UNIVERSITAT POLITÈCNICA DE CATALUNYA
BARCELONATECH
Department of Civil and Environmental Engineering
Geotechnical Engineering and Geosciences

CIMNE
EXCELENCIA SEVERO OCHOA

eurad
European Joint Programme on Radioactive Waste Management

EXPERIMENTAL MULTI-SCALE INSIGHT INTO GAS TRANSPORT AND SELF-SEALING CAPACITY
A DETAILED RESEARCH METHODOLOGY ON BOOM CLAY

Laura Gonzalez-Blanco
Enrique Romero
CIMNE / UPC

The project leading to this application has received funding from the European Union's Horizon 2020 research and innovation programme under grant agreement n° 847593.

OUTLINE OF THE LECTURE

1. Motivation
2. Insight into gas transfer and self-sealing
3. Some observations regarding gas testing (experimental protocols)
4. A detailed research methodology on Boom Clay:
    - Material characterization
    - Stress paths followed
    - Gas test protocols
    - Test results at different scales (macroscopic results and microstructural features)
5. Final comments. Future challenges

WHY GAS TRANSPORT ISSUES ARE OF INTEREST?

Understanding gas transport process is an important issue in the **assessment of radioactive waste repository performance** and other **energy / environmental geotechnics related fields** (shale gas, CO_2 capture, landfill design, …)

Landfill design (methane, …)

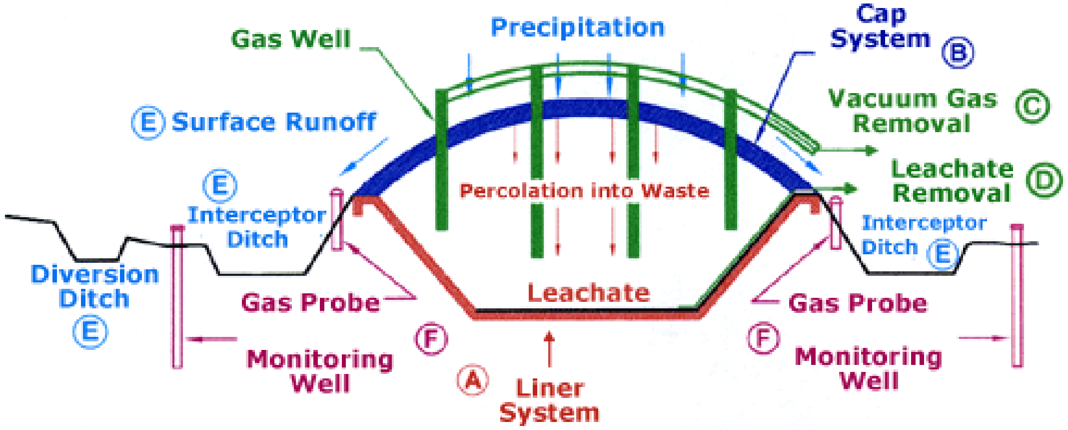

Conventional/unconventional gas reserves

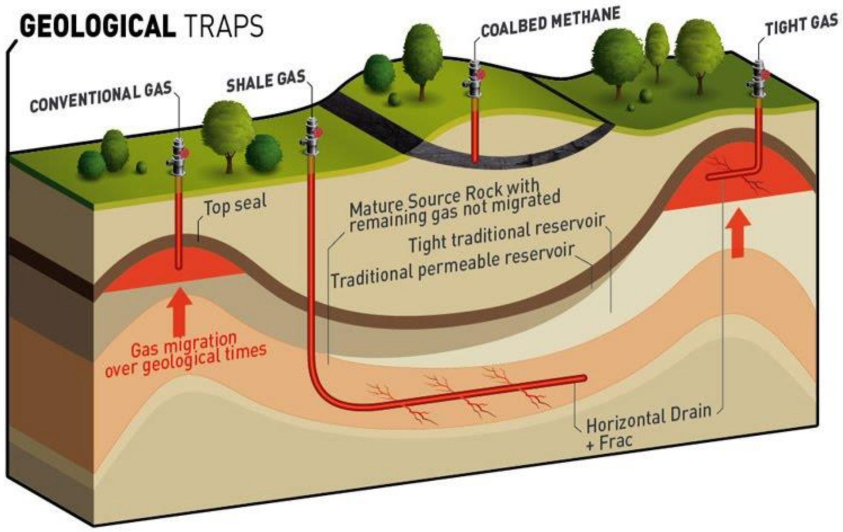

Safely storing CO_2

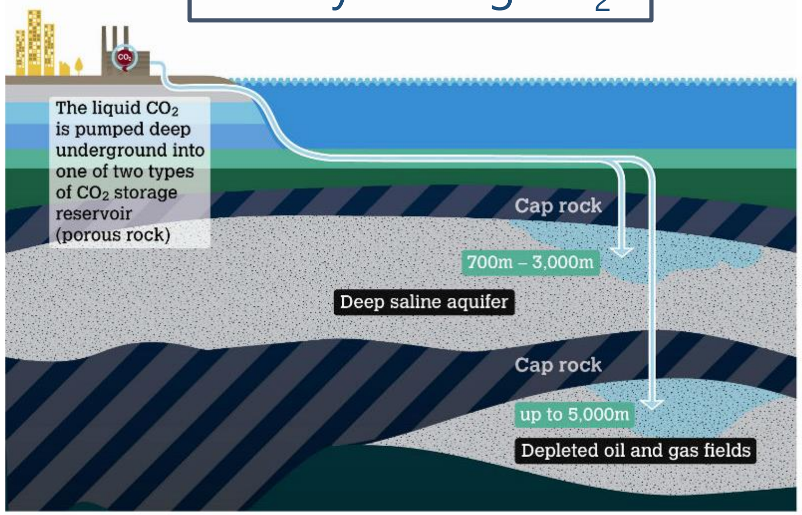

Peterhead CCS Project (UK)

GEOLOGICAL DISPOSAL FACILITIES

Based on the multi-barrier system concept for long-term isolation

- **Artificial barriers:**
  - Waste canister
  - Metallic overpack
  - **Sealing and buffer materials EBS** to prevent / delay the release of radionuclides, gases and other contaminants

- **Natural barriers:**
  - Geosphere: **geological formation** and groundwater (host rock)

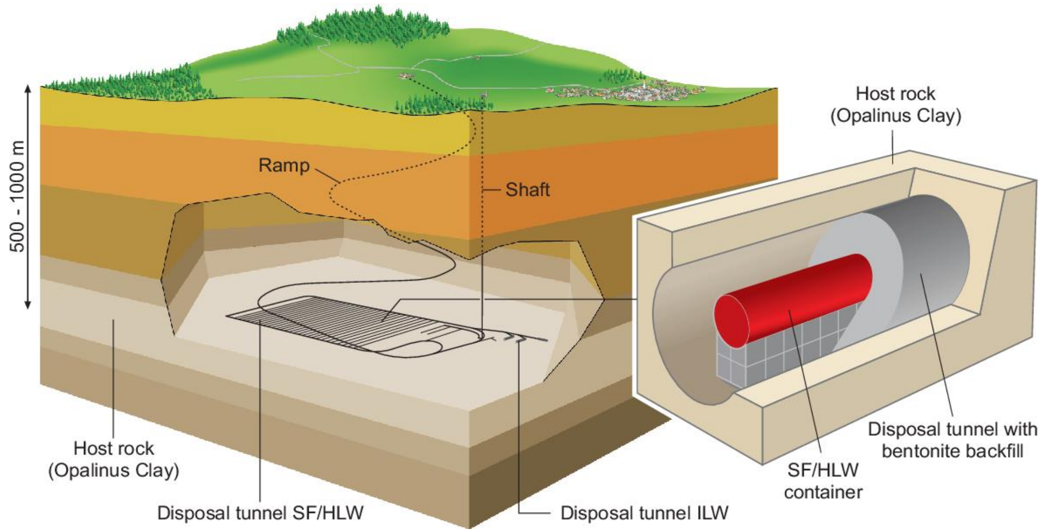

Swiss concept (NAGRA)

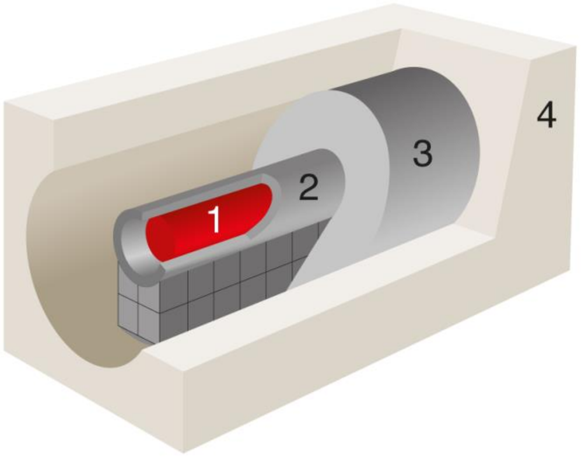

1. Glass matrix, containing radioactive material
2. Metal container
3. **Backfill with bentonite**
4. **Host rock**

GAS GENERATION SOURCES

- **Degradation of organic matter: Methane and Carbon Dioxide**
- **Radiolysis: Hydrogen, Oxygen, Carbon Dioxide, Methane, etc**
- **Alpha decay process: Helium**
- **Anaerobic corrosion of ferrous materials in metallic overpacks (largest source and production of Hydrogen)**

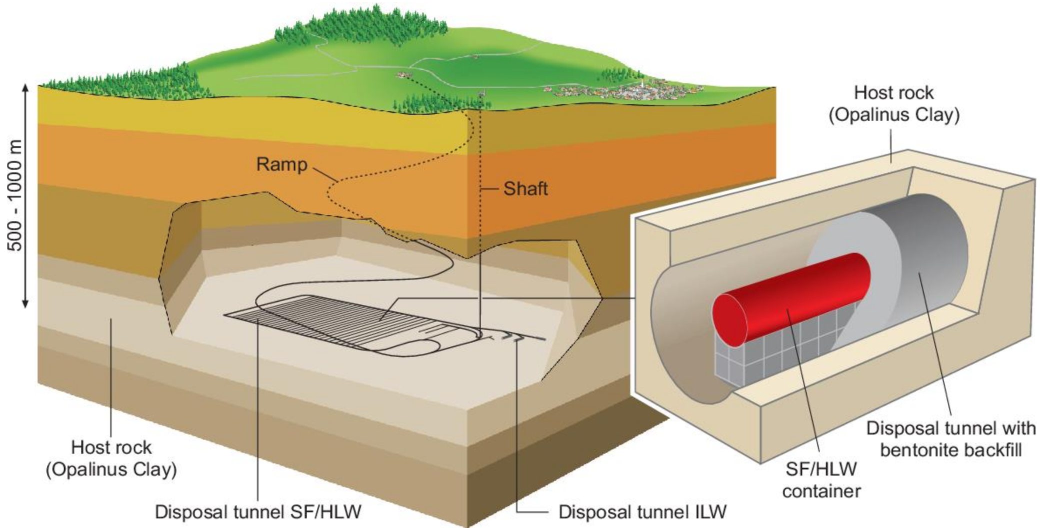

Gas pressure → Gas production rate

Gas pressure → Transport properties of EBS and host formations

Swiss disposal concept for HLW and L/ILW

- Total volume of produced gas: **20 Mio m³ (STP)**
- Total pore volume of backfilled underground structures: **400000 m³**
- **Maximum gas overpressure above the hydrostatic pressure: 1-3 MPa**
- **Upper limit of gas pressure: 16 MPa**

Gas pressure build-up may cause the failure of the EBS and the possible release of radionuclides into environment

MULTI-BARRIER PERFORMANCE

- **Large number of past THM-C processes** and phenomena that interact
- **No overlapping with bentonite saturation and EDZ self-sealing**
- Predictions required for **long periods of time**

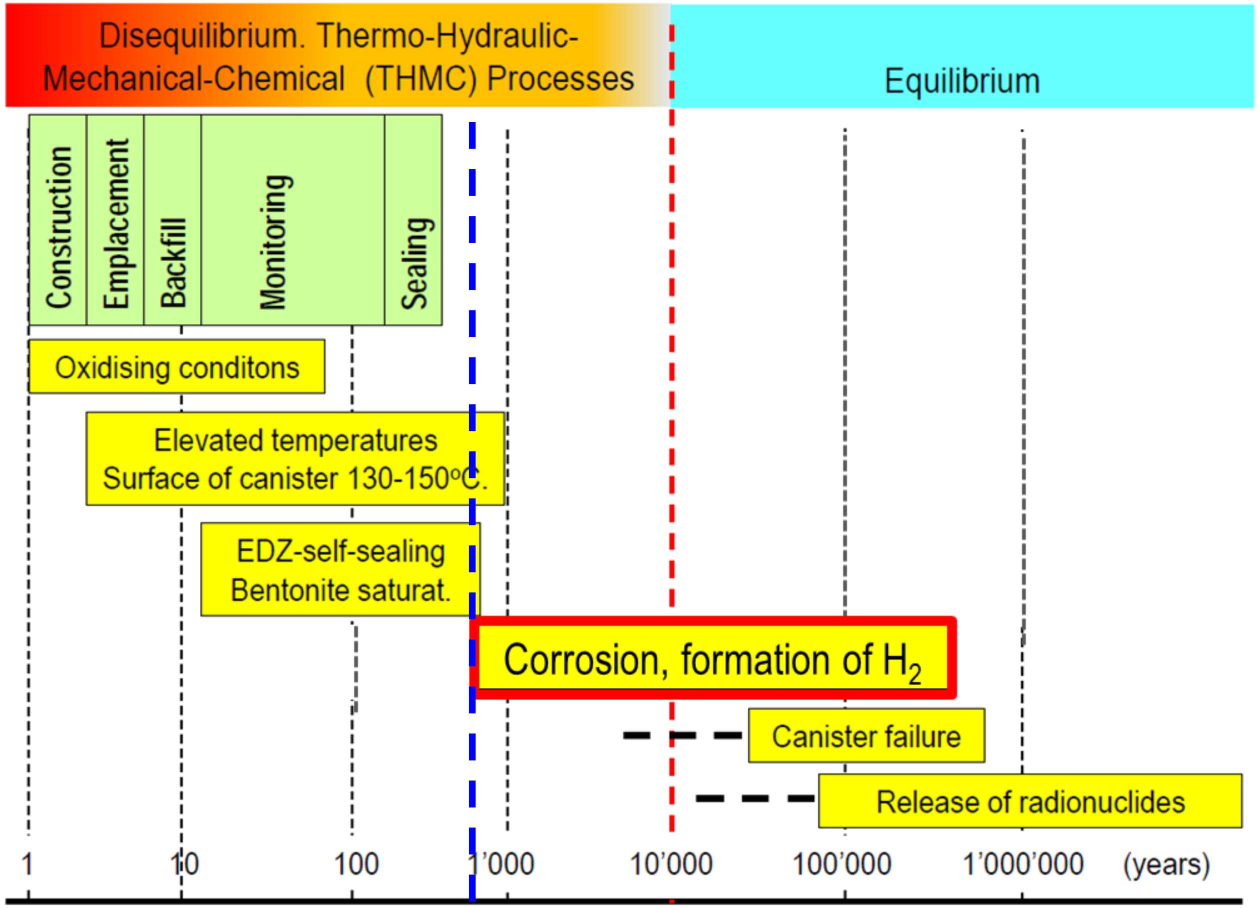

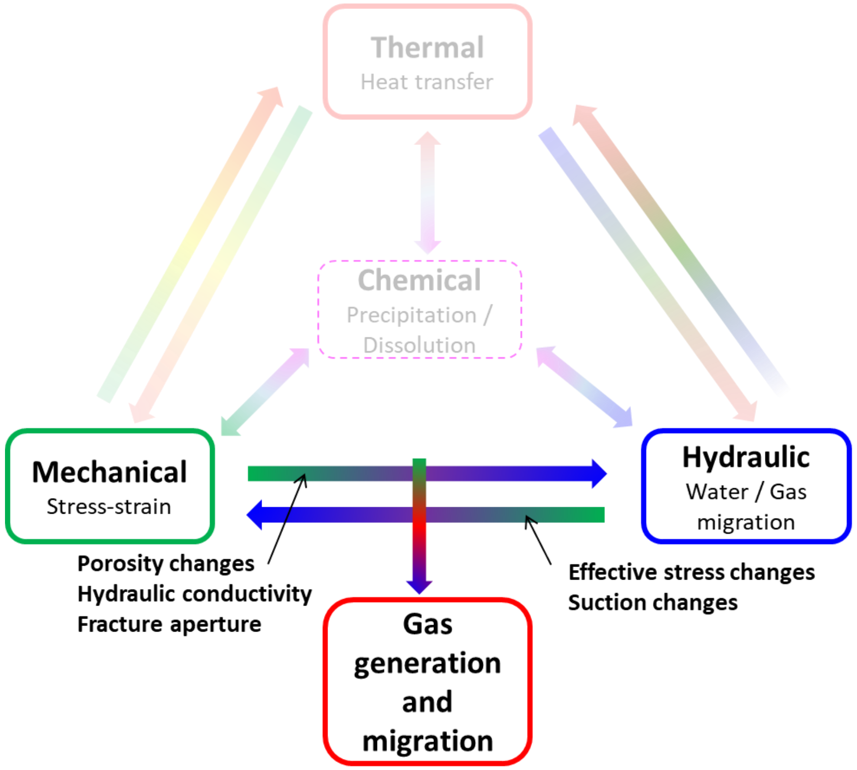

LONG-TERM

Small thermal interactions (thermal history has impact)
EBS and host rock close to saturated conditions (reduced chemical interactions)

NAGRA (www.mont-terri.ch)

WHAT IS THE MOTIVATION OF THIS LECTURE? SOME COMMENTS

To present an **updated perspective** on the use of multi-scale **laboratory techniques** (multi-physics testing)

Macroscopic (phenomenological) features of advective gas transport and self-sealing in saturated clayey materials. Evaluation of stress paths and effective permeability to water and gas flow for the safety assessment.

Macroscopic laboratory tests are necessary to improve the understanding of the basics and to provide data for the development of predictive tools.

Microstructural tests to evaluate the pore size distribution, reconstruct the fissure/pathway patterns, estimate the total volume of pathways and their connectivity, and observe the closure of the gas pathways upon re-saturation (self-sealing).

Microstructural description of discontinuities, fractures and heterogeneity play an important role and should be to be taken into account for modelling.

WHAT IS THE MOTIVATION OF THIS LECTURE? SOME COMMENTS

- **Experimental techniques** used to study coupled multi-physics process **do not always present the complete picture of understanding** (information on local behavior usually remains unknown). Often, theoretical and/or **numerical models must accompany the interpretation of the physical tests to better exploit the information provided by measurements** and to offer additional confidence on the experimental results (validation of the experimental techniques).

- **Advective gas tests** are associated with so-called **'critical phenomena'** that are at the **verge of predictability** (particularly at specimen scale), and **microstructural features set on compaction / stress paths** affecting pore size distribution and connectivity issues (multiple gas pathways, dominant single cluster, ….) are admitted to **play an important role in the scatter**.

eurad

OUTLINE OF THE LECTURE

1. Motivation
2. **Insight into gas transfer and self-sealing**
3. Some observations regarding gas testing (experimental protocols)
4. A detailed research methodology on Boom Clay:
   - Material characterization
   - Stress paths followed
   - Gas test protocols
   - Test results at different scales (macroscopic results and microstructural features)
5. Final comments. Future challenges

eurad

GAS MIGRATION IN SATURATED POROUS MEDIA: GAS TRANSPORT MECHANISMS

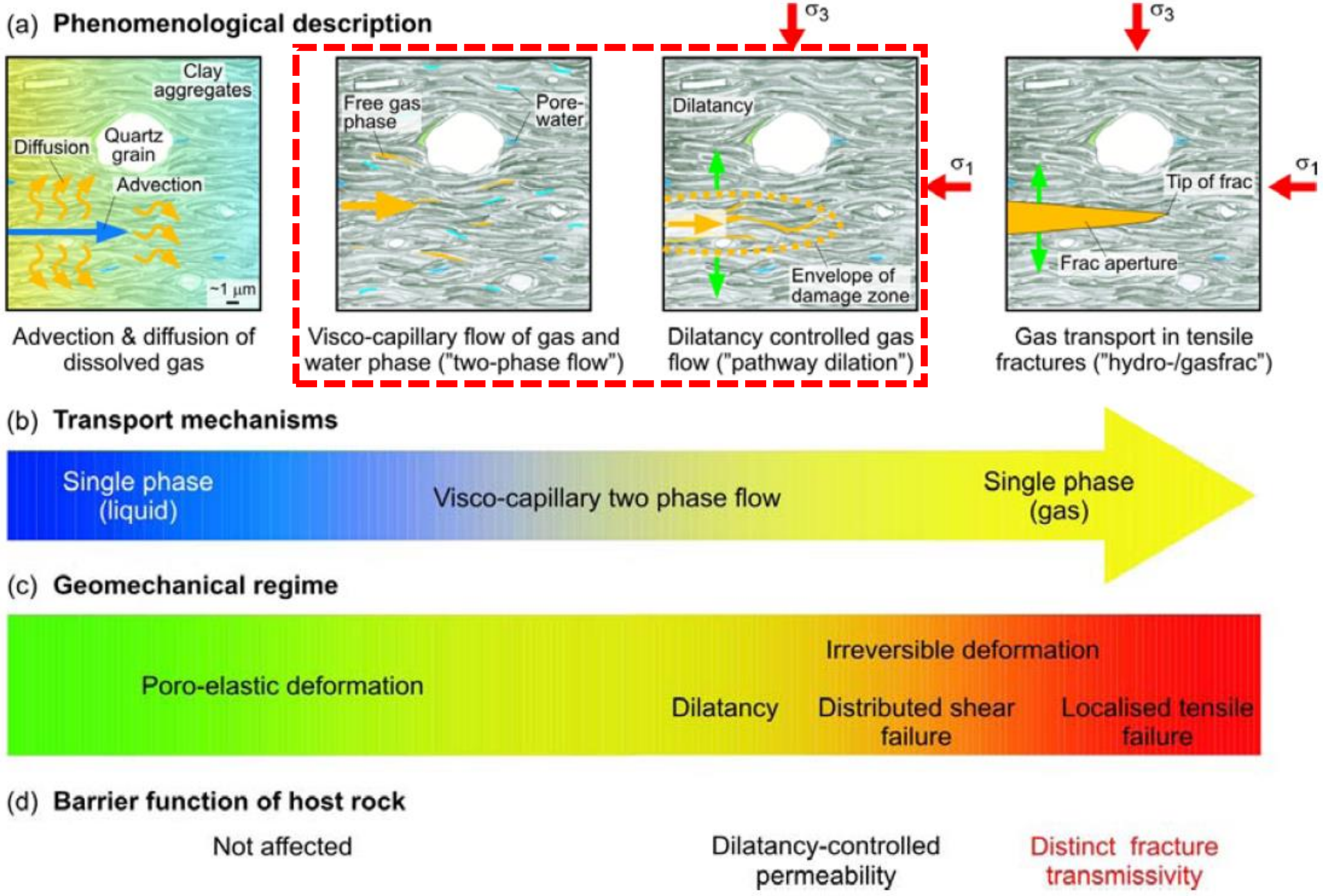

Marschall et al. (2005)

Gas dissolved in water migrates through diffusion (low gas generation rates)

- Gas pressure builds up due to the slow diffusive transport in low permeable media (high gas generation rates)

Gas flow through the matrix partially displacing water (two-phase flow)

- Flow affected by mechanical effects (intrinsic permeability affected by porosity changes)

Gas flow through pressure-dependent pathways/fractures (existing/induced) (microscopic fissuring, macroscopic fracture)

- Flow properties affected by mechanical effects and fracture aperture

eurad

GAS TRANSPORT PATHWAYS

Plastic host rock: gas migration along bedding planes or discontinuities in the EDZ that can be initially close

Extension of EDZ in Connecting Gallery
(Boom Clay, HADES URL, Belgium)

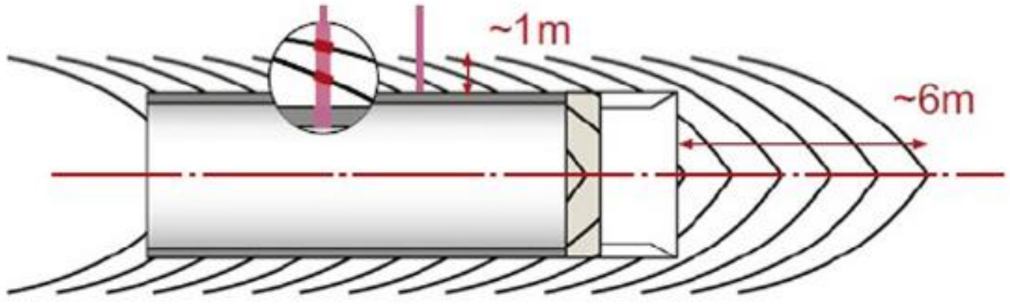

Salehnia et al. (2015)

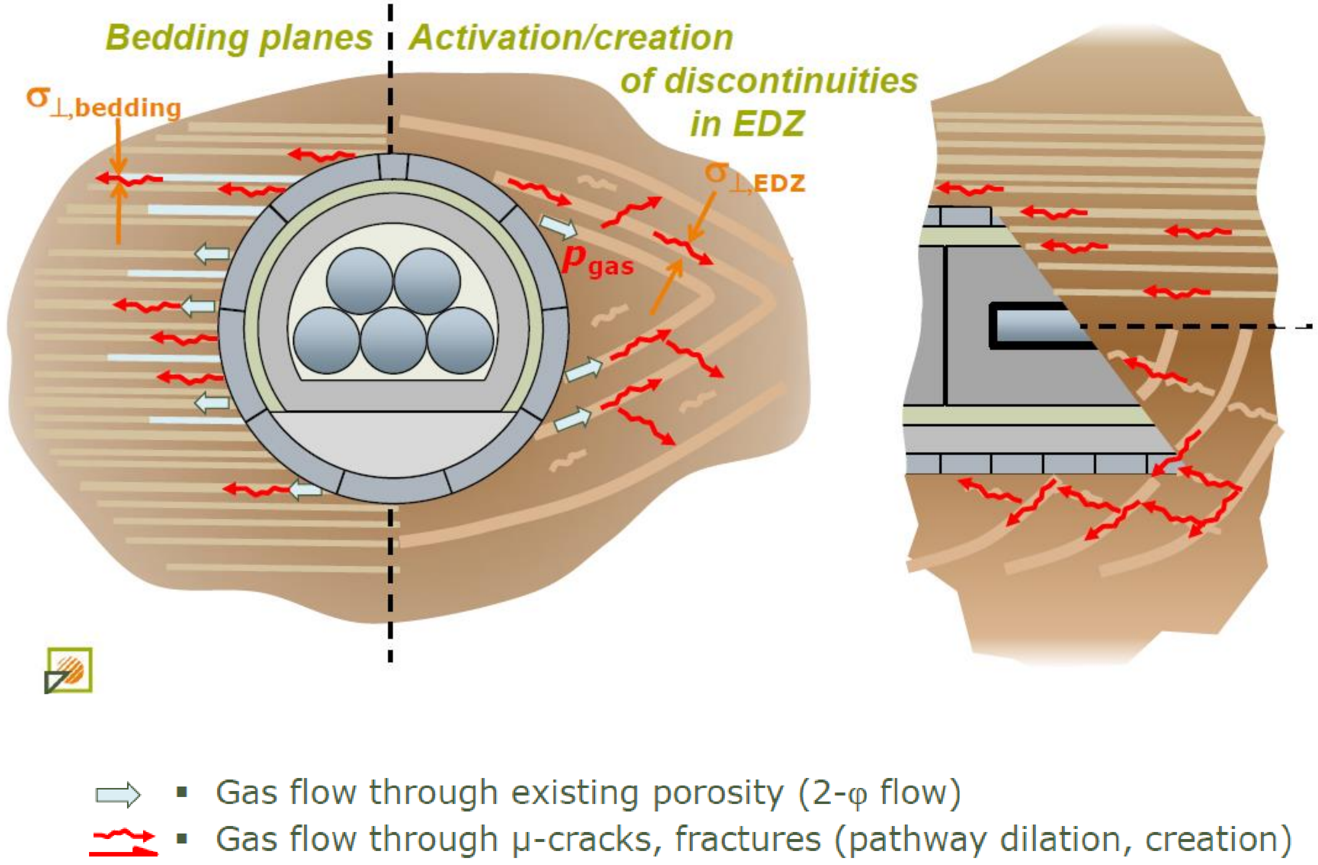

ONDRAF/NIRAS ***(2016)***

GAS INJECTION EXPERIMENTS

Gas injection tests on Opalinus Clay formation (Switzerland)

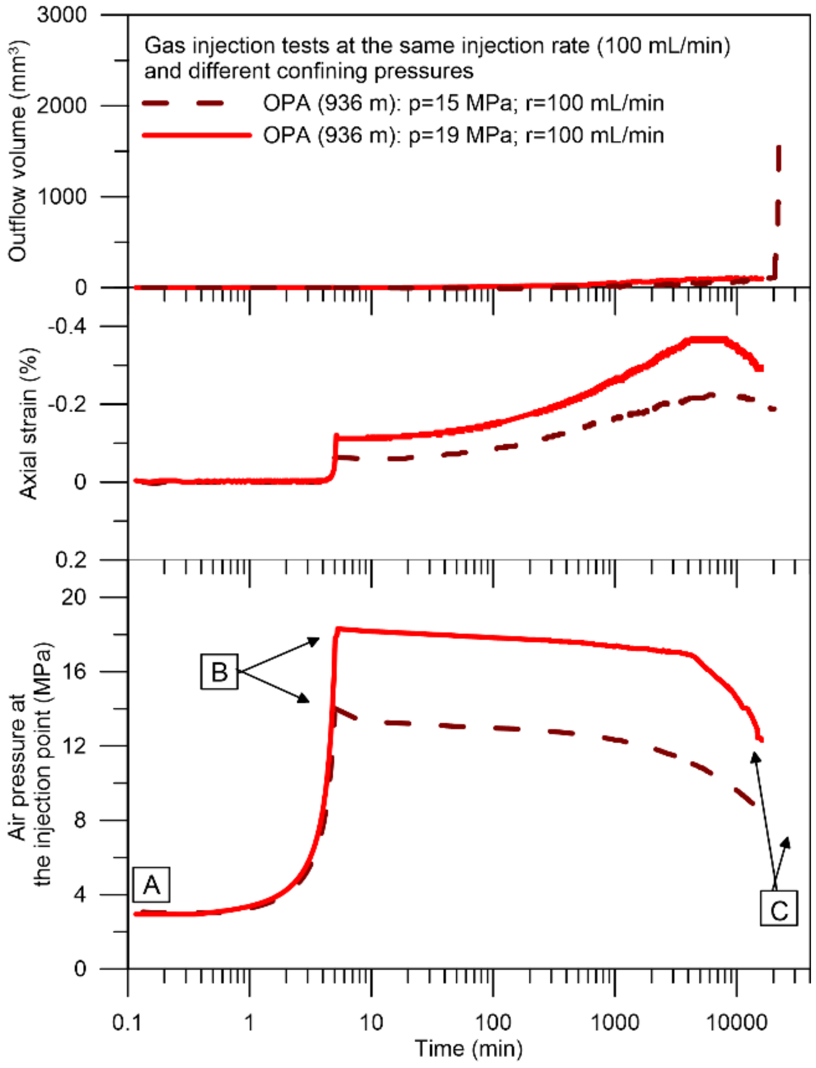

A→B: Gas injection at constant volume rate

B: Shut-off phase (constant injection volume)

B→C: Dissipation phase (constant injection volume)

Volumetric response during gas injection

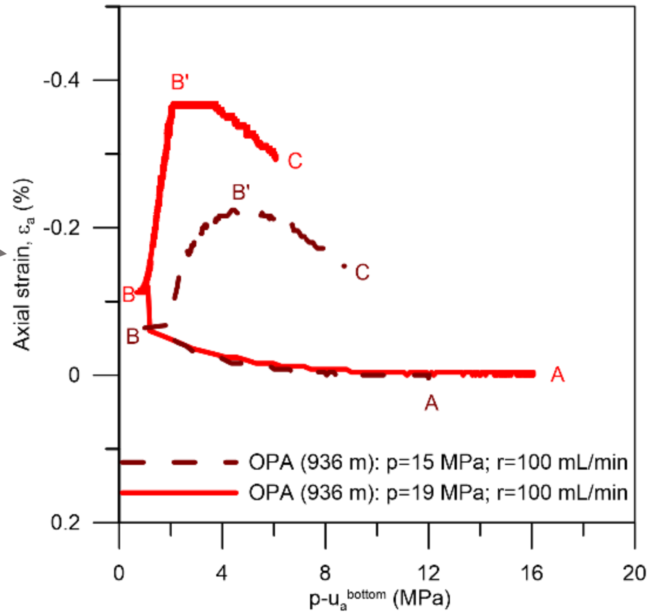

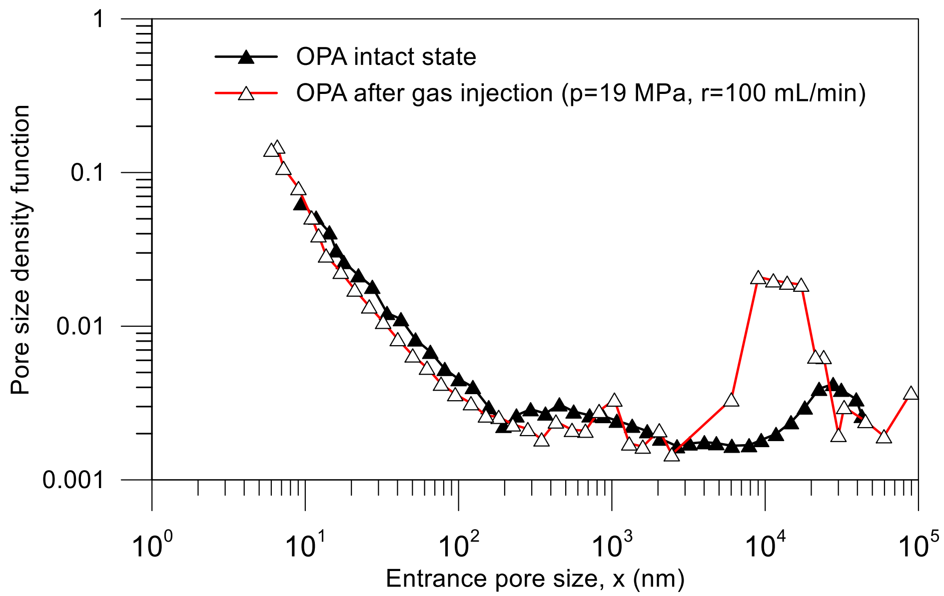

Change in the pore size distribution

Gonzalez-Blanco et al. (2022)

MICROSTRUCTURE (TECHNIQUES)

Multi-scale characterisation of porosity in Boom Clay (HADES-level, Mol, Belgium)

Hemes et al. (2015)

MIP (450 μm and 7 nm)

100 μm 10 μm 1 μm 100 nm

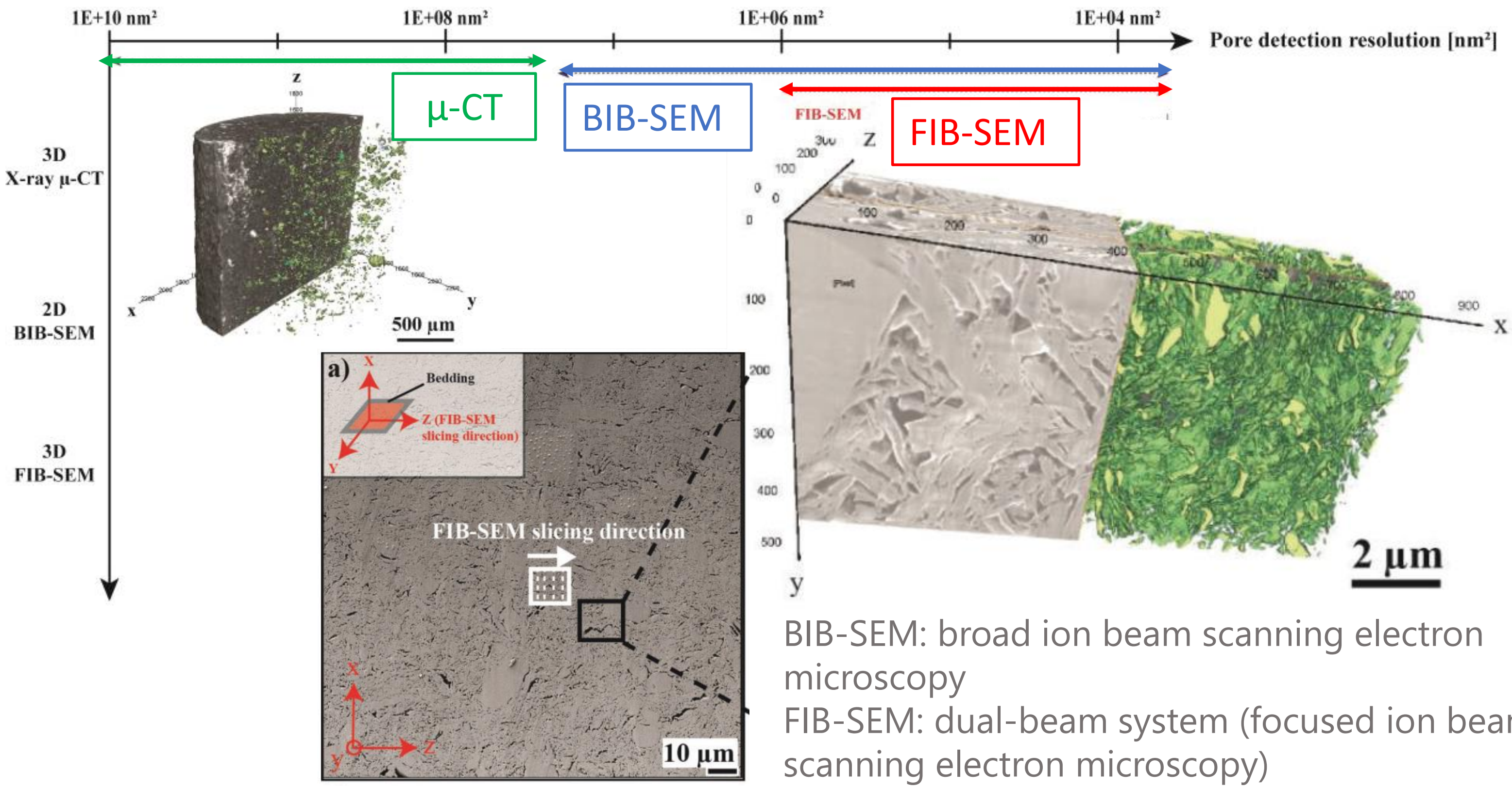

BIB-SEM: broad ion beam scanning electron microscopy
FIB-SEM: dual-beam system (focused ion beam scanning electron microscopy)
MIP: Mercury Intrusion Porosimetry
μ-CT: Micro-focus X-ray computed tomography

Digital image analyses (X-ray μ-CT, BIB-SEM / FIB-SEM tomography) (rendering graphics software ImageJ, Avizo, ...)

3D volume reconstruction from slice-and-view images, and stacking multiple planar images with a known separation

Resolution depending on system and sample size (typically between 0.01 to 100 μm) (1/1000-2000 times the object cross-section diameter)

EXPERIMENTAL DATA AT MULTI-SCALE LEVEL NECESSARY FOR THE DEVELOPMENT AND VALIDATION OF CONSTITUTIVE MODELS

Embedded fracture permeability model
(*Olivella & Alonso, 2008*)

Fracture aperture
$$b = \begin{cases} b_0 + \Delta b & b < b_{max} \\ b = b_{max} & b \geq b_{max} \end{cases} \qquad \Delta b = a\Delta\varepsilon$$

Equivalent permeability
$$k = k_{matrix} + \frac{b^3}{12a}$$

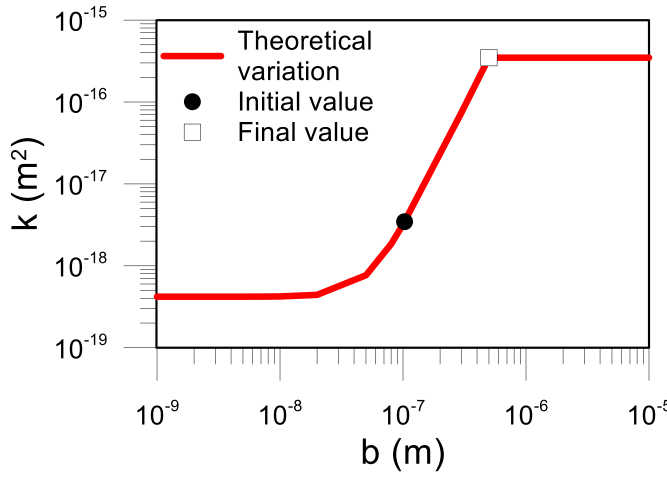

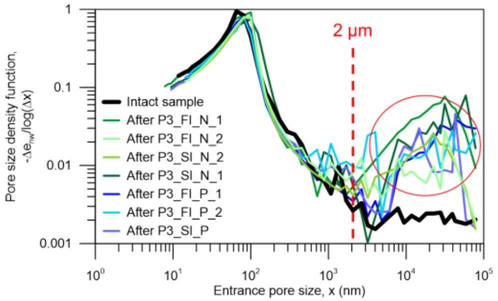

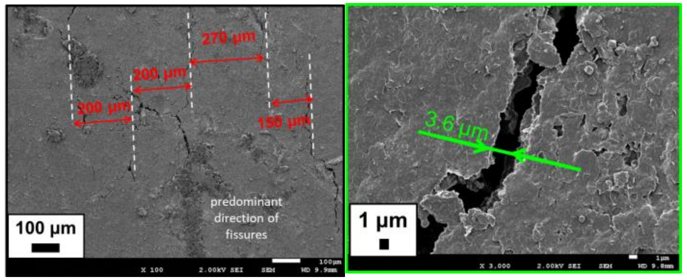

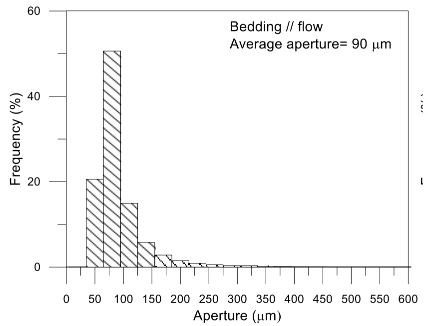

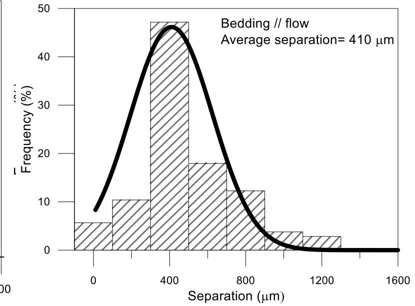

	MIP	FESEM	μ-CT
Aperture: b (μm)	> 2	3 - 10	90// - 150⊥
Separation: a (μm)	-	150 - 270	410// - 560⊥

Gonzalez-Blanco et al. (2016)

APPLICATION OF THE EMBEDDED FRACTURE MODEL

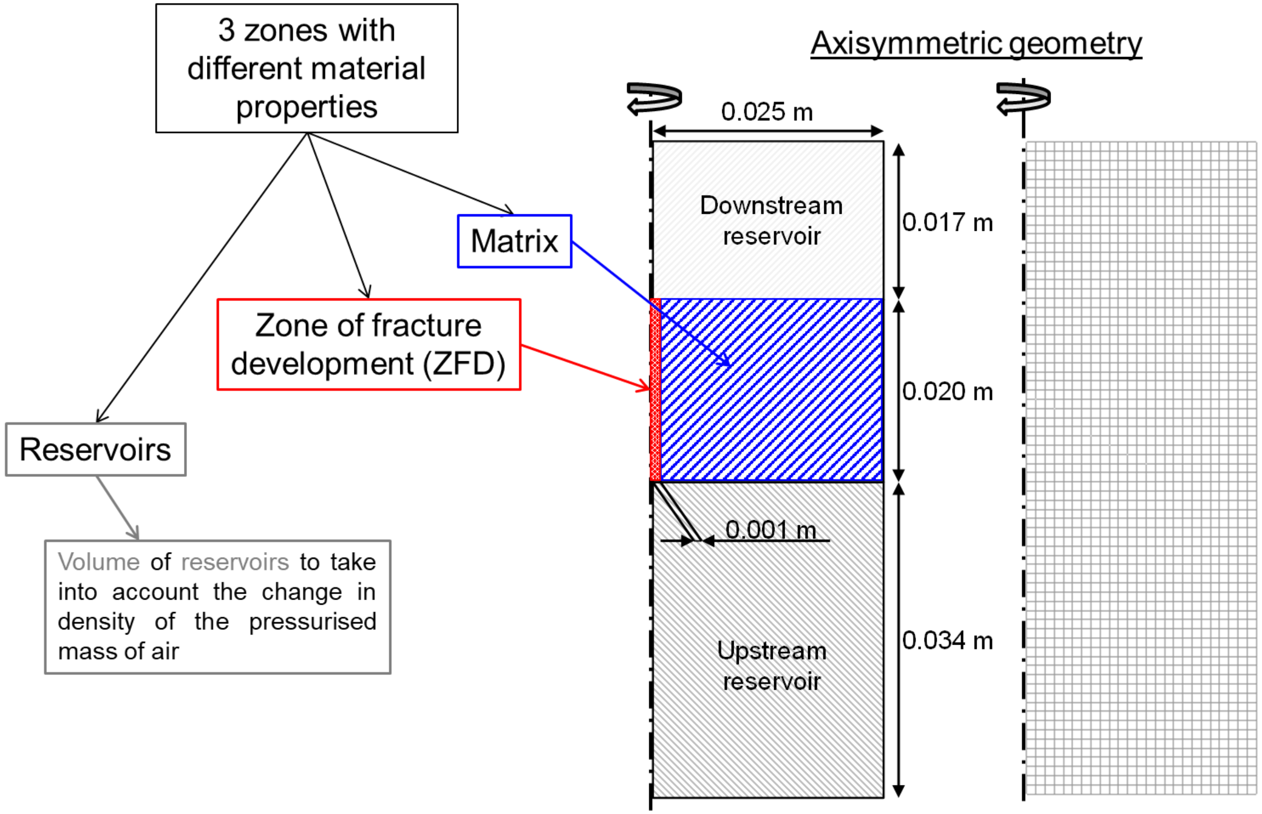

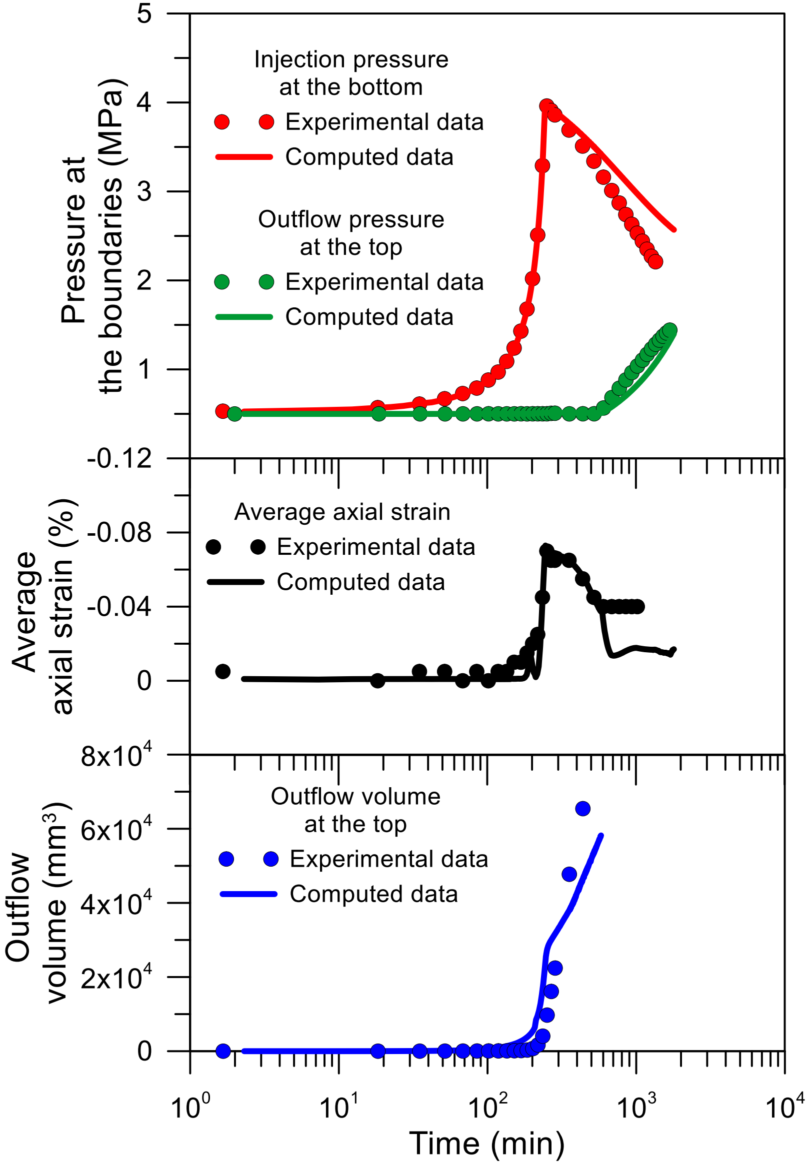

Gonzalez-Blanco et al. (2016)

SIMULATION OF EXPERIMENTAL RESULTS ALLOWED BETTER EXPLOITING THE INFORMATION PROVIDED BY MEASUREMENTS

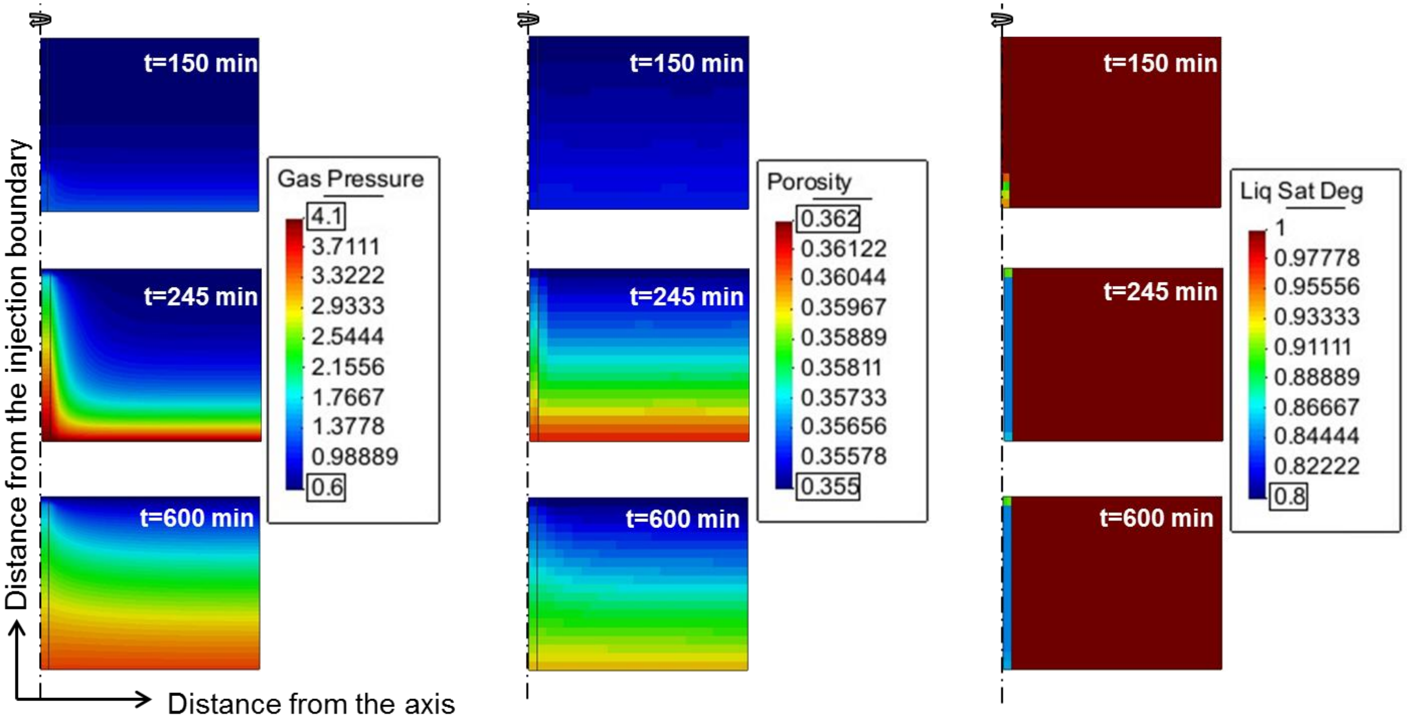

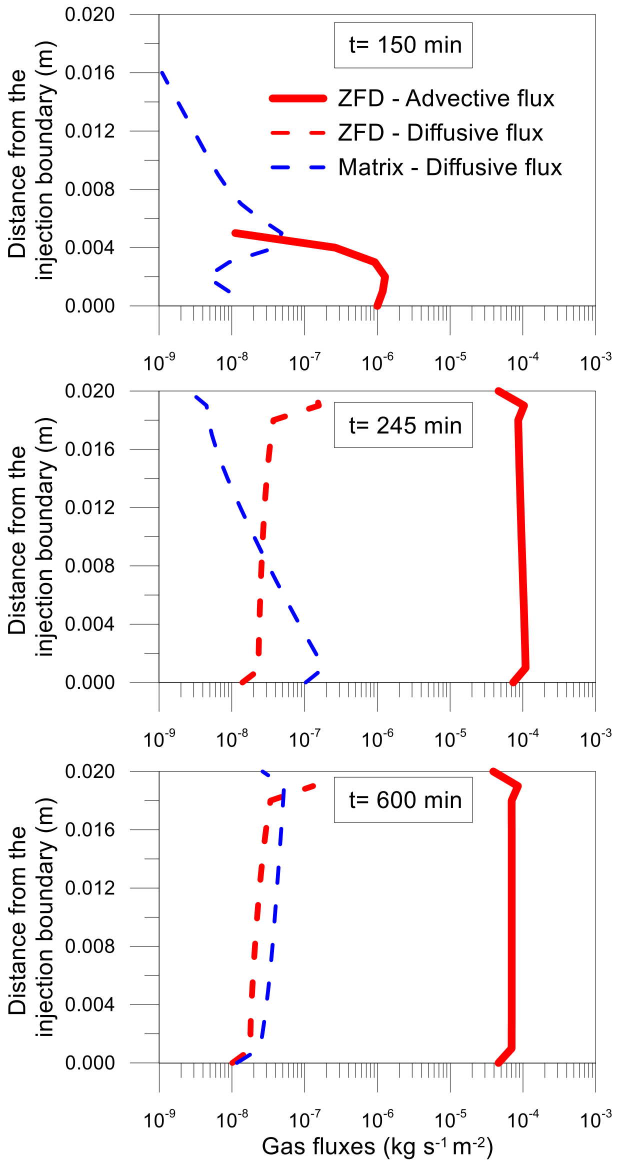

t= 150 min → During gas injection
t= 245 min → At shut-off (end of the injection)
t= 600 min → During gas dissipation

Gonzalez-Blanco et al. (2016)

eurad

SELF-SEALING / SELF-HEALING

Sealing → Reduction of fracture permeability by any hydro-mechanical, hydro-chemical or hydro-biochemical processes

Healing → Sealing with loss of memory of the pre-healing state

Self → The process of healing or sealing happens spontaneously in the rock mass without interference by intentional human actions

Possible mechanisms:

- Increase of the stress state
- Pore-pressure changes
- Creep
- Swelling of clay minerals
- Oxidation/precipitation
- Mineralogical changes (crystallisation)
- etc.

Bernier et al. (2007) SELFRAC Project

eurad

SELF-SEALING / SELF-HEALING IN ARTIFICIALLY FRACTURED CLAYEY ROCKS

Hydraulic conductivity reduction due to self-sealing

BOOM CLAY

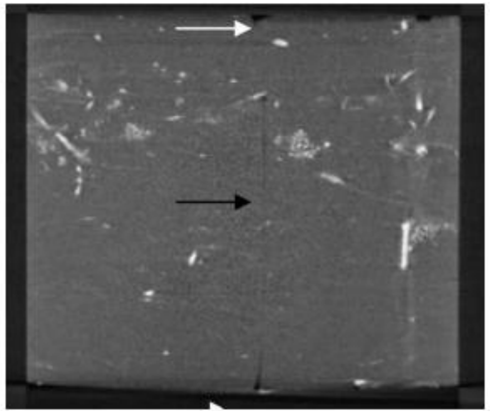

After loading

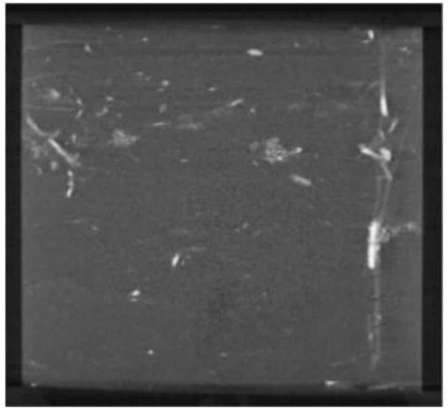

After permeability testing

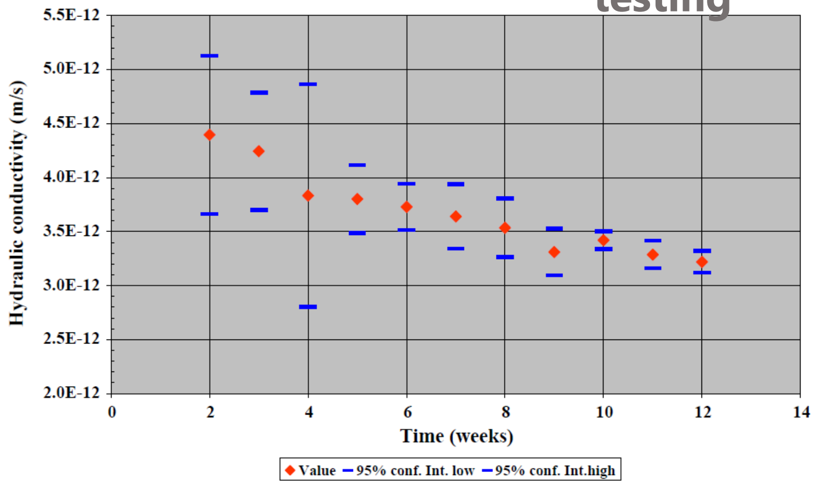

OPALINUS CLAY

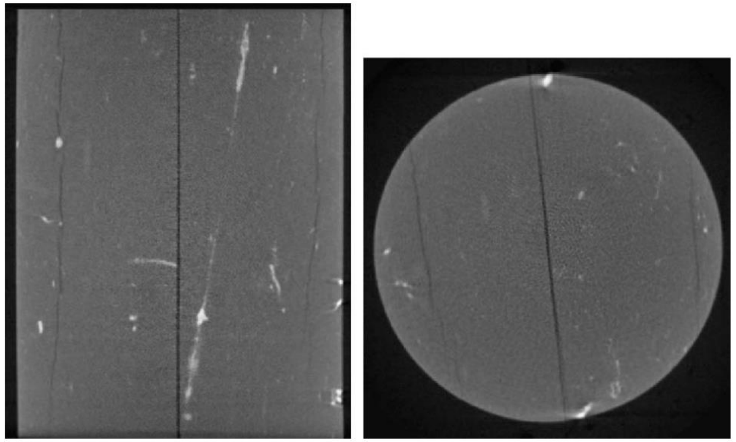

Initial state

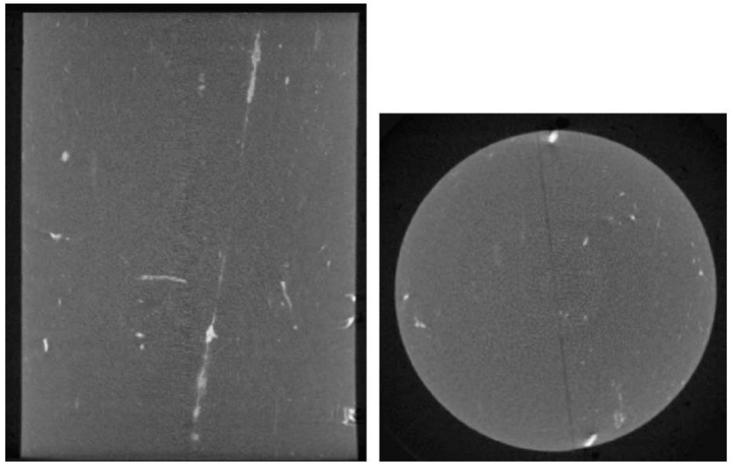

After permeability testing

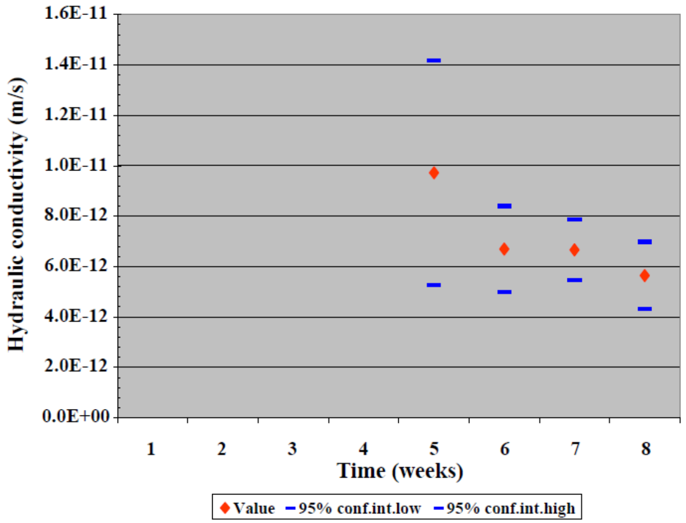

SELFRAC Project

Van Geet et al. (2008)

FRACTURE CLOSURE

CALLOVO-OXFORDIAN CLAY

Artificially-fractured

OPALINUS CLAY

Naturally-fractured

Effect of normal stress on fracture closure

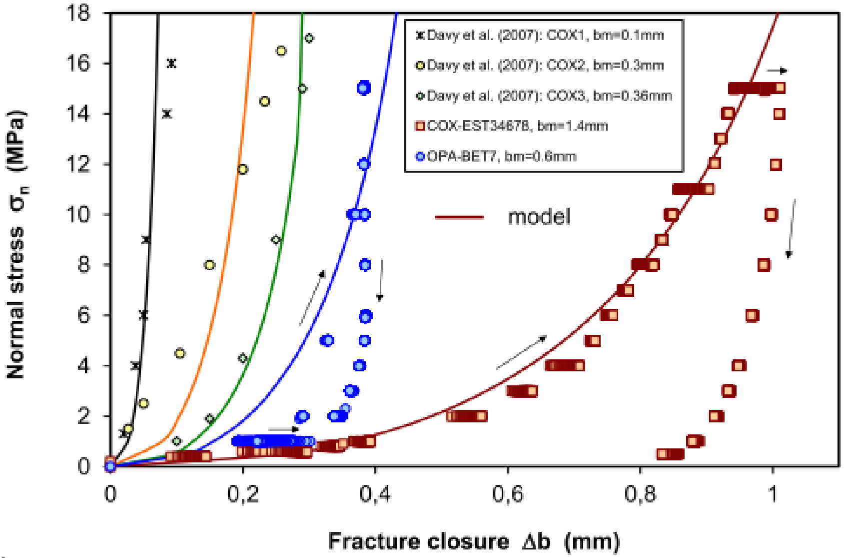

Zhang et al. (2013)

Sealing of fractures in COX claystone during water flowing under various confining stresses

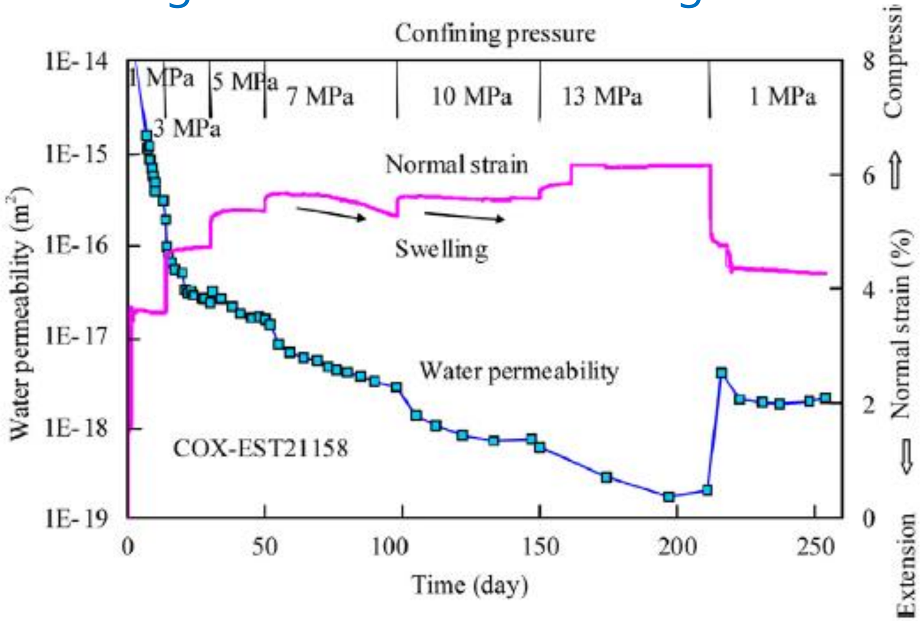

Effects of wetted gas flow on fracture sealing

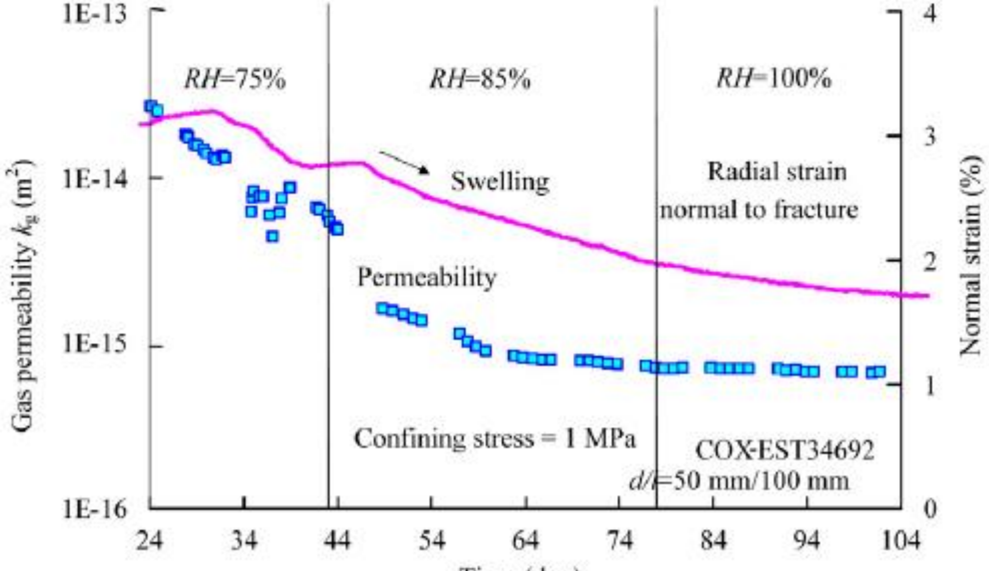

SELF-SEALING / SELF-HEALING IN NATURALLY FRACTURED CLAYEY ROCKS

Water flow while increasing confining pressure

OPALINUS CLAY

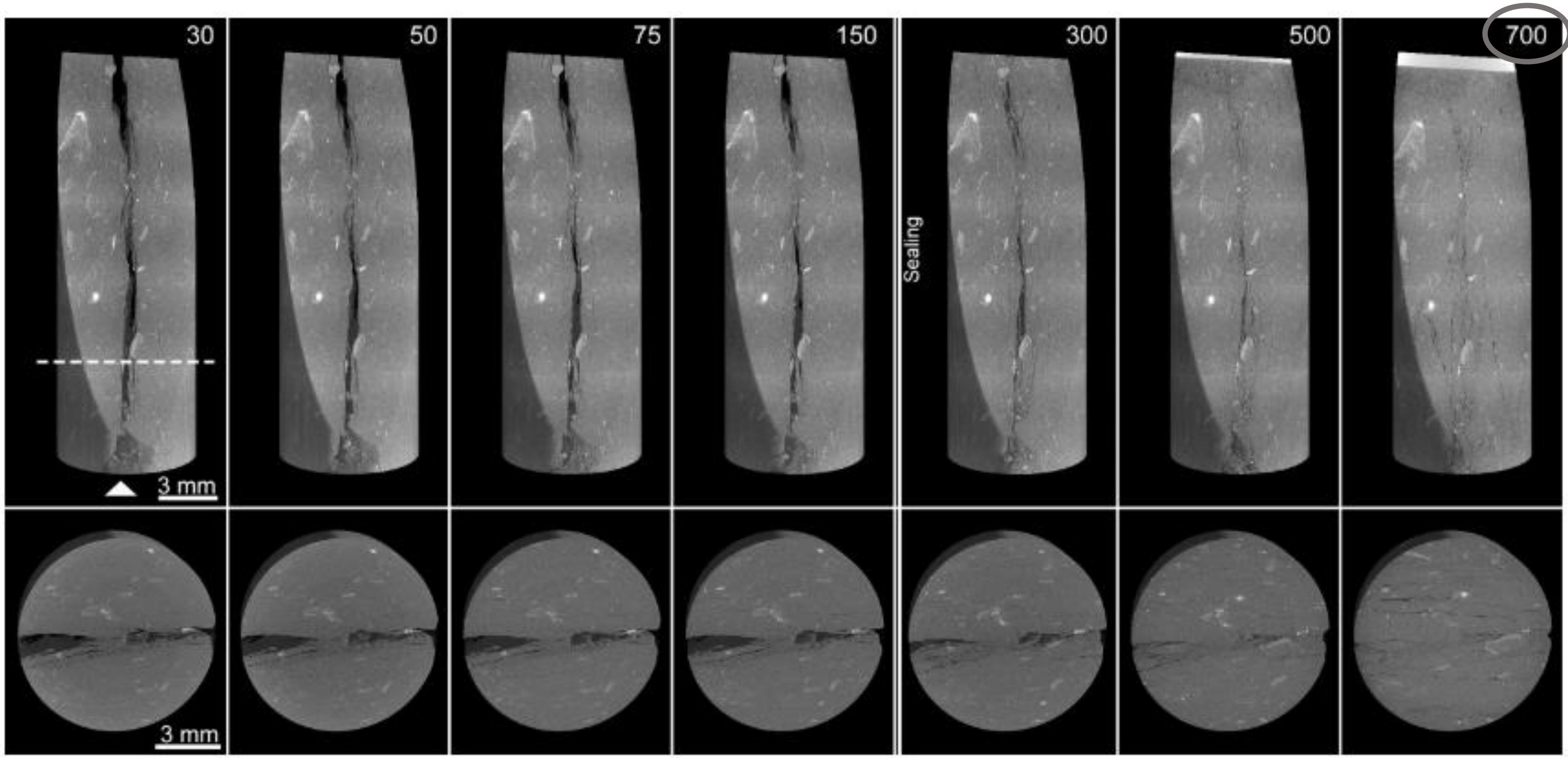

Confining pressure minus back-pressure (psi)

Synchrotron X-Ray Micro-Tomography

Voltolini & Ajo-Franklin (2020)

SELF-SEALING / SELF-HEALING IN ARTIFICIALLY FRACTURED CLAYEY ROCKS

Effect of wetting / drying cycles on fracture closure and re-opening

CALLOVO-OXFORDIAN CLAY

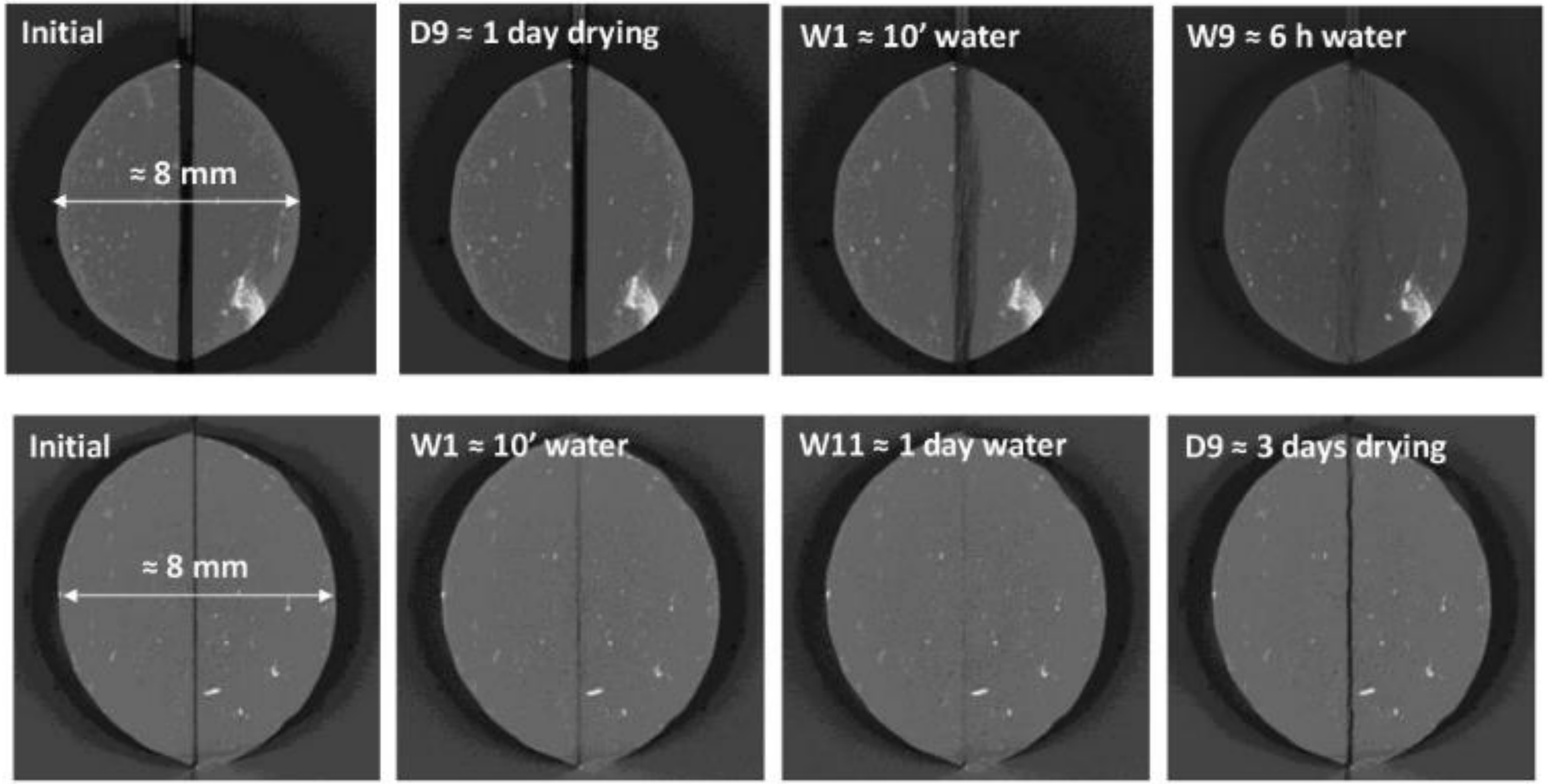

Initial gap 425 µm
Voxel size 15 µm

Initial gap 75 µm
Voxel size 13.5 µm

Di Donna et al (2022)

EFFECT OF GAS INJECTION ON SELF-SEALED FRACTURED CLAYEY ROCKS

Gas invasion in previously fractured and sealed indurated clay samples

CALLOVO-OXFORDIAN CLAY

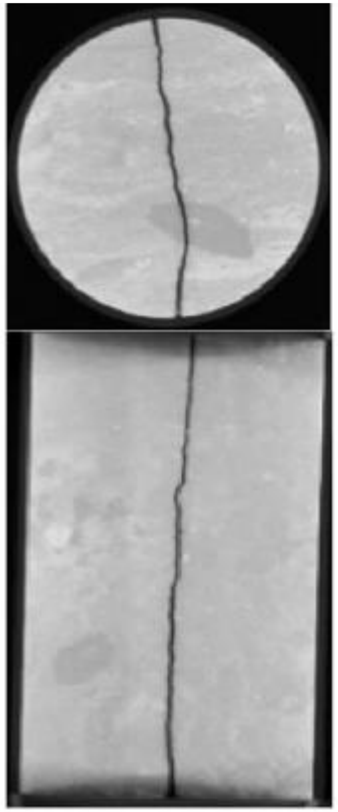

OPALINUS CLAY

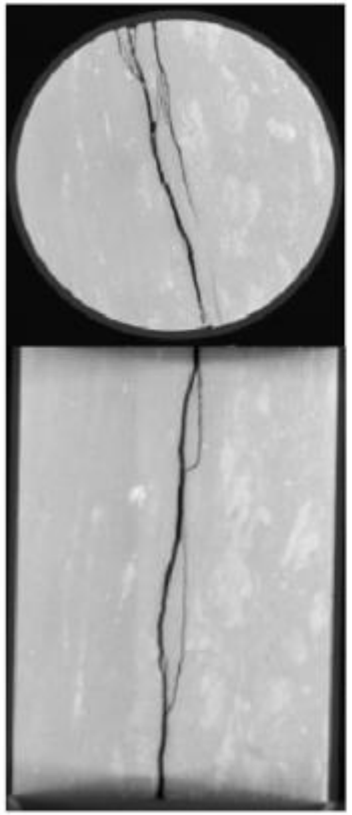

Zhang & Talandier (2022)

Decrease of water permeability due to fracture closure

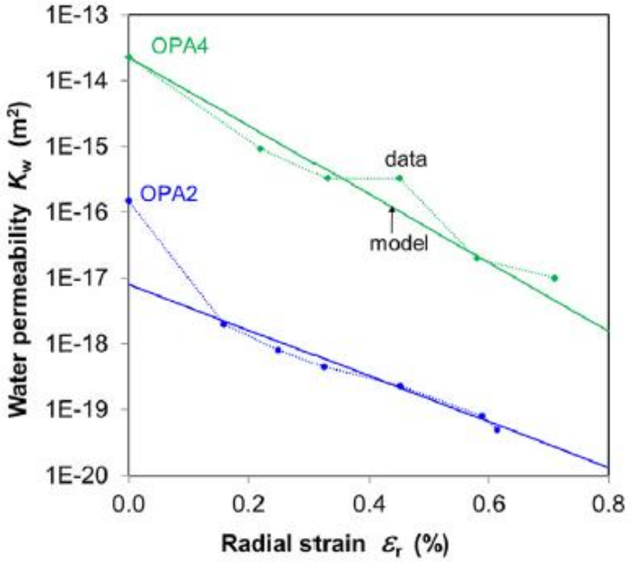

Water permeability **before and after gas invasion**

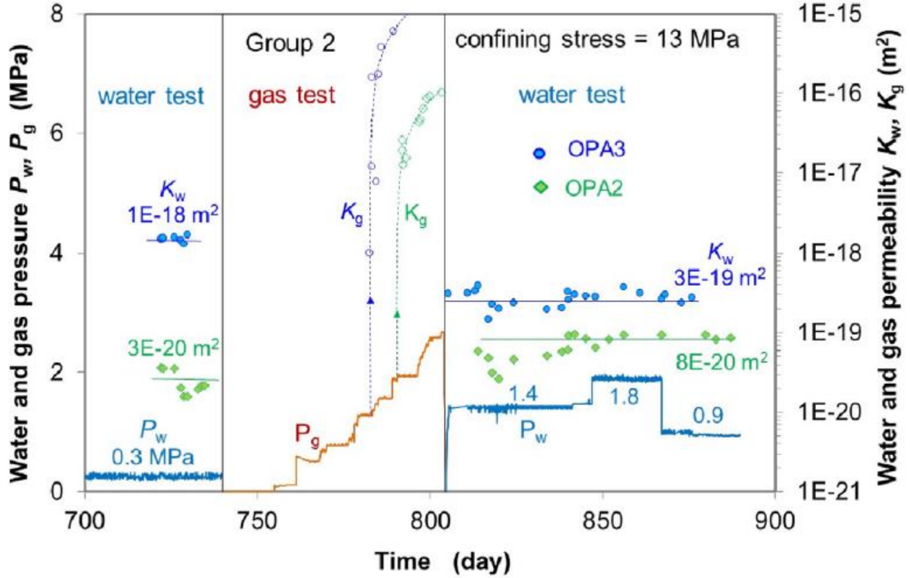

OUTLINE OF THE LECTURE

1. Motivation
2. Insight into gas transfer and self-sealing
3. Some observations regarding gas testing (experimental protocols)
4. A detailed research methodology on Boom Clay:
   - Material characterization
   - Stress paths followed
   - Gas test protocols
   - Test results at different scales (macroscopic results and microstructural features)
5. Final comments. Future challenges

eurad

ADVECTIVE GAS EXPERIMENTS AT LAB SCALE: SOME ISSUES OF CONCERN

- Effects of the **stress state** and **stress history (mechanical, saturation, thermal)** on gas migration
- **Volume change behaviour** during the stress history and along gas injection / dissipation (changes in gas and liquid pressures and their impact on gas permeability).
- **Stress changes** during gas injection under constant volume conditions
- Role played by natural **discontinuities and their orientation (anisotropy)**
- **Changes in the pore / fissure network and their connectivity** due to gas injection / dissipation (opening of bedding planes / fissures / pathways)
- **Liquid displacements (desaturation of pathways)** during gas injection / dissipation
- Influence of the **gas injection rate and gas type**
- **Gas migration after re-saturation** (reopening of fissures)

Simple concepts but **not-so-simple tests to perform and interpret**. Need for **coupled modelling to complement the information** not provided by measurements ('boundary value tests')

HOW TO PERFORM ADVECTIVE GAS INJECTION/DISSIPATION TESTS?

Importance of:

- Hydro-mechanical characterization of tested material (uncertainty / variability assessment)

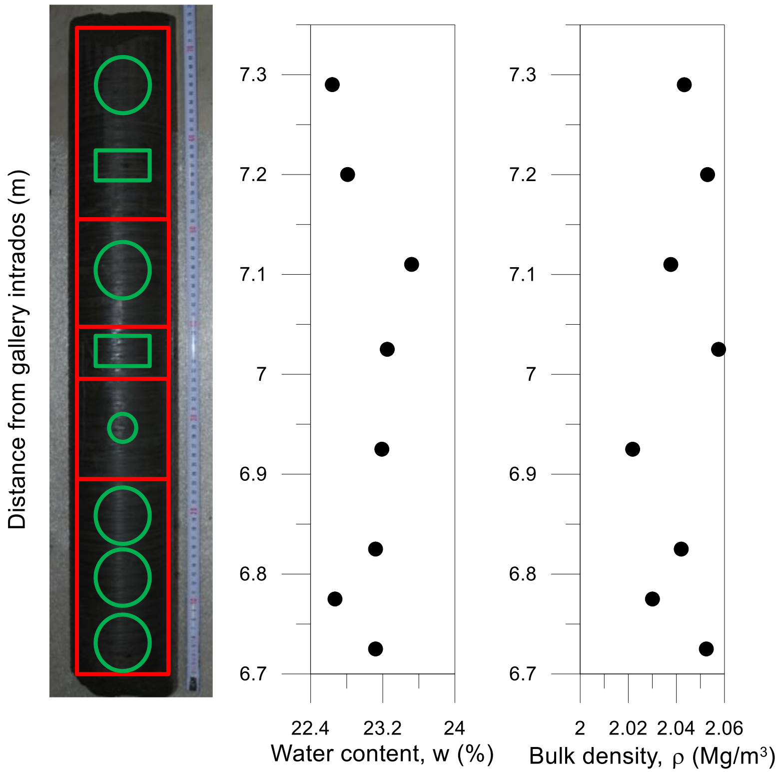

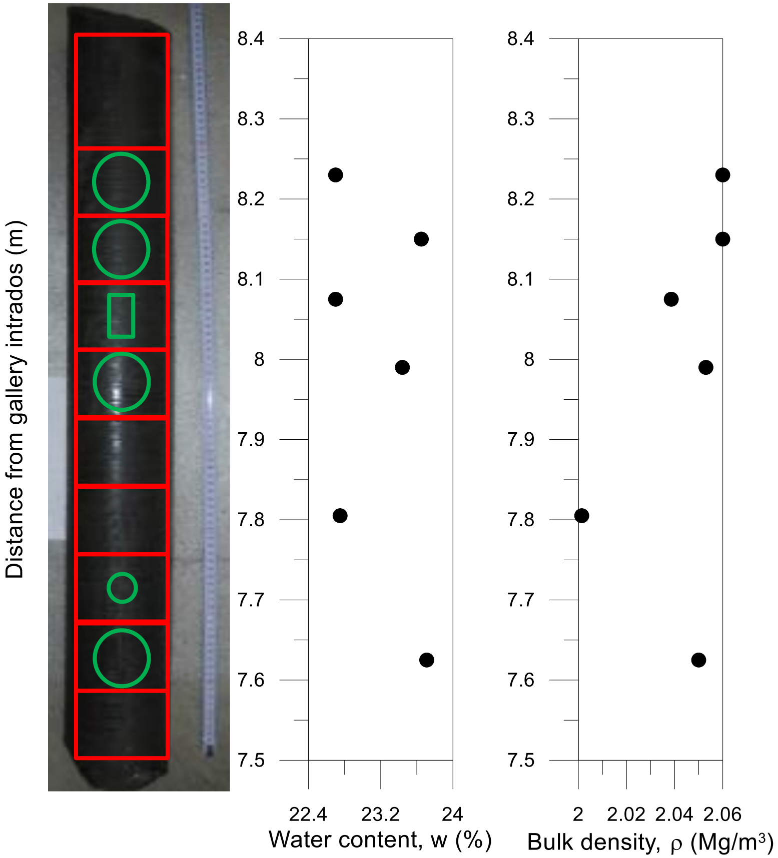

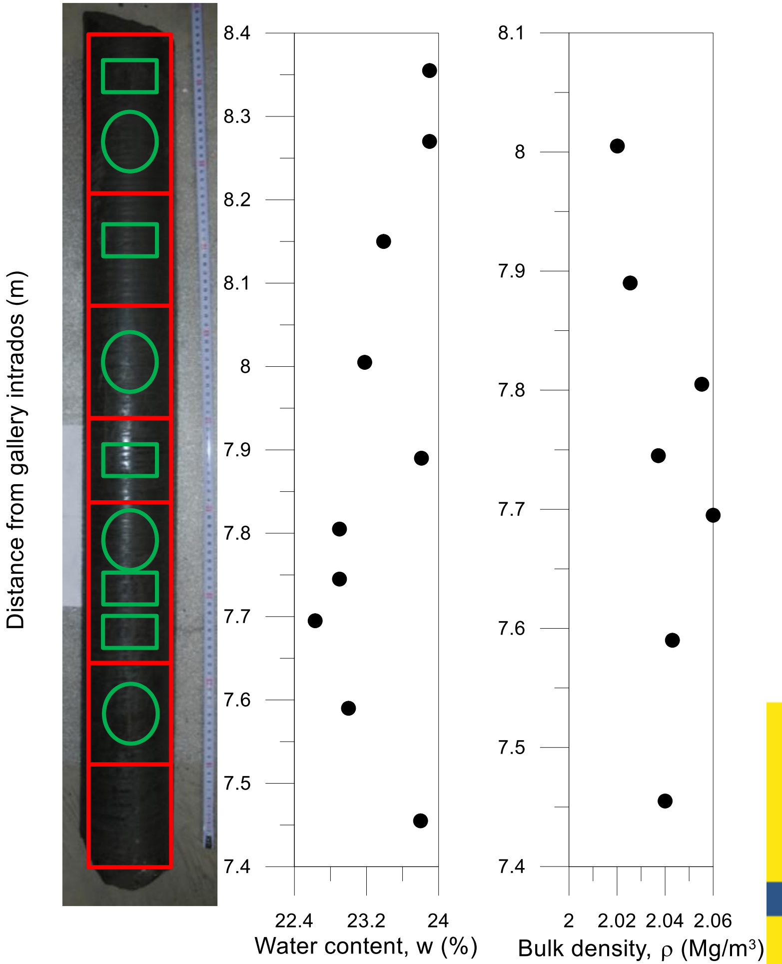

Gonzalez-Blanco (2017)

HOW TO PERFORM ADVECTIVE GAS INJECTION/DISSIPATION TESTS?

Importance of:

- Restoring in situ stress state (effective stress) (natural samples)

Occurrence of (matric) suction despite the nearly saturated state:

- Release of total stresses under water undrained conditions upon retrieval
- Some drying undergone during sampling, transportation, storage and preparation

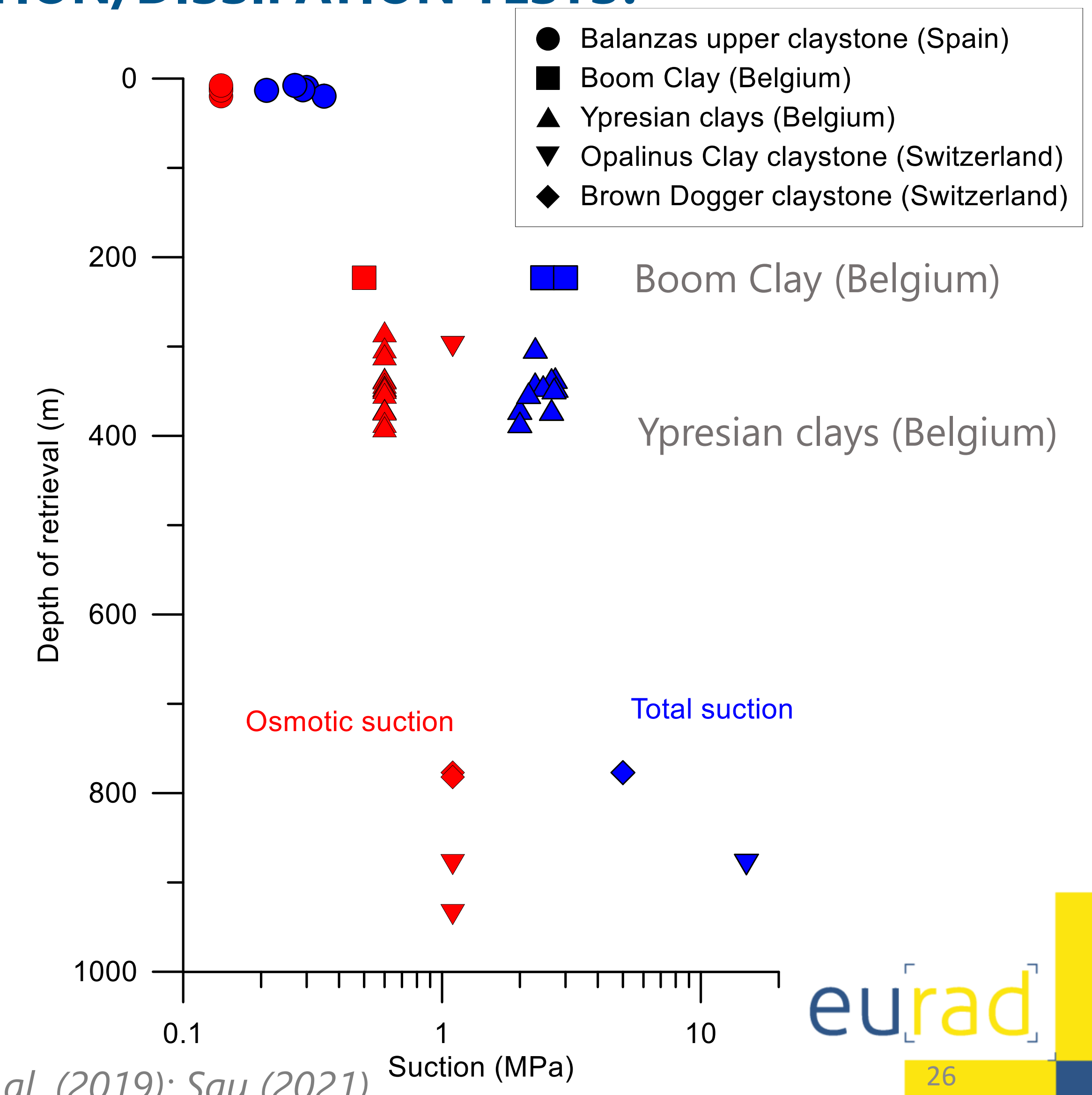

Sau et al. (2019); Sau (2021)

HOW TO PERFORM ADVECTIVE GAS INJECTION/DISSIPATION TESTS?

Importance of:

- Defining the stress paths to follow prior to gas injection (saturation path)

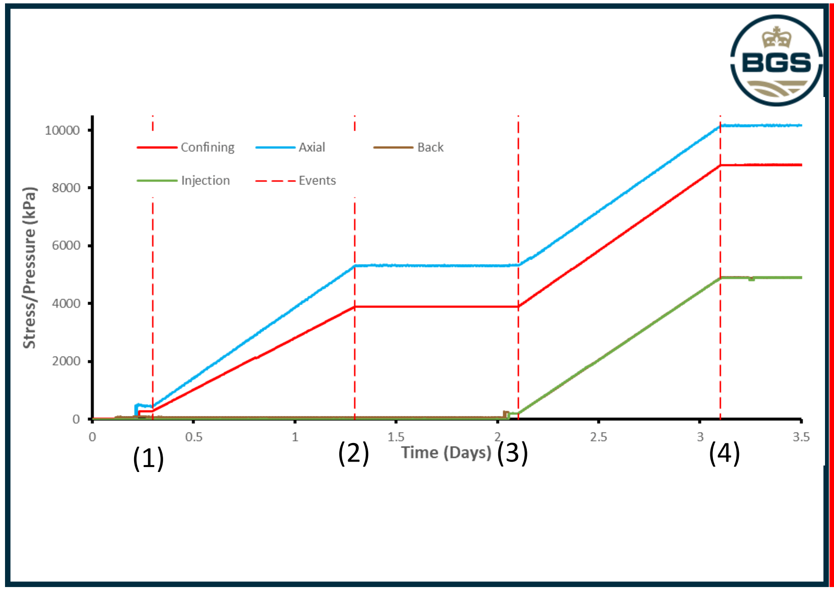

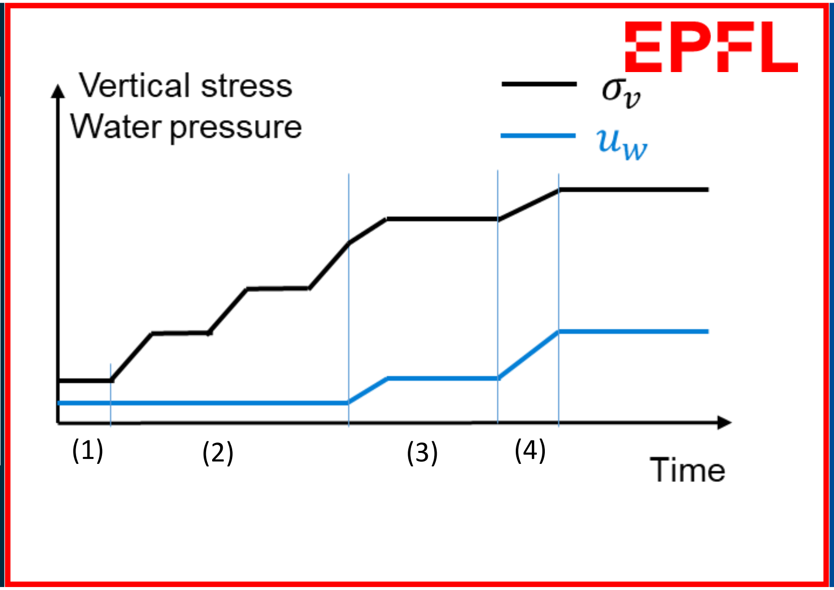

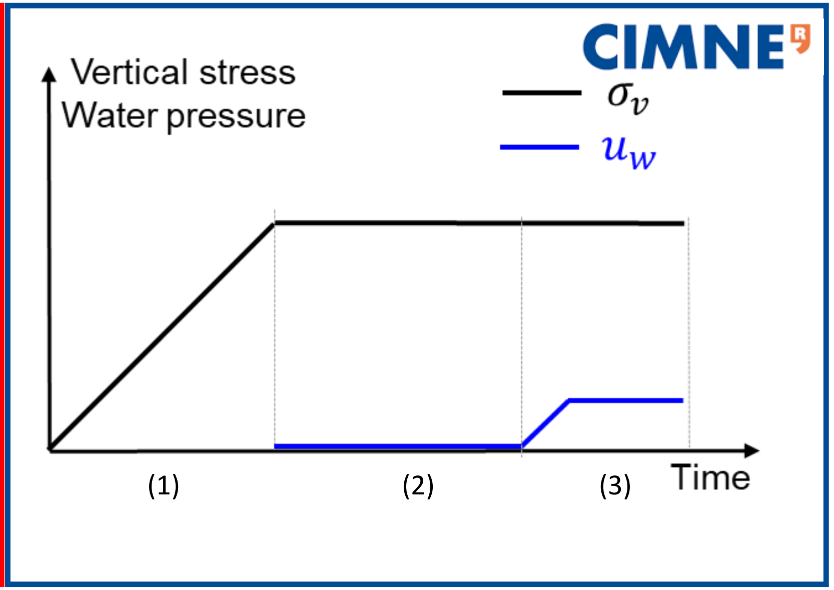

HOW TO PERFORM ADVECTIVE GAS INJECTION/DISSIPATION TESTS?

Importance of:

- Measuring volume changes in stress-controlled tests or stress state under isochoric conditions

Air injection tests under isotropic conditions on Brown Dogger shale formation (Switzerland)

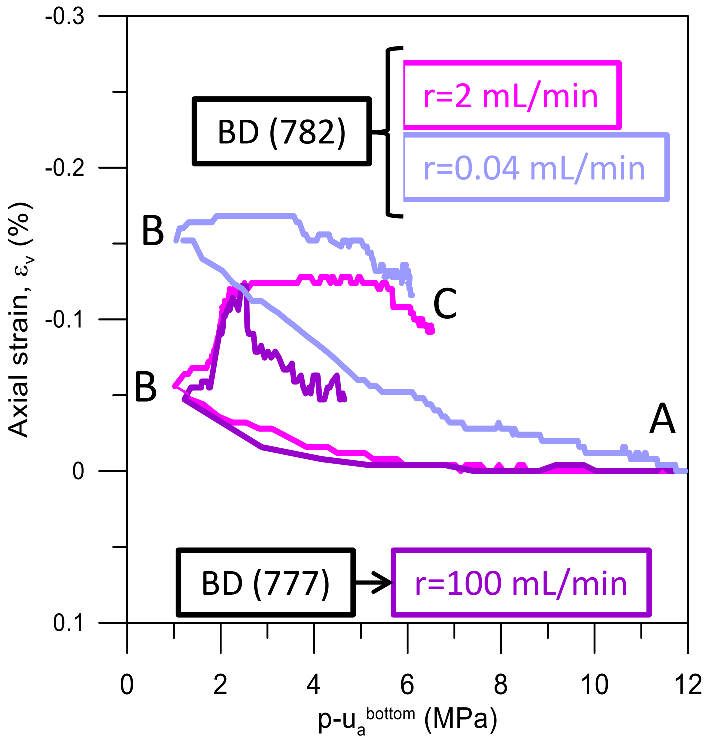

A→B: Gas injection at constant volume rate

B: Shut-off phase (constant injection volume)

B→C: Dissipation phase (constant injection volume)

Gonzalez-Blanco et al. (2022)

eurad

HOW TO PERFORM ADVECTIVE GAS INJECTION/DISSIPATION TESTS?

Importance of:

- Gas injection protocol: some decisions to make

➢ Gas type (air / N_2 / He …)

➢ Type of fluid at the boundaries (gas – gas) / (gas – liquid)

➢ Relative humidity of gas (dry gas / wet gas)

Air injection test on Opalinus Clay

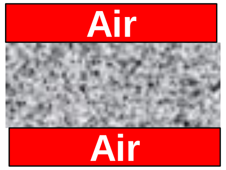

- Progressive desaturation of the sample
- Air injection pressure decays
- Breakthrough process does not occur

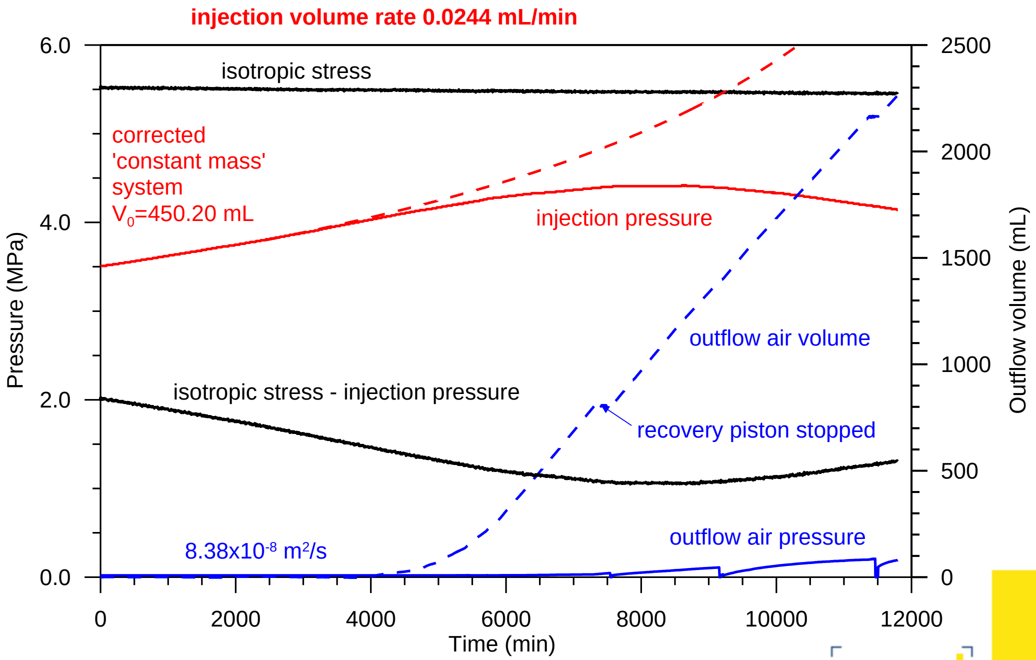

Romero et al (2010)

HOW TO PERFORM ADVECTIVE GAS INJECTION/DISSIPATION TESTS?

Importance of:

- Gas injection protocol:

➢ Flow direction with respect to bedding orientation (anisotropy features) 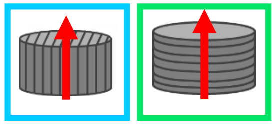

➢ Surface to apply gas injection (gas on entire sample surface, point injection)

➢ Gas injection method (pressure ramp / pressure steps / volumetric ramp / …)

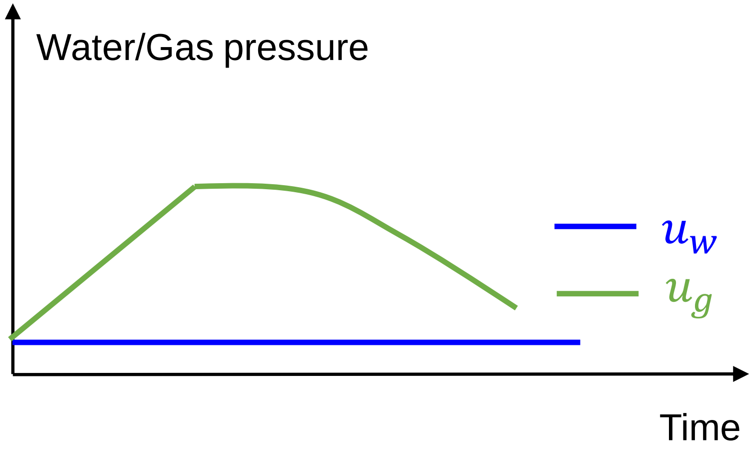

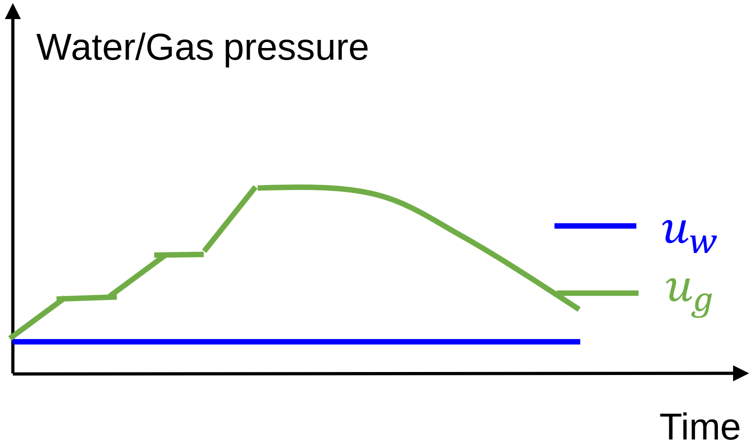

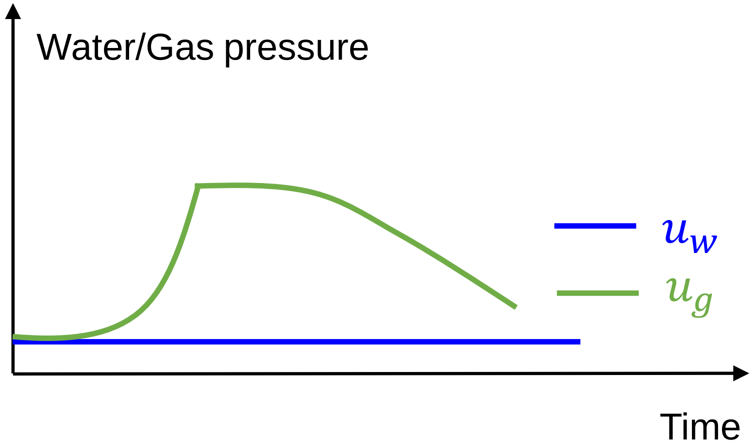

HOW TO PERFORM ADVECTIVE GAS INJECTION/DISSIPATION TESTS?

Importance of:

- Gas injection protocol:

➢ Gas injection rate (slow – fast) (dynamic effects on water retention curve)

➢ Information on system volumes (inflow/outflow volumes, dead volume up to valves, gaps)

Air injection test on Opalinus Clay

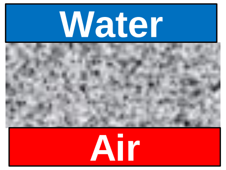

Air diffusion phenomena are important to consider when the injection rate is too slow

Injection volume rate: 0.1 mL/min

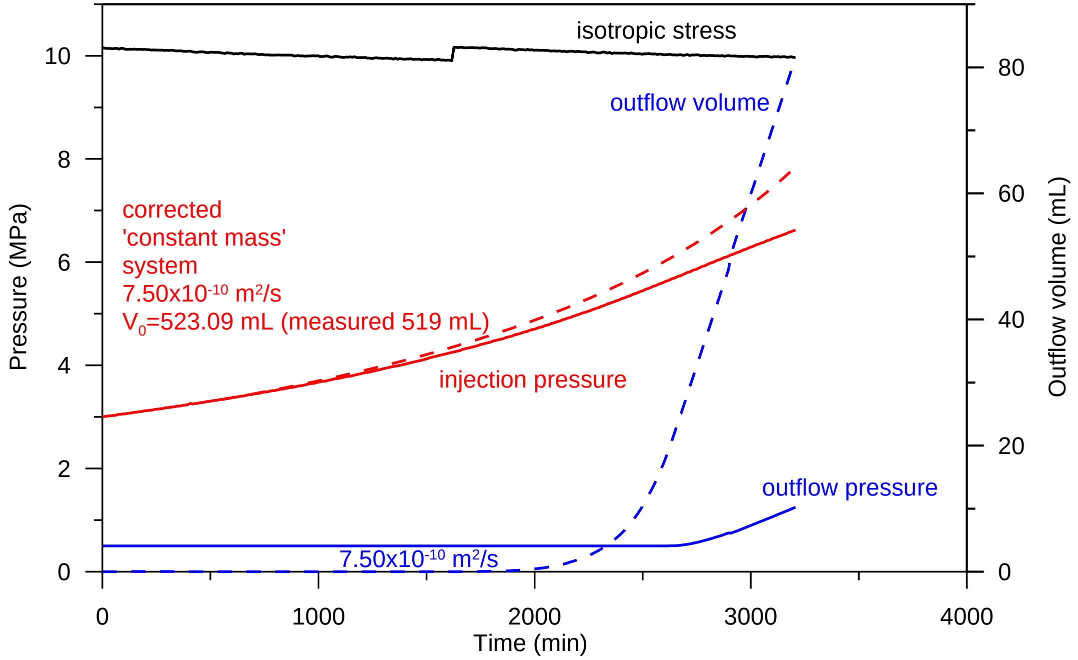

Romero et al. (2010)

eurad

HOW TO PERFORM ADVECTIVE GAS INJECTION/DISSIPATION TESTS?

Importance of:

- Gas injection protocol:

➢ Type of test ('soft breakthrough' with maximum pressure close to AEV / 'hard breakthrough' until gas outflow close to the minimum total stress)

$u_{g\ ini}$ → > AEV
$u_{g\ ini}$ → < AEV

➢ Stress state and gas pressure (maximum gas pressure)

$\sigma_1 - u_{g\ max}$ → < 1 MPa (flow through interface)
$\sigma_1 - u_{g\ max}$ → > 1 MPa (flow through sample)

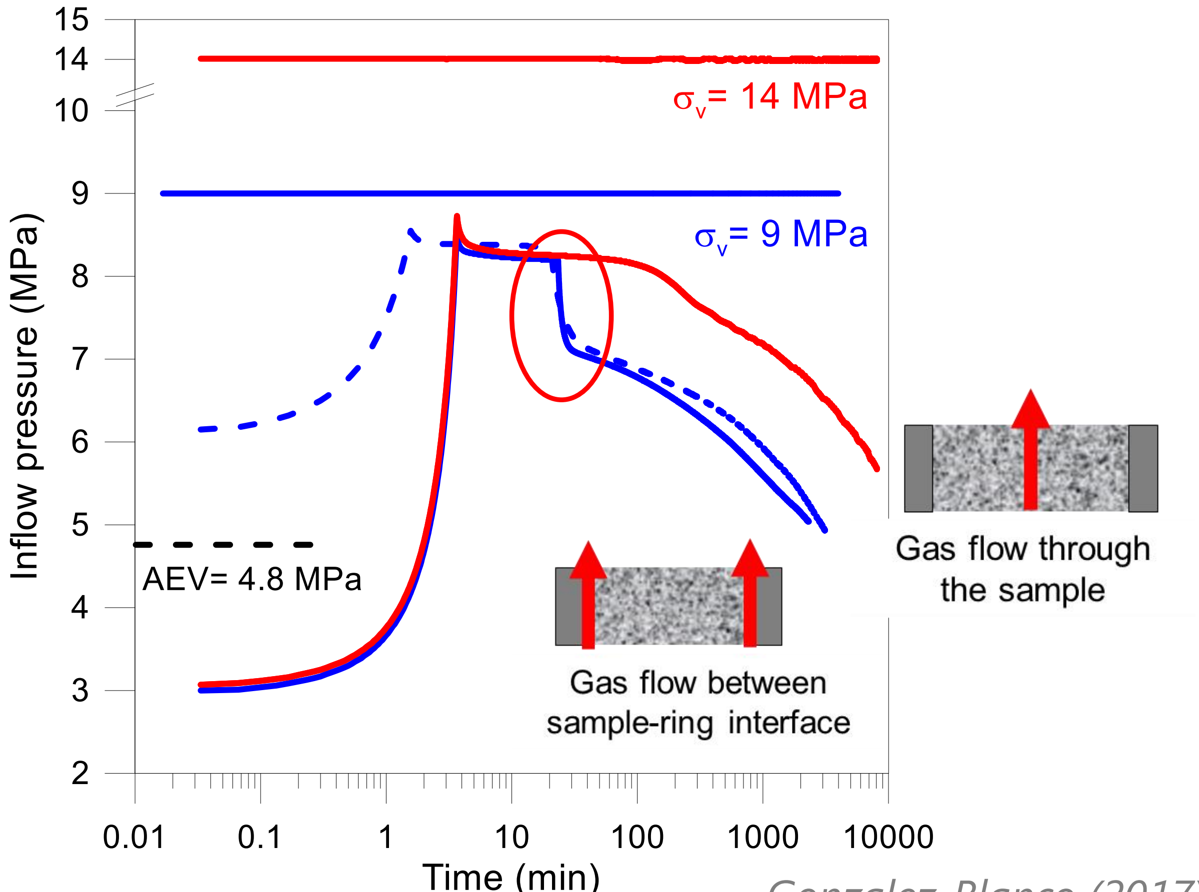

Gonzalez-Blanco (2017)

$\sigma_1 - u_{g\ max}$ > 1 MPa to avoid air passage between sample-ring interface

⇩

Development of oedometer cell with lateral stress measurement

eurad

OUTLINE OF THE LECTURE

1. Motivation
2. Insight into gas transfer and self-sealing
3. Some observations regarding gas testing (experimental protocols)
4. A detailed research methodology on Boom Clay:
   - Material characterization
   - Stress paths followed
   - Gas test protocols
   - Test results at different scales (macroscopic results and microstructural features)
5. Final comments. Future challenges

BOOM CLAY

Marine sediment of the Cenozoic (Rupelian age, 30 My)

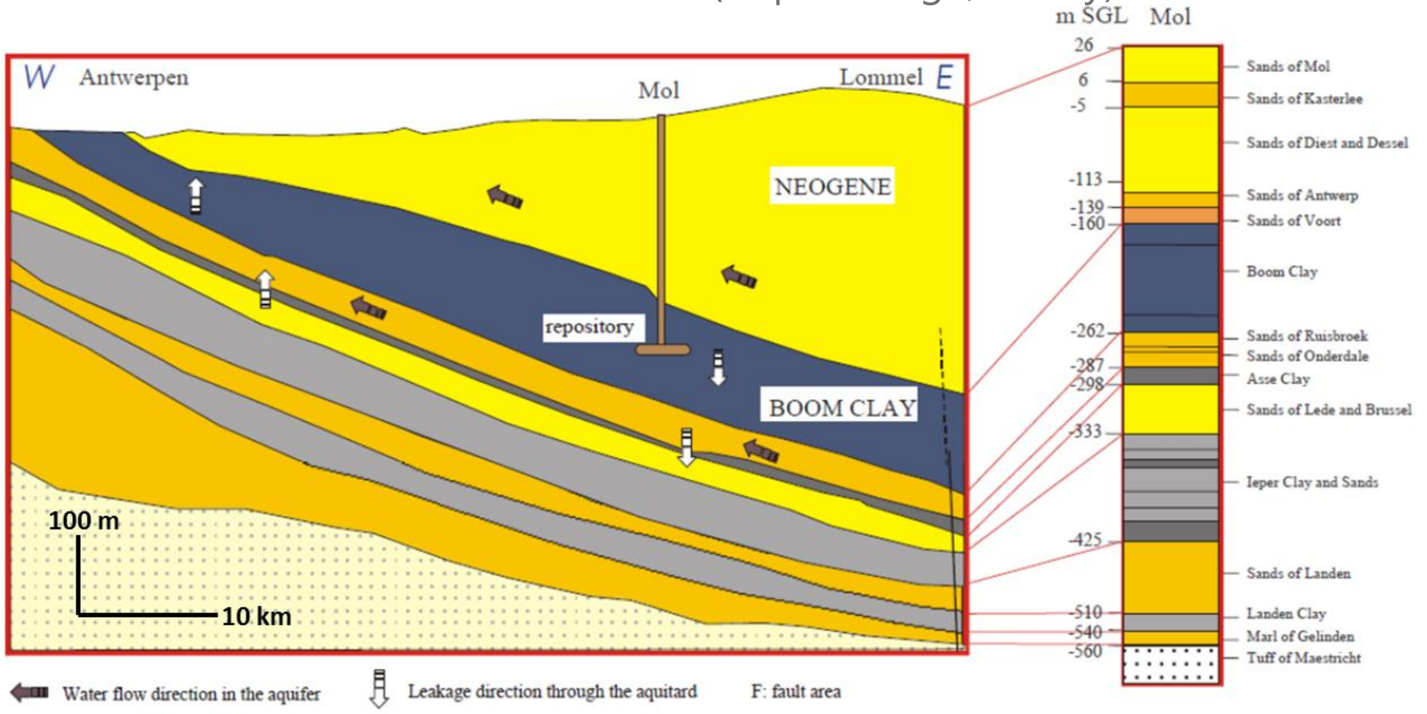

Sillen & Marivoet (2007)

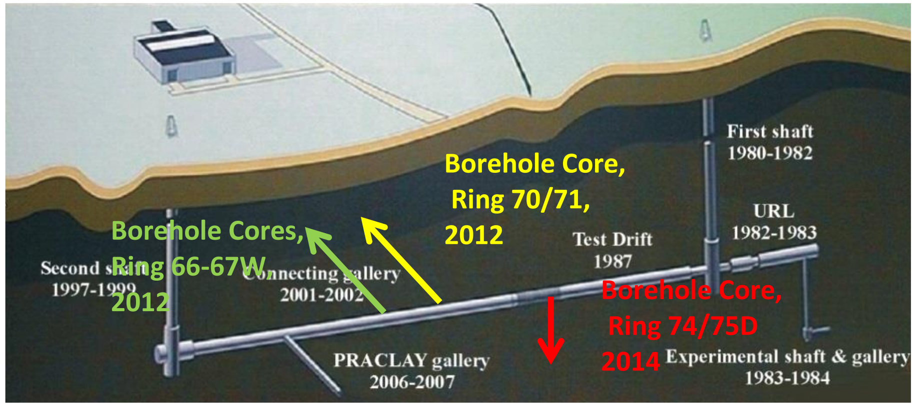

Samples retrieved at **HADES URL** level (223 m depth) in boreholes horizontally drilled

EXPERIMENTAL CHARACTERIZATION

Parameter	Value
Geotechnical properties	
Density of soils, ρ_s (Mg/m^3)	2.67
Liquid limit w_L (%)	67
Plasticity index, I_P (%)	38
Initial conditions	
Density, ρ (Mg/m^3)	2.02-2.06
Dry density, ρ_d (Mg/m^3)	1.63-1.69
Porosity, n	0.37-0.39
Void ratio, e	0.58-0.63
Water content, w (%)	22.6-24.0
Degree of saturation	close to 1
Total suction after retrieval, Ψ (MPa)	2.45
Air-entry value from MIP (MPa)	4.8
Dominant pore mode from MIP(nm)	70

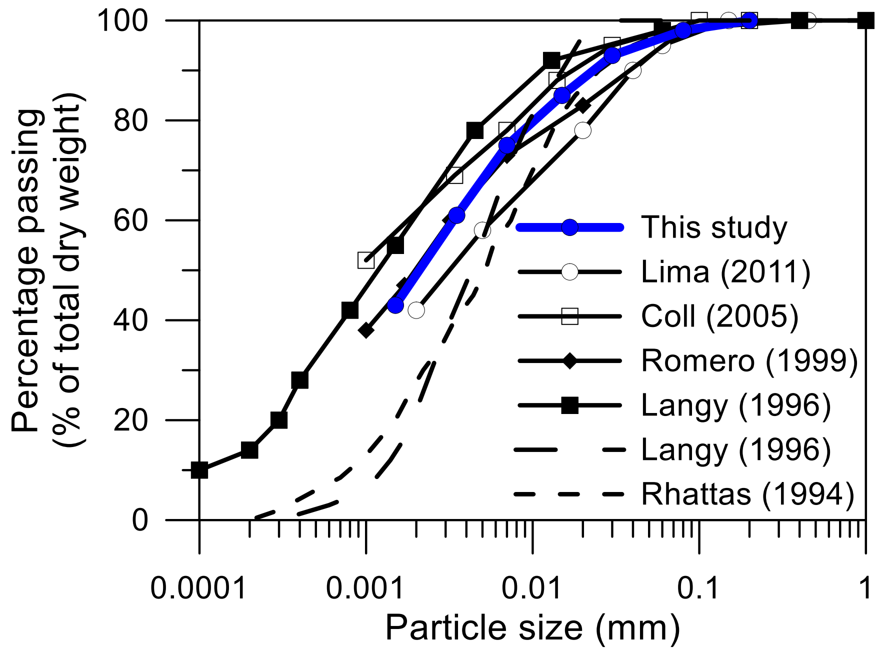

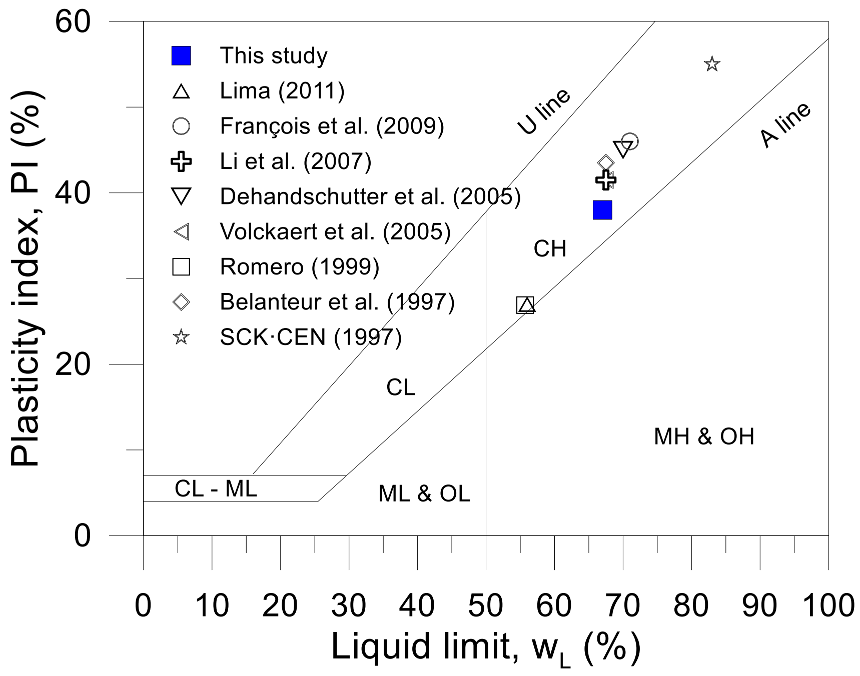

EXPERIMENTAL CHARACTERIZATION

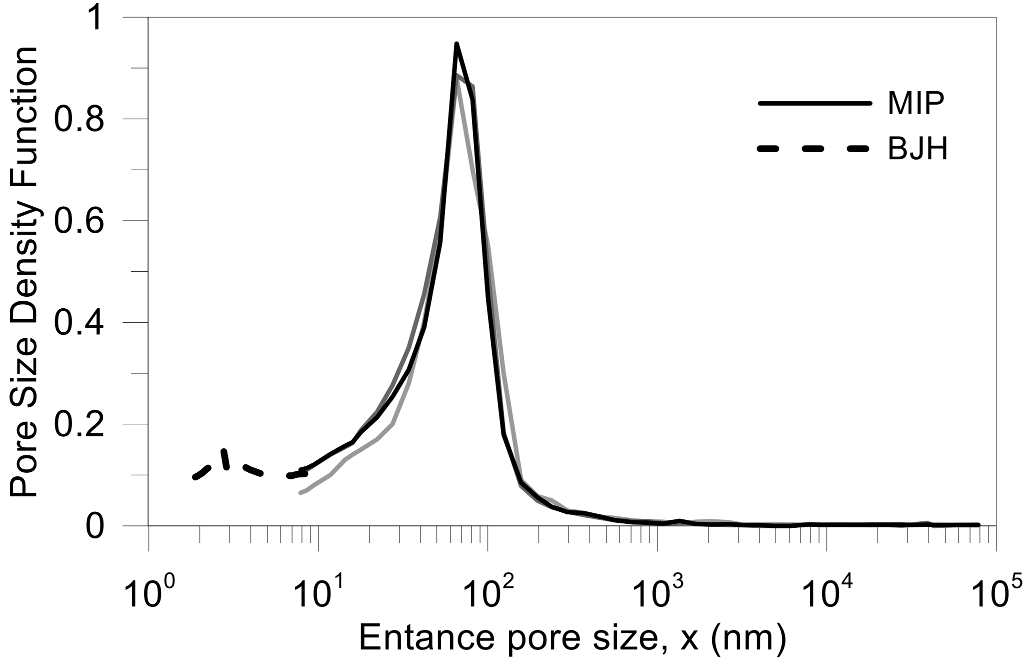

Mono-modal pore size distribution from MIP:

- dominant pore mode around 70 nm
- AEV ~ 4.8 MPa

Drying path of the water retention curve:

- initial total suction after retrieval 2.45 MPa
- AEV ~ 4.5 MPa

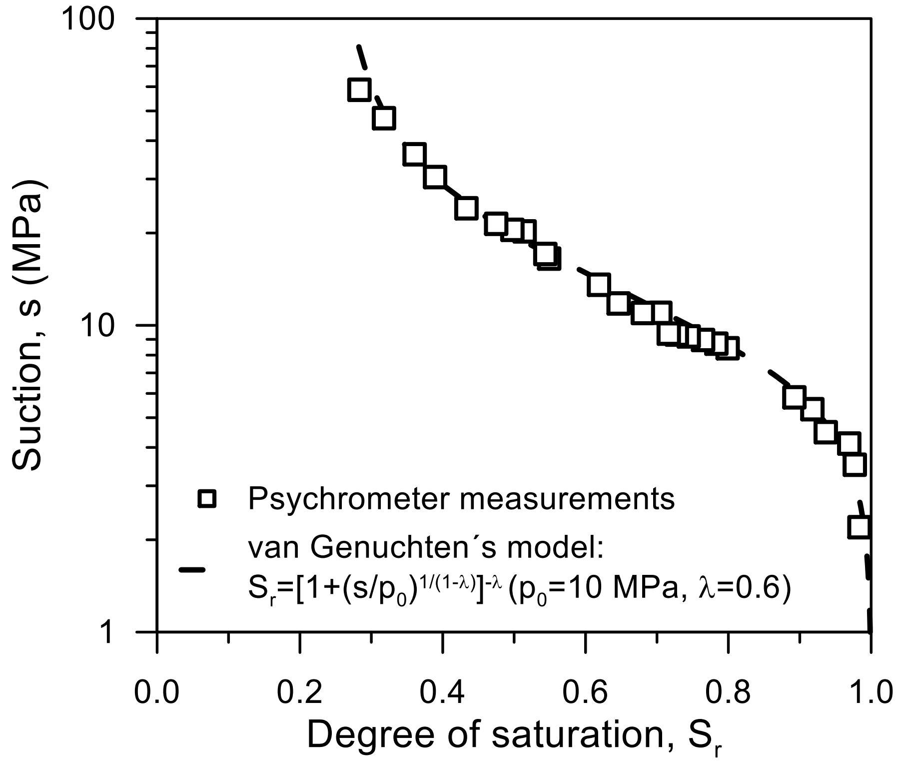

eurad

EXPERIMENTAL SET-UPS

Old oedometer cell

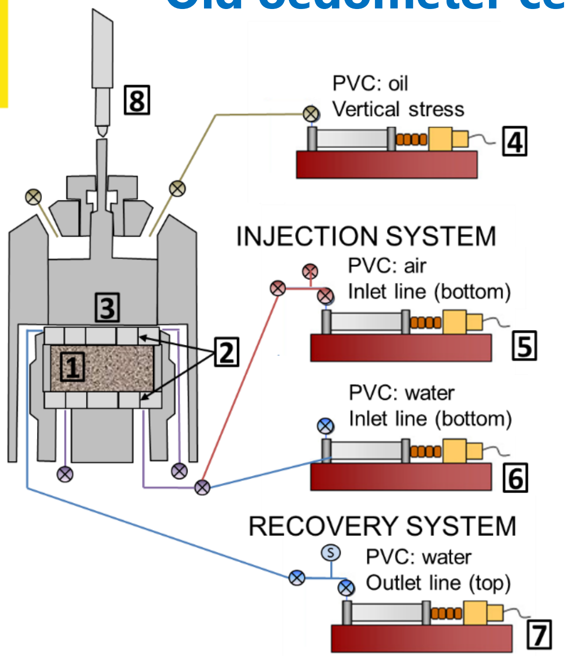

Sample size
- 20 mm in height
- 50 mm in diameter

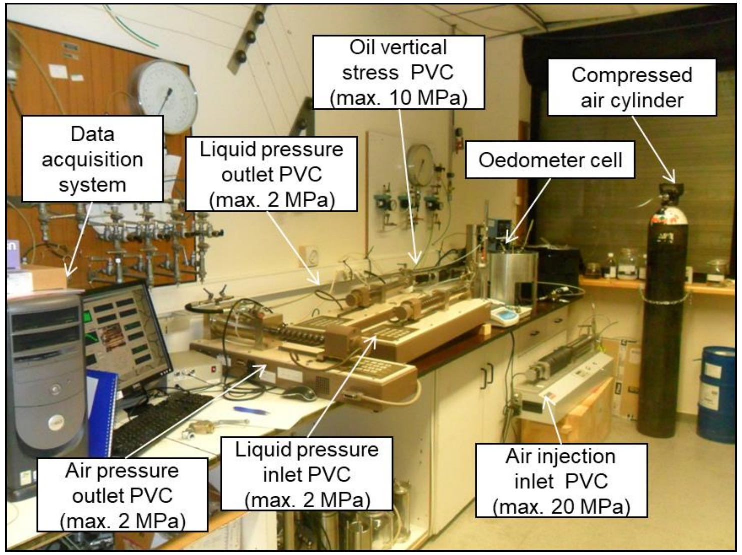

New oedometer cell with lateral stress measurement

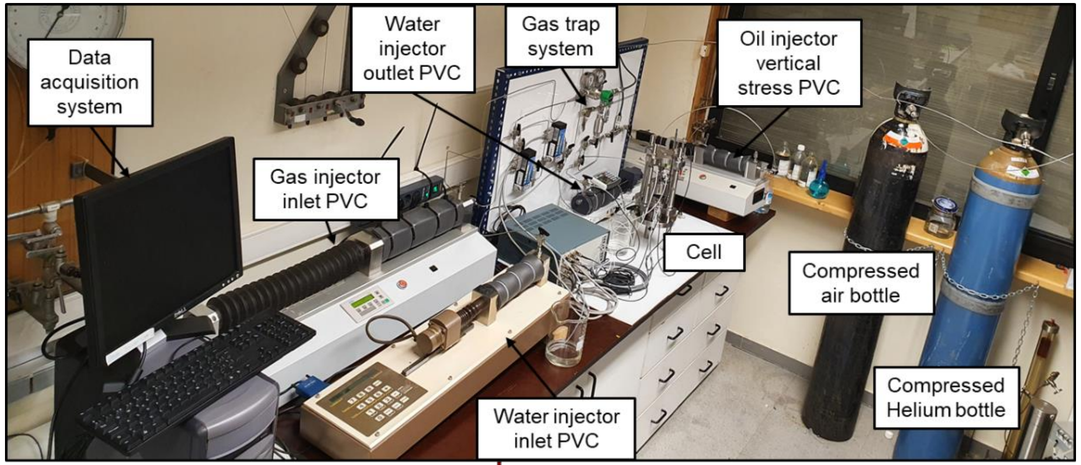

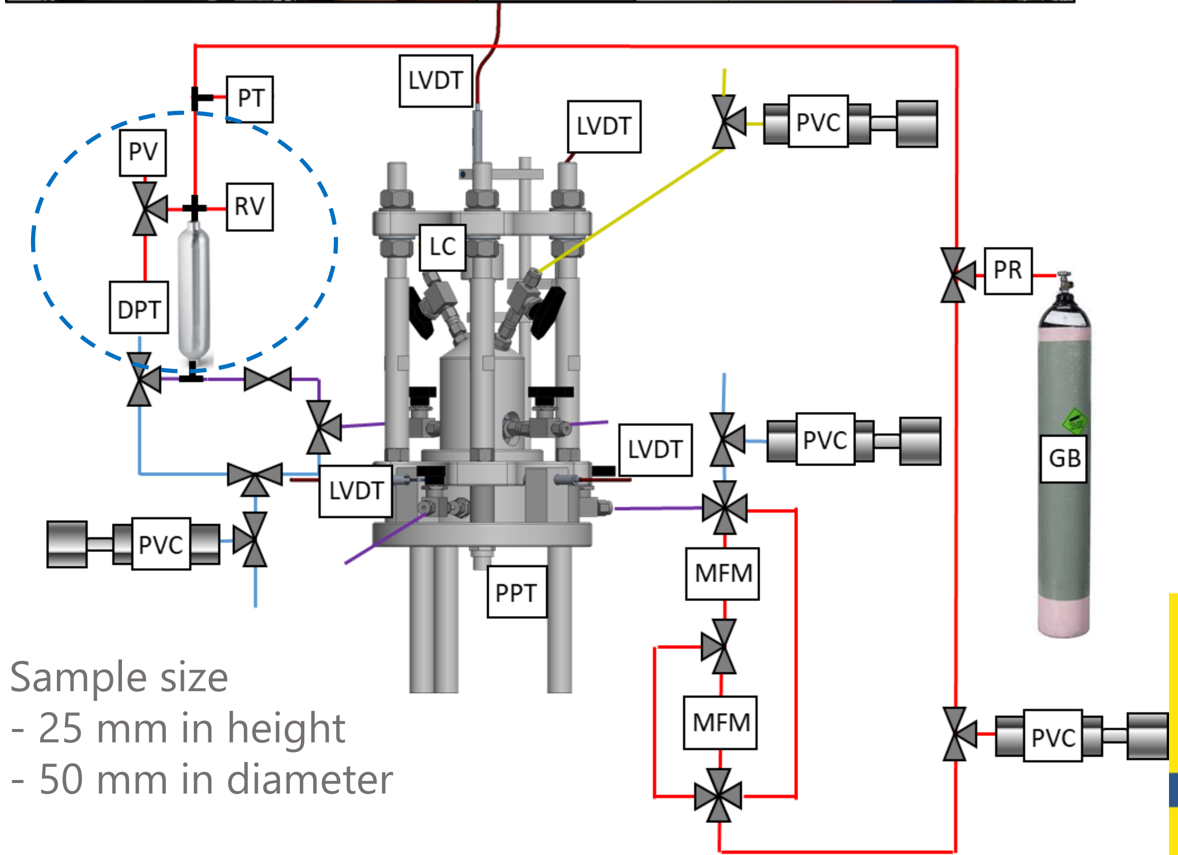

Sample size
- 25 mm in height
- 50 mm in diameter

EXPERIMENTAL SET-UPS

New oedometer cell with lateral stress measurement

Deformable Ring to indirectly measure the lateral stress

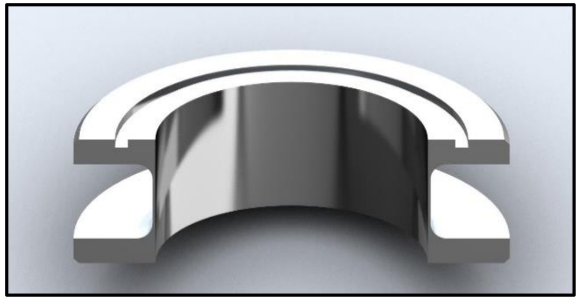

Lateral displacement measurement with **2 LVDTs**

- Measure range: $\pm$ 1 mm
- Accuracy: 0.3% FS
- Resolution: 0.15 µm

Maximum lateral displacement 35 µm ⟹ LVDT measures 233 steps

0.14% (some small loss of K_0 condition) between 0.02% and 0.15% for semi-rigid systems

Resolution in terms of **lateral stress** = Full Scale (≈ 4000 kPa) / steps ≈ **20 kPa**

eurad

TEST PROTOCOL

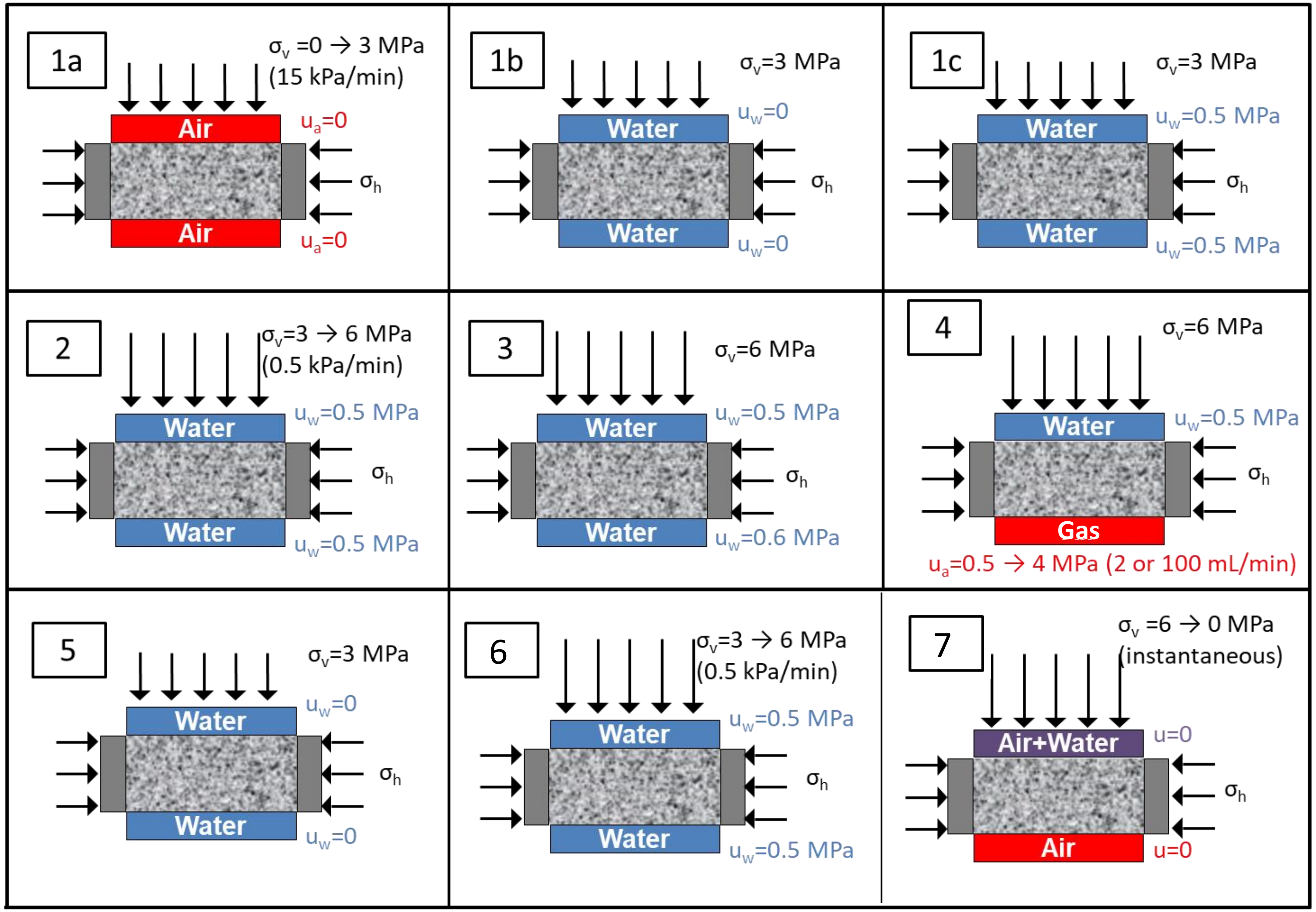

1. Pre-conditioning path
   1a. Undrained loading
   1b. Contact with water
   1c. Water pressurization
2. Drained loading
3. Water permeability
4. Gas injection/dissipation
5. Re-saturation for self-sealing
6. Water permeability
7. Undrained unloading

Additional tests:

- to study the K_0 evolution
- to analyse the post-yield behaviour
- to determine the water permeability variation with porosity
- to see the effect of a second gas injection

PRE-CONDITIONING STAGE

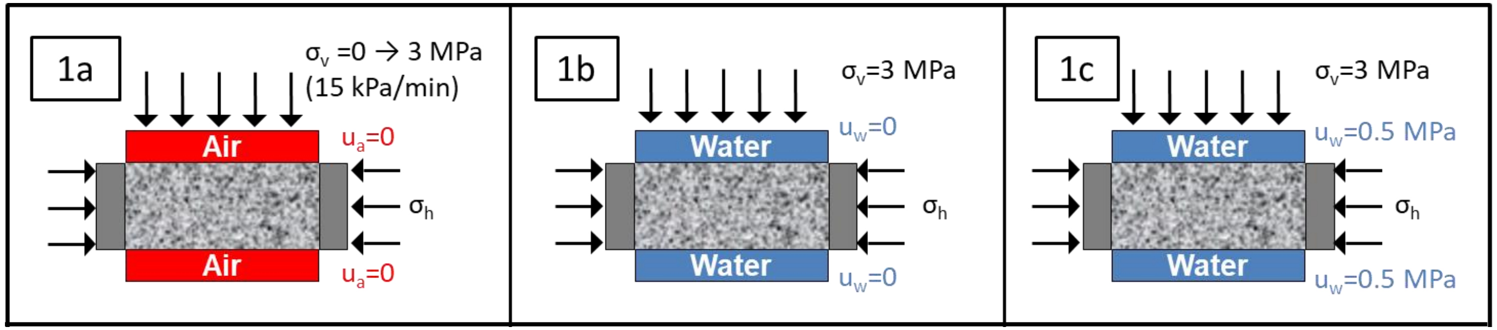

Objectives:

- to apply similar stress state than *in situ*
- to reduce initial suction
- to avoid expansion and degradation of the sample induced by suction reduction at low stress levels

At 223 m depth
(*in situ* conditions)

$$\sigma_{1v} = 4.50\ MPa$$
$$u_{wi} = 2.25\ MPa$$
$$\sigma'_{1i} = 2.25\ MPa$$
$$\sigma_1'^{max} = 5.2\ MPa$$

After retrieval
(undrained unloading)

$$\Delta\sigma_1; \Delta\sigma_3 \rightarrow \Delta u_w = B\left[\Delta\sigma_3 + \frac{1}{3}A(\Delta\sigma_1 - \Delta\sigma_3)\right]$$
$$B = 1;\ A = 1/3$$
$$\Delta u_w = \frac{\Delta\sigma_1 + 2\Delta\sigma_3}{3} = \Delta p = -4.5\ MPa$$
$$u_{wf} = u_{wi} + \Delta u_w = -2.25\ MPa$$

Post-storage

$$\Psi = 2.45\ MPa$$
$$S_r \backsim close\ to\ 1$$

High initial suction
due to stress relief

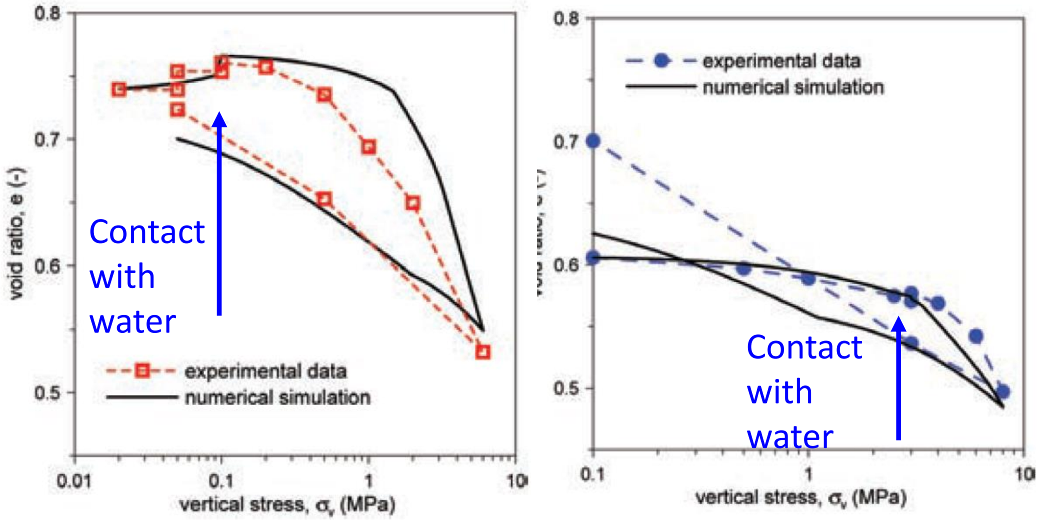

Large deformation when soaking at 0.02 MPa

Soaking at 3 MPa

Della Vecchia et al (2011)

PRE-CONDITIONING STAGE: AXIAL STRESS-STRAIN

Some deformation occurred:

→ Deformation due to suction changes and stress changes

Slightly higher compressibility on loading of sample with bedding planes orientated normal to the axis (**anisotropy in the elastic domain**)

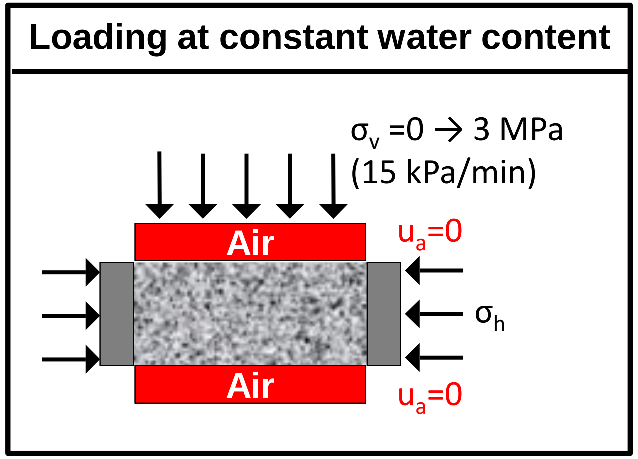

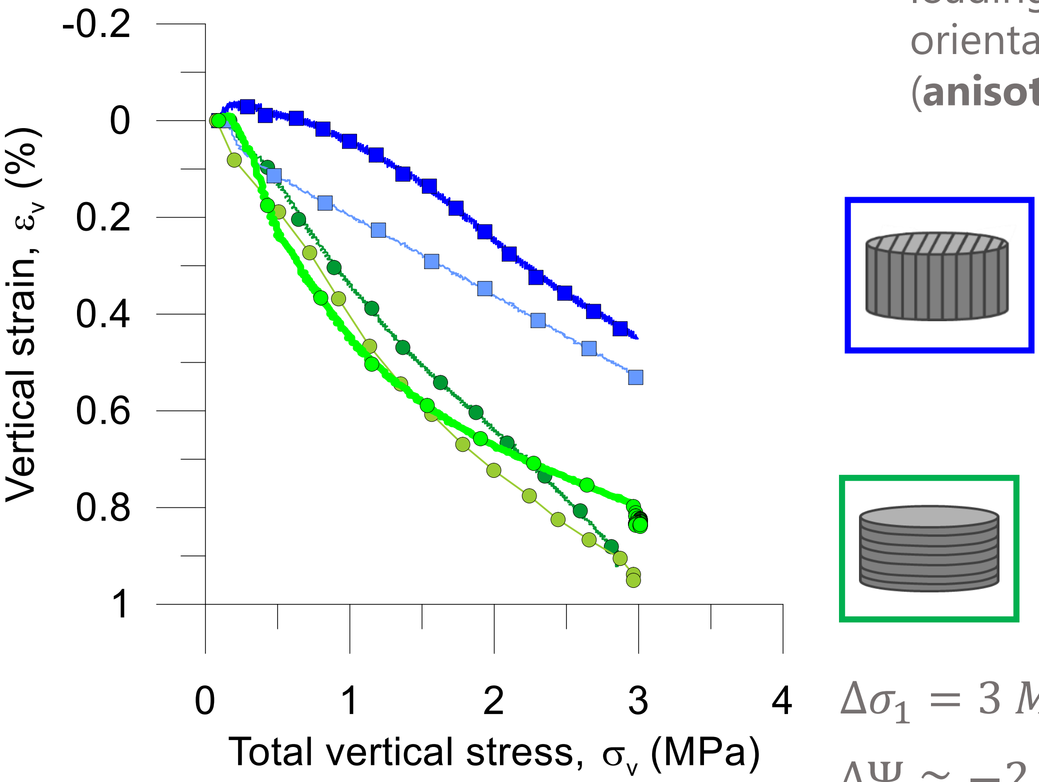

$$\Delta\sigma_1 = 3\ MPa$$

$$\Delta\Psi \simeq -2.3\ MPa$$

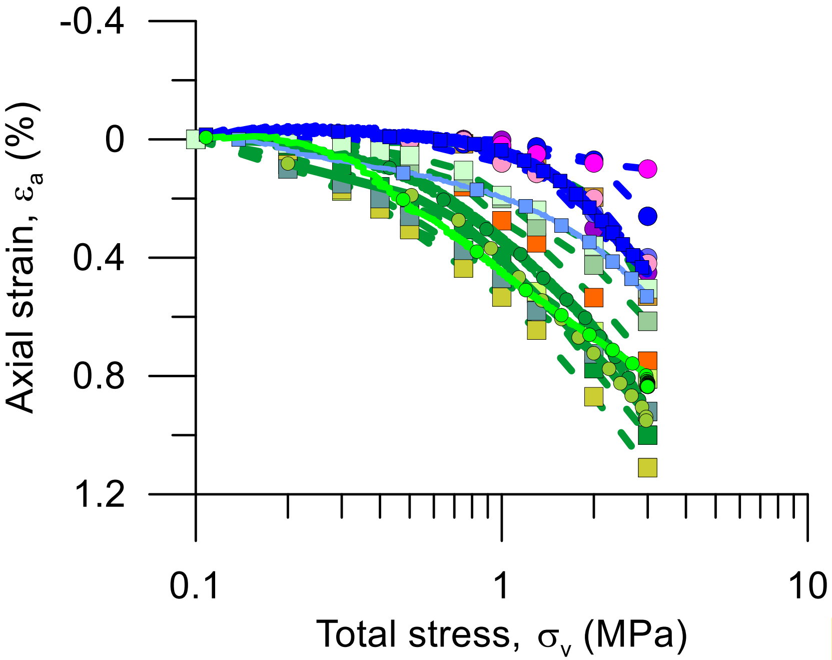

*Values of initial compressibility have been corrected after the new calibration of the cell compressibility

PRE-CONDITIONING STAGE: HORIZONTAL STRESS

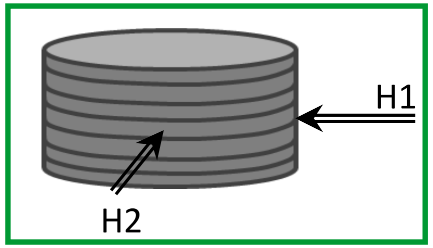

H1 ≈ H2

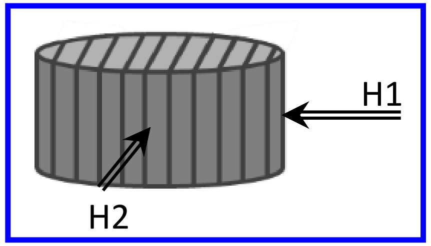

H1 > H2

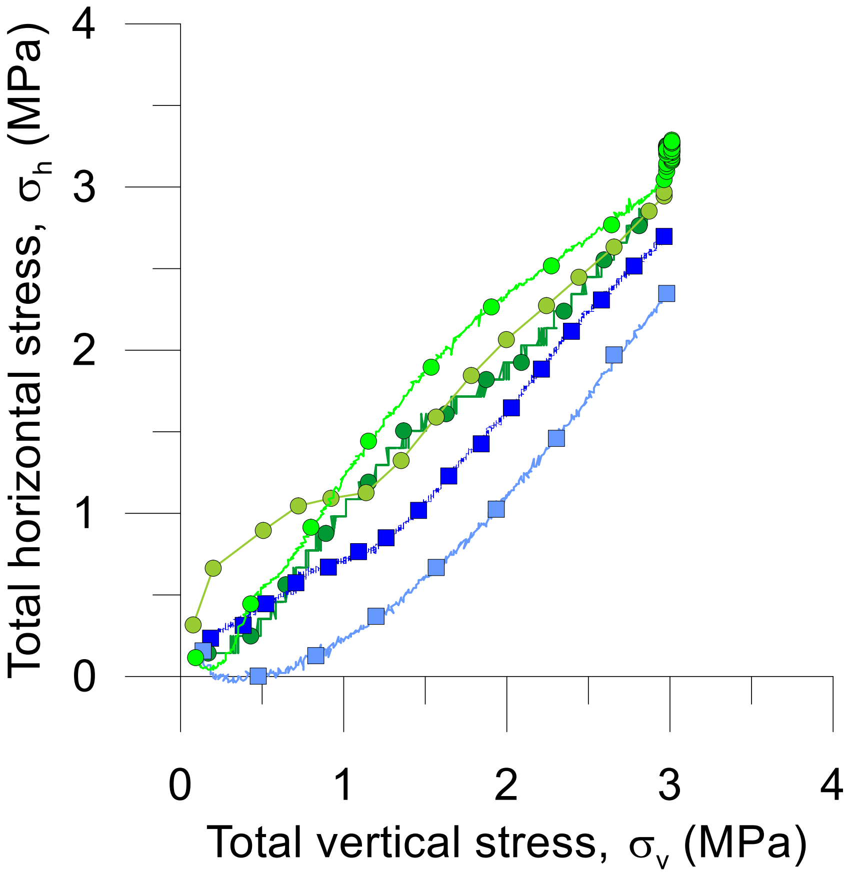

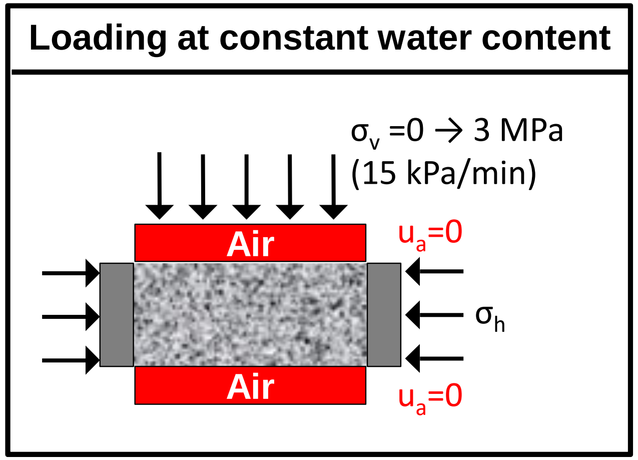

Initial total horizontal stress calibrated:
$\sigma_{h0} \approx 150\ kPa$

*Total horizontal stress computed as the average stress measured at both sensors

PRE-CONDITIONING STAGE: SWELLING STRAIN

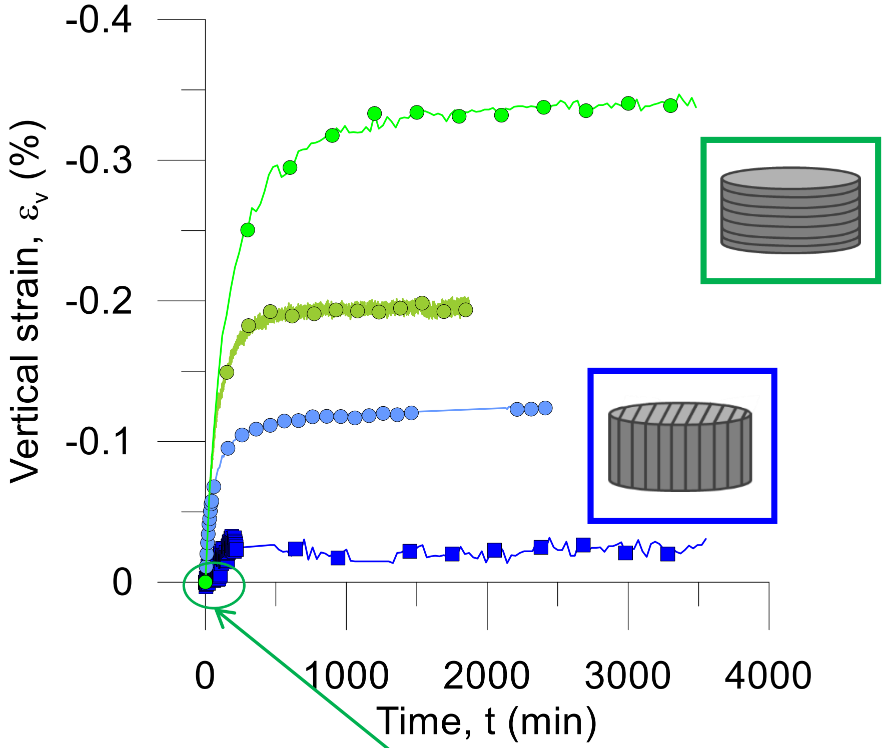

At $\sigma_v = 3\ MPa$
$s = 0.15\ MPa$ measured
$s = 0.20\ MPa$ computed

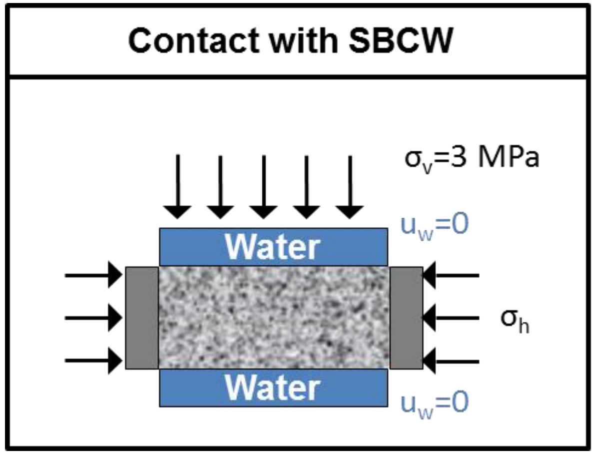

Swelling strains recorded during soaking due to some remaining suction

Samples with bedding planes normal to flow underwent higher swelling (anisotropy in the elastic domain)

PRE-CONDITIONING STAGE: HORIZONTAL STRESS

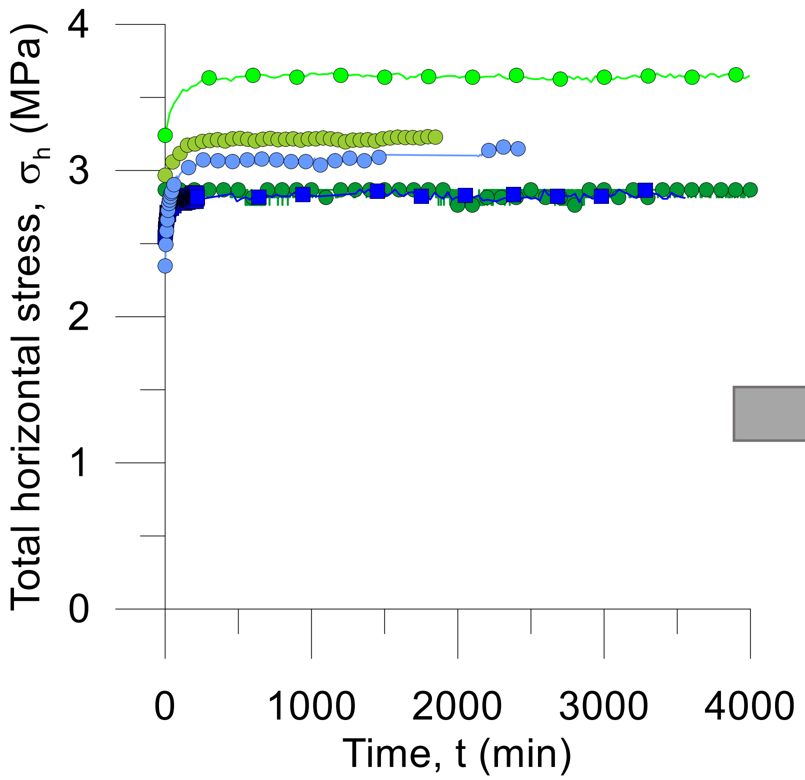

Values after restoring the in situ conditions*

$K_0 = 1.20$ $\sigma_h = 3.64$

$K_0 = 0.99$ $\sigma_h = 2.97$

$K_0 = 1.08$ $\sigma_h = 3.24$

$K_0 = 0.95$ $\sigma_h = 2.85$

$K_0 = 1.03$ $\sigma_h = 3.09$

*Slightly affected by the initial horizontal stress and very sensitive to the sensor location with respect to bedding planes

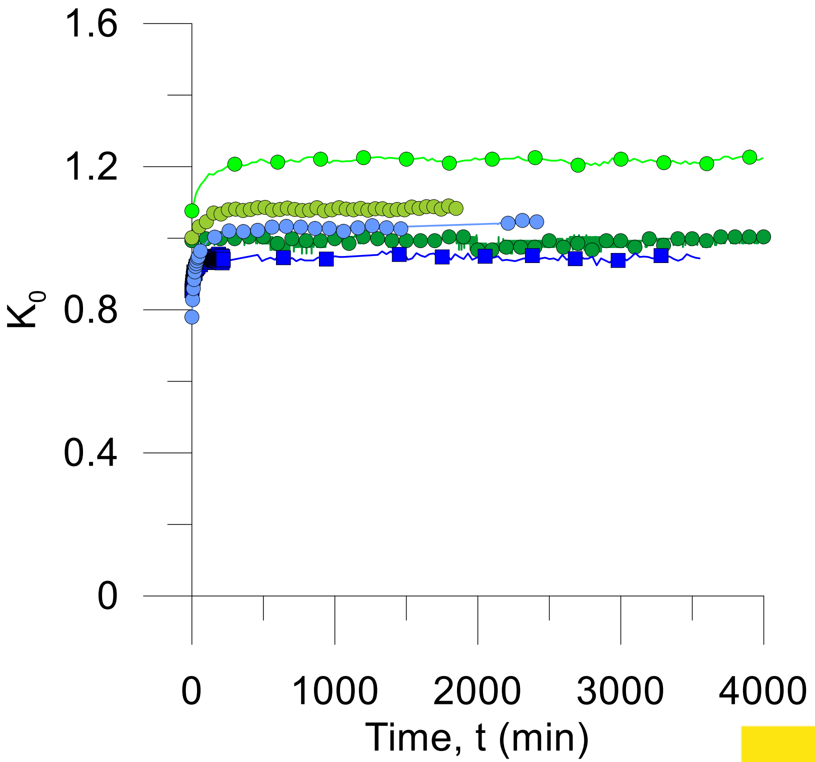

eurad

DRAINED LOADING

- Small anisotropy in elastic domain

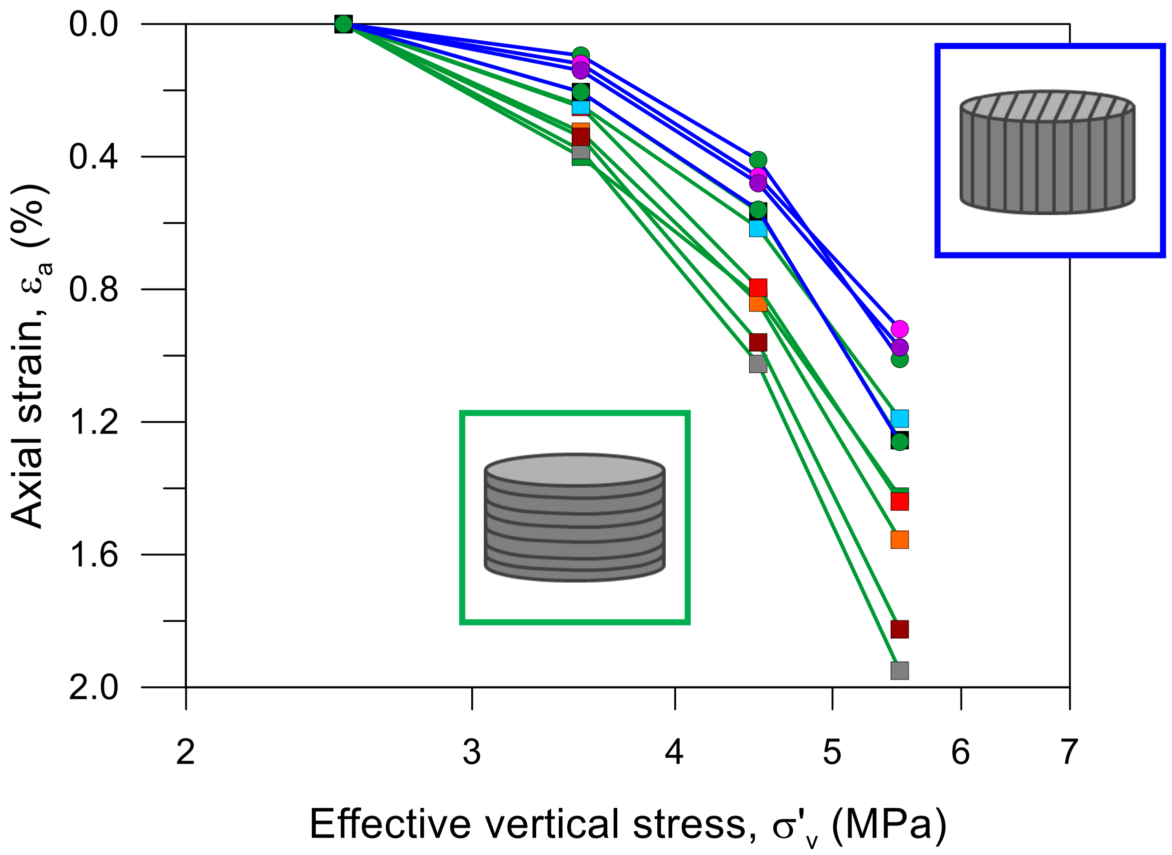

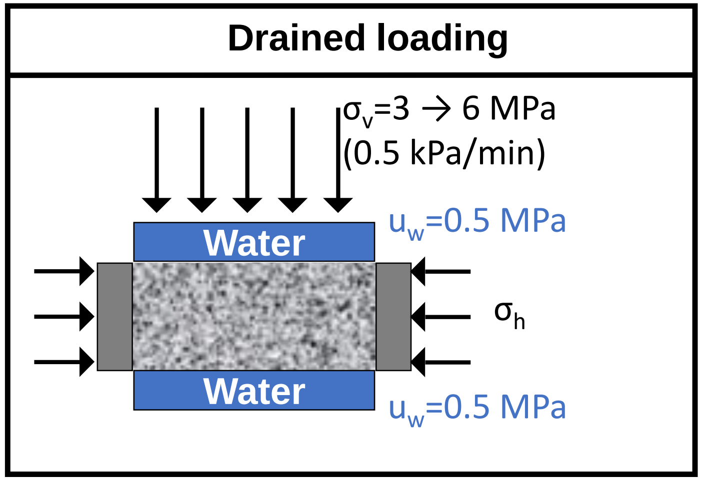

ADDITIONAL HYDRO-MECHANICAL PATHS TO STUDY K_0

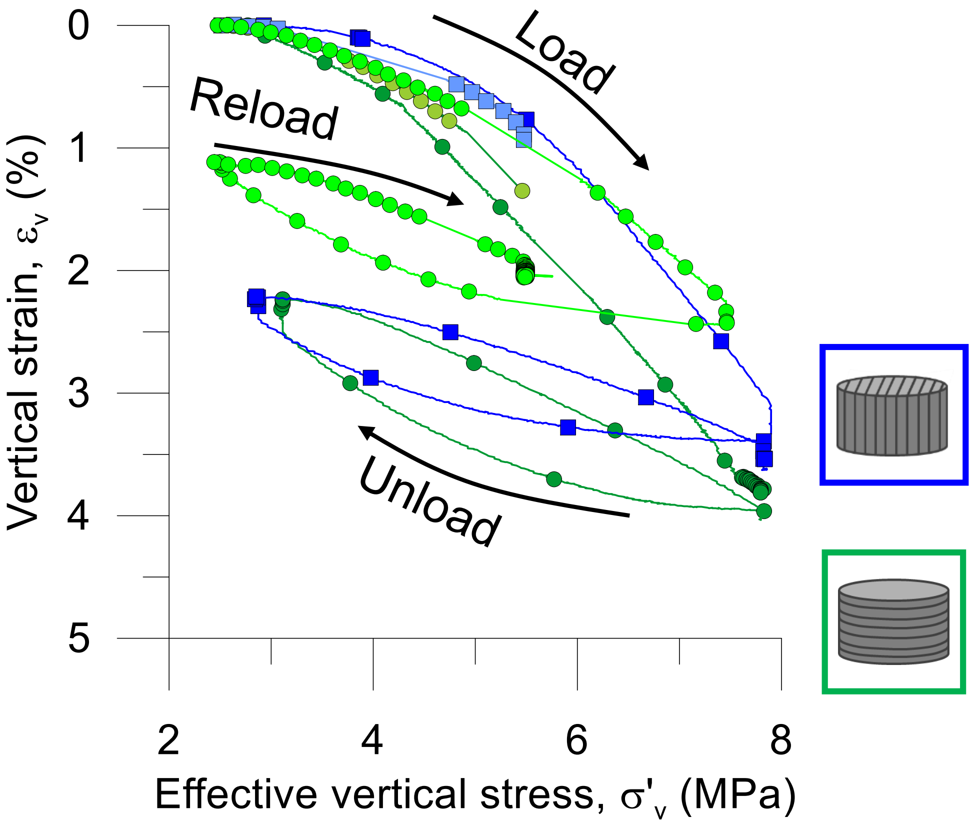

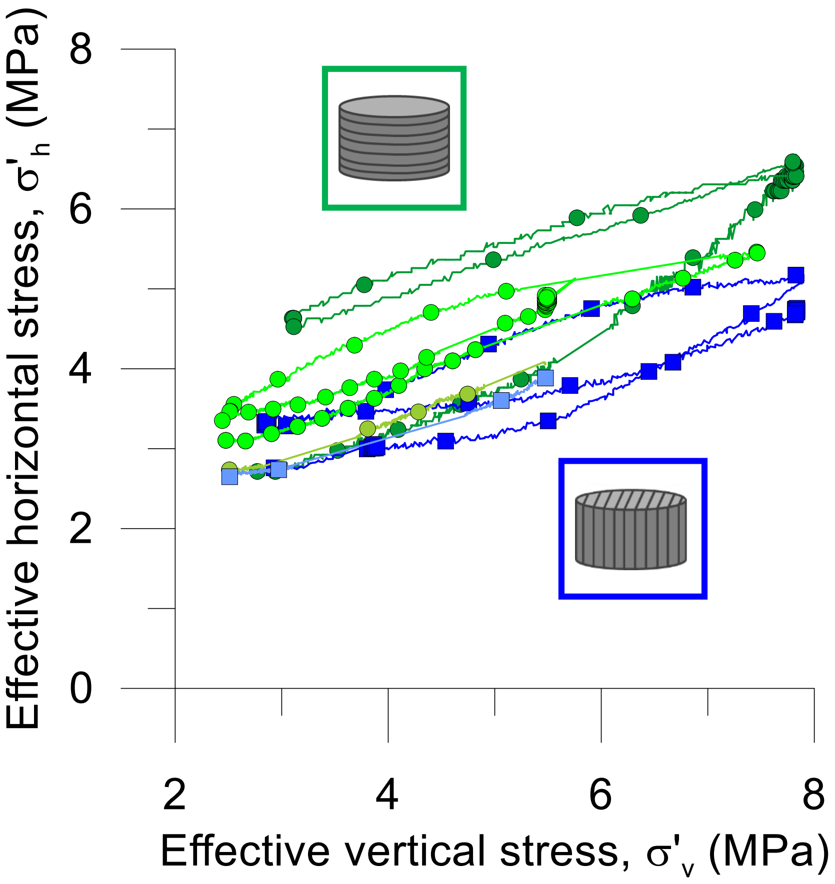

ADDITIONAL HYDRO-MECHANICAL PATHS TO STUDY K_0

Drained unload stage

$$K_0^{OC} = K_0^{NC} \cdot OCR^n$$

$n = \sin(\phi') = 0.326$ with $\phi' = 19°$

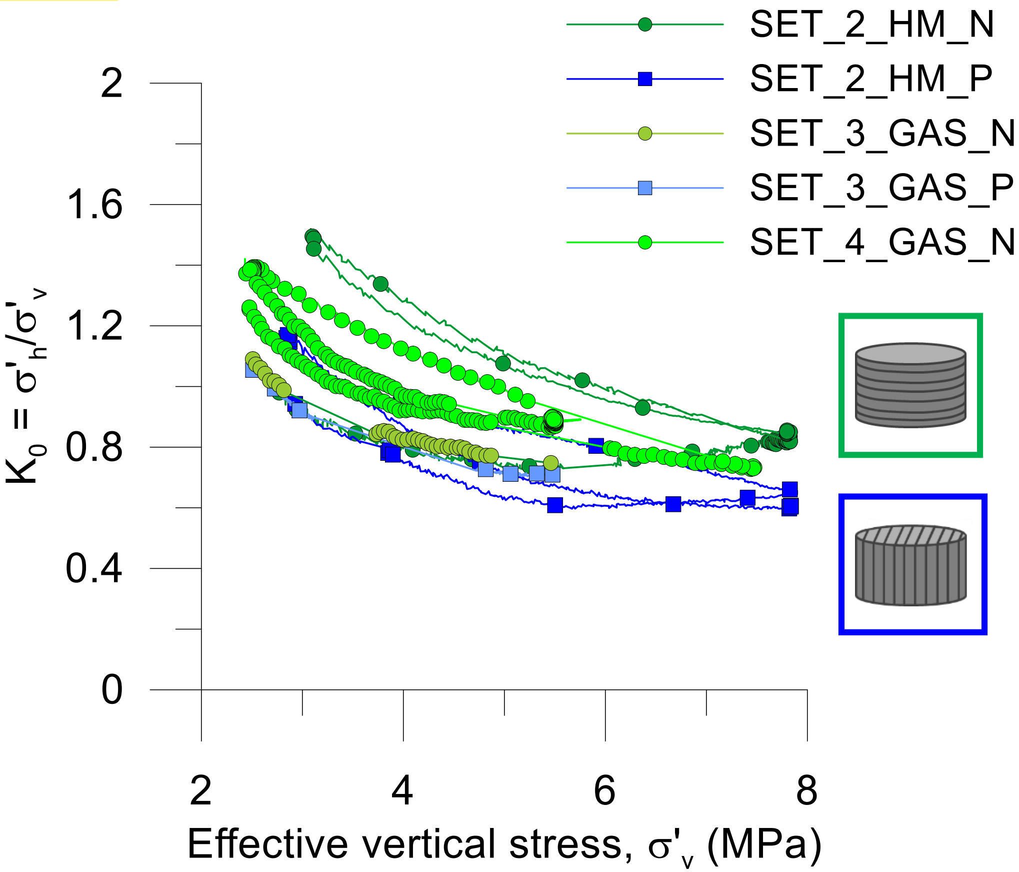

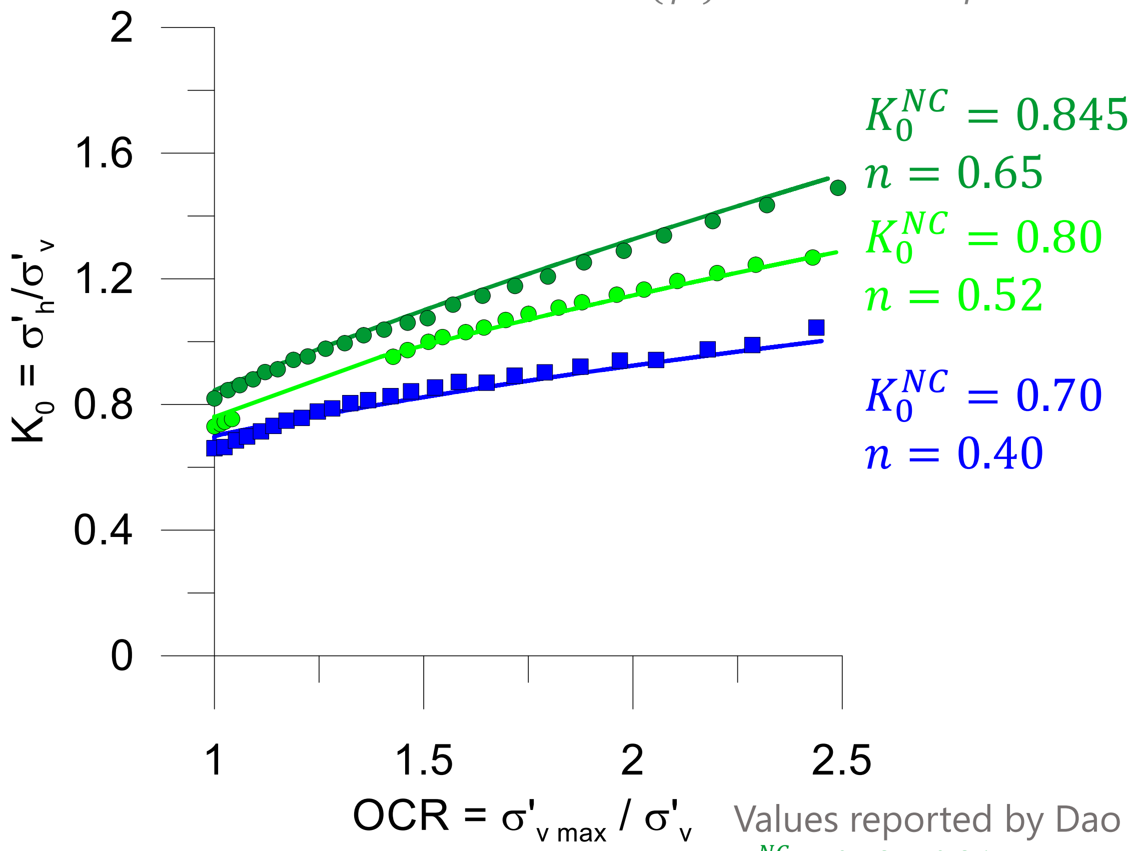

Values reported by Dao (2015)
$K_0^{NC} = 0.78 - 0.86$
$K_0^{NC} = 0.65 - 0.7$

OCR is computed in terms of the vertical effective stress, but it can be also expressed in terms of mean effective stresses

eurad

ADDITIONAL HYDRO-MECHANICAL PATH

❖ **SET2_HM_N**

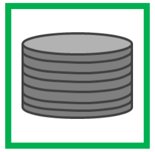

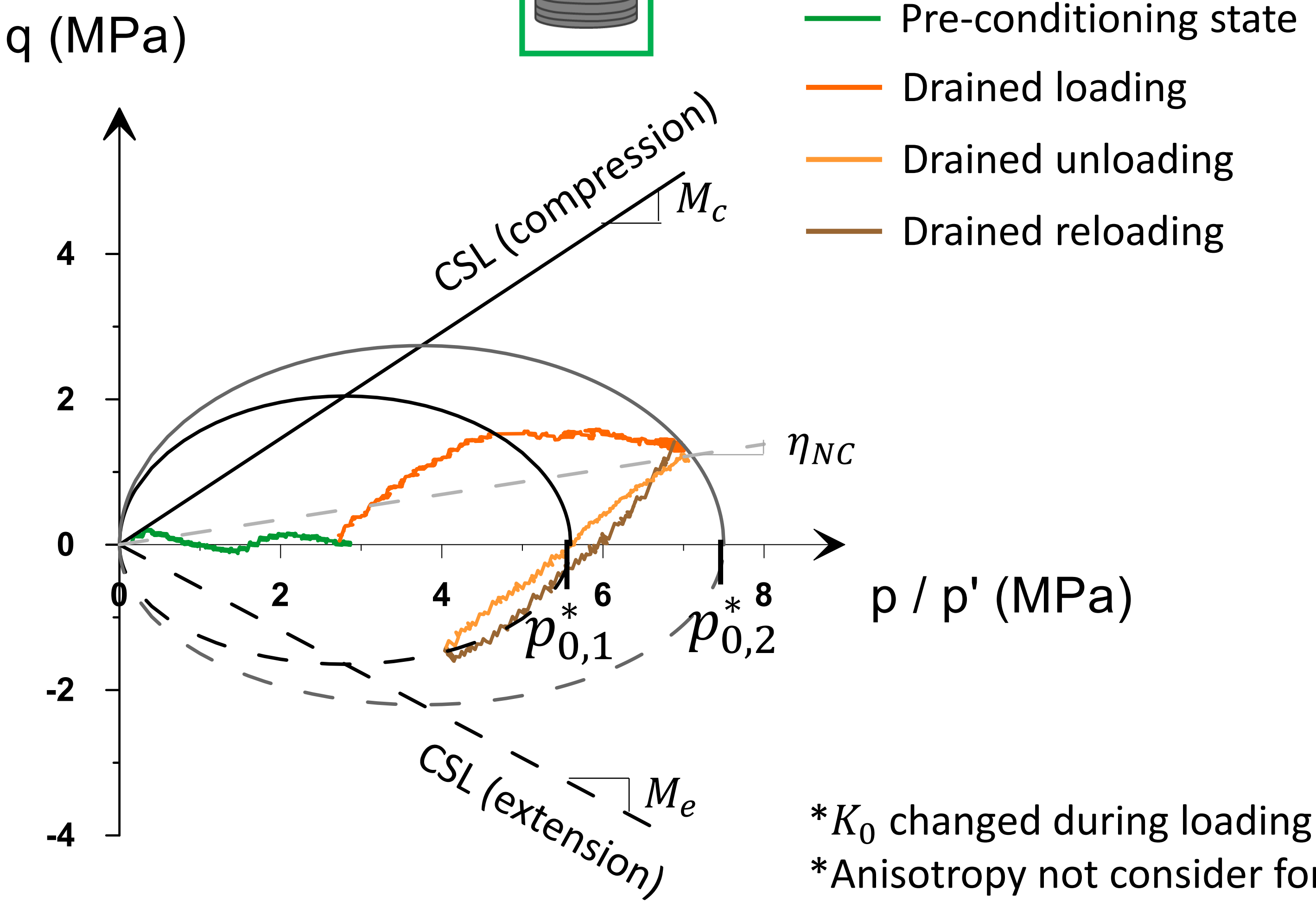

❖ Barcelona Basic Model Parameters:

- $\phi' = 19°$
- $M_c = 0.73$
- $M_e = 0.58$
- $p^*_{0,1} = 5.6\ MPa$
- $p^*_{0,2} = 7.5\ MPa$

$$p = \frac{1}{3}(\sigma_1 + 2\sigma_3) \qquad p' = \frac{1}{3}(\sigma'_1 + 2\sigma'_3)$$

$$q = (\sigma_1 - \sigma_3)$$

$$M_c = \frac{6\sin(\phi')}{3 - \sin(\phi')} \qquad M_e = \frac{6\sin(\phi')}{3 + \sin(\phi')}$$

$$\eta_{NC} = \frac{3(1 - K_0)}{(1 + 2K_0)}$$

*K_0 changed during loading
*Anisotropy not consider for M_c and M_e

ADDITIONAL HYDRO-MECHANICAL PATH

❖ **SET2_HM_P**

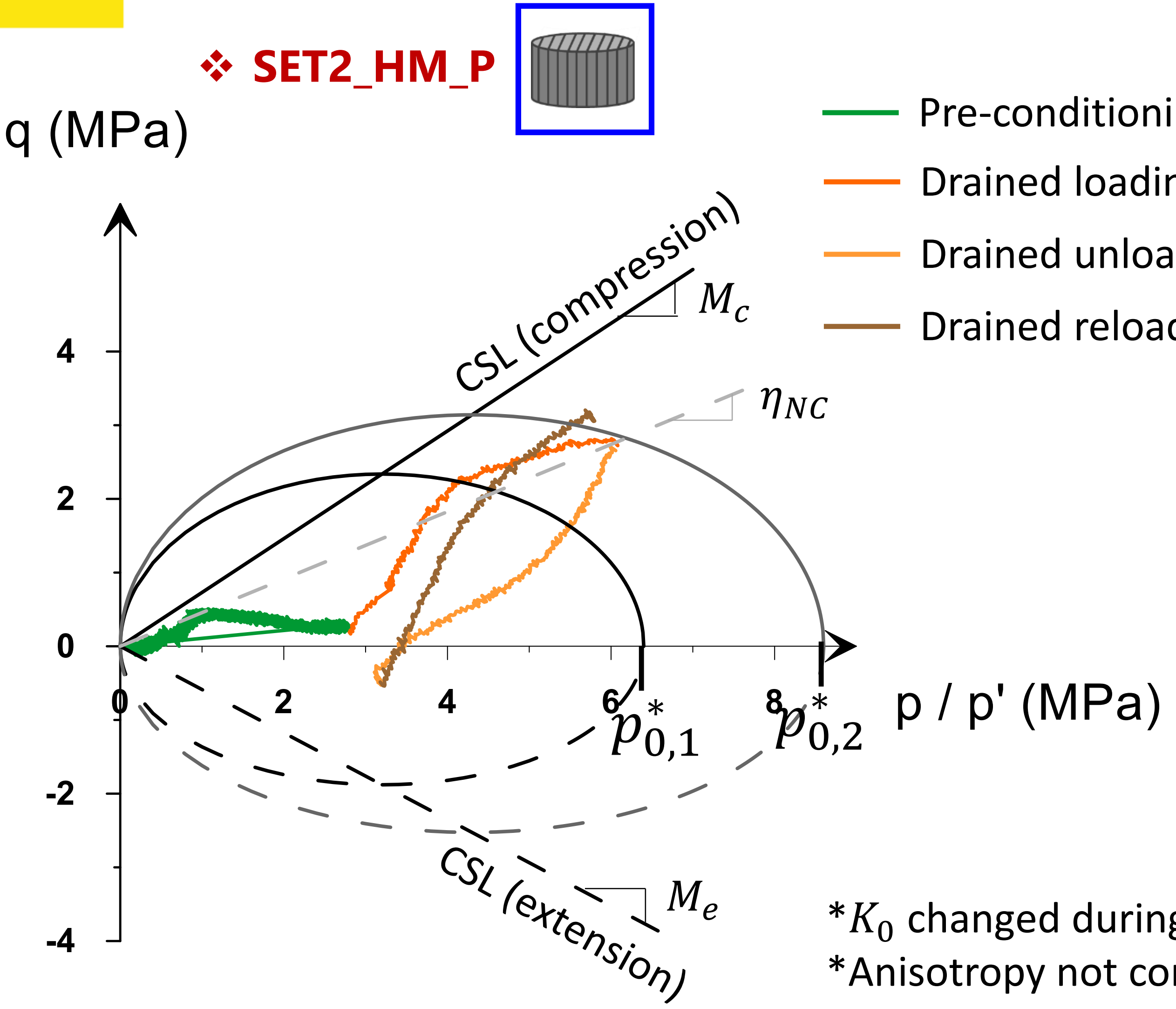

❖ Barcelona Basic Model Parameters:

- $\phi' = 19°$
- $M_c = 0.73$
- $M_e = 0.58$
- $p^*_{0,1} = 6.4\ MPa$
- $p^*_{0,2} = 8.6\ MPa$

$$p = \frac{1}{3}(\sigma_1 + 2\sigma_3) \qquad p' = \frac{1}{3}(\sigma'_1 + 2\sigma'_3)$$

$$q = (\sigma_1 - \sigma_3)$$

$$M_c = \frac{6\sin(\phi')}{3 - \sin(\phi')} \qquad M_e = \frac{6\sin(\phi')}{3 + \sin(\phi')}$$

$$\eta_{NC} = \frac{3(1 - K_0)}{(1 + 2K_0)}$$

*K_0 changed during loading
*Anisotropy not consider for M_c and M_e

ADDITIONAL HYDRO-MECHANICAL PATH TO ANALYSE THE POST-YIELD BEHAVIOUR

- Slope of post-yield compression line similar for both orientations

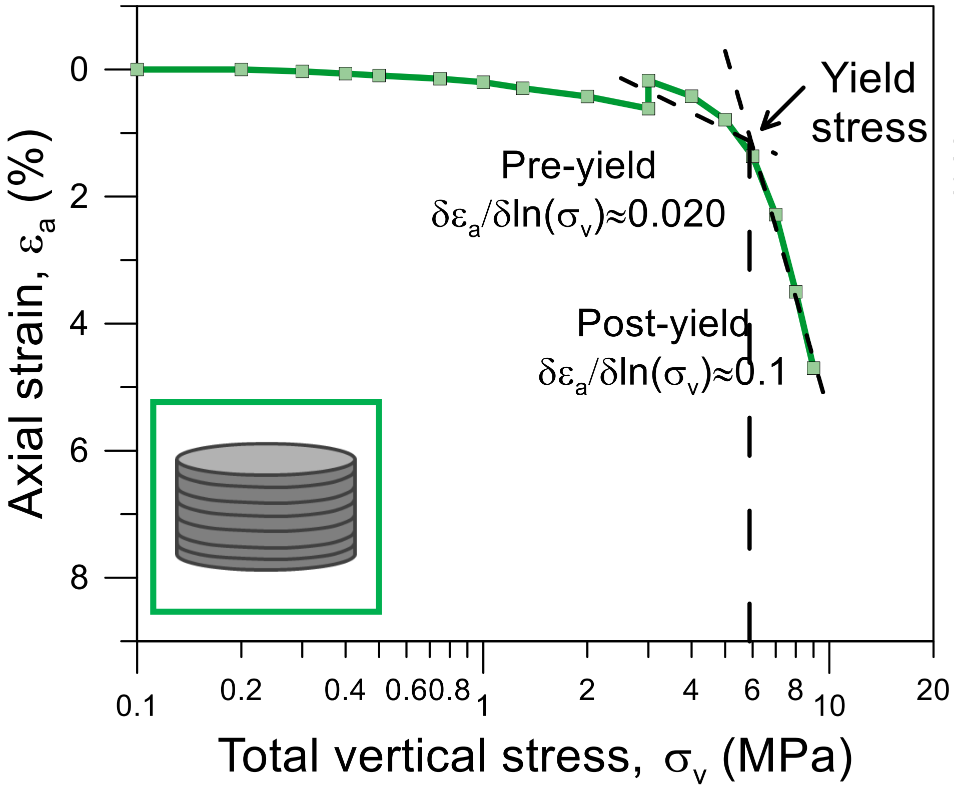

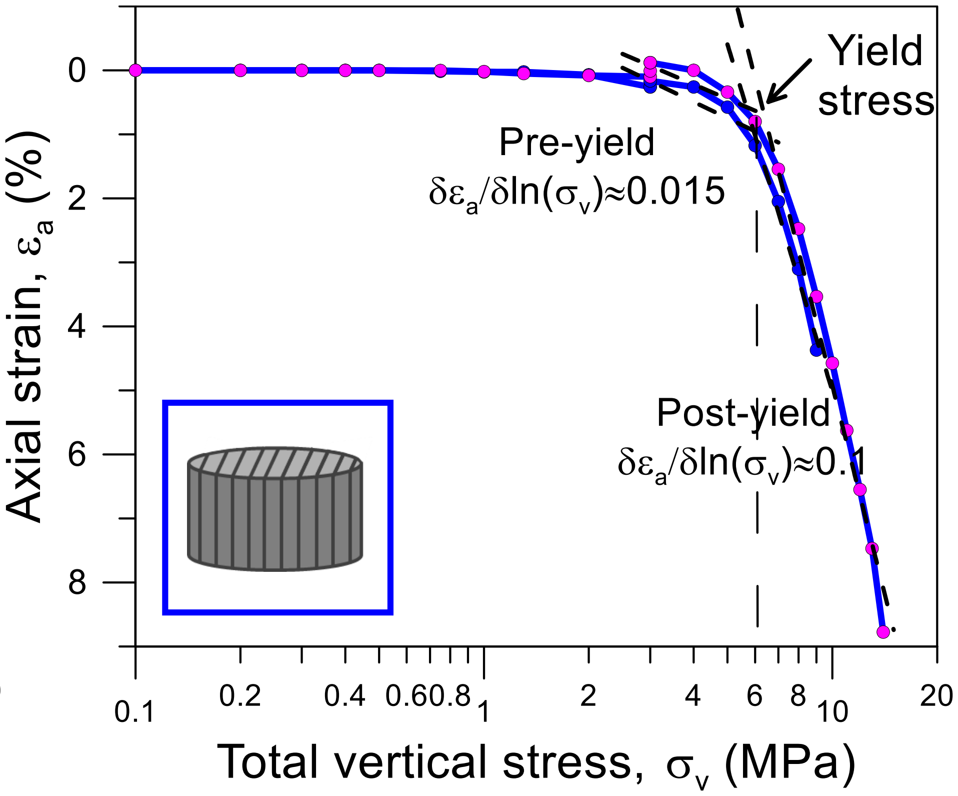

WATER PERMEABILITY

- Dependence of water permeability on porosity
- Higher water permeability with flow parallel to bedding planes (**anisotropy**)
- Loading to 8 MPa and unloading to 6 MPa causes a significant decrease in water permeability

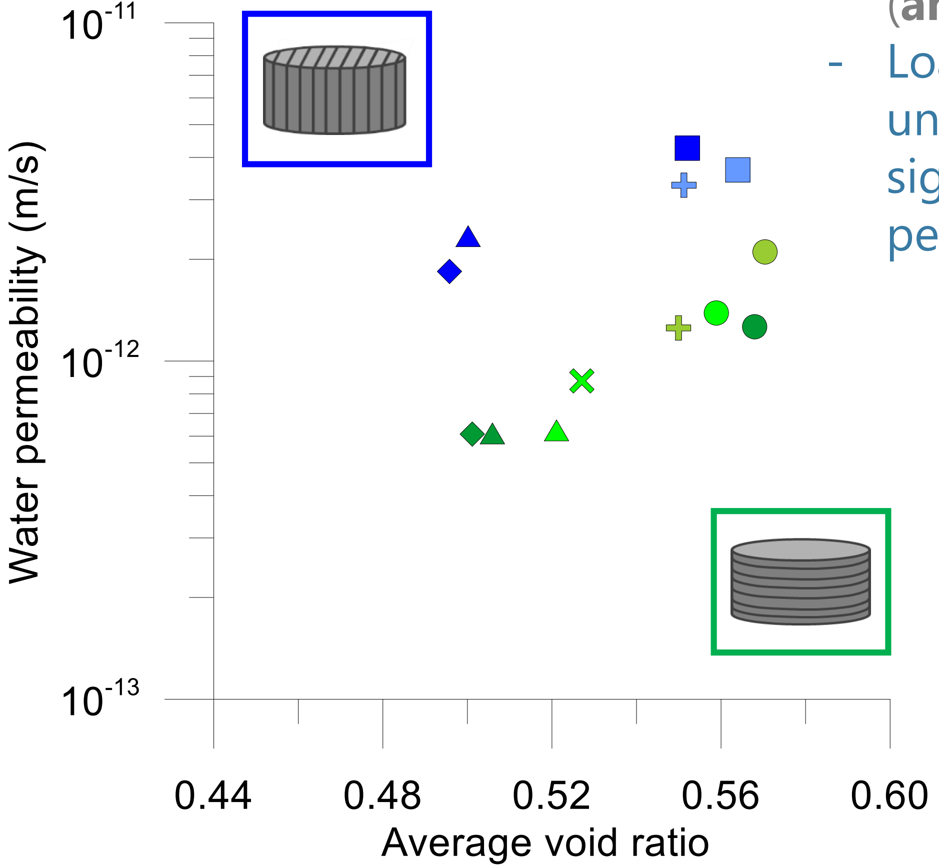

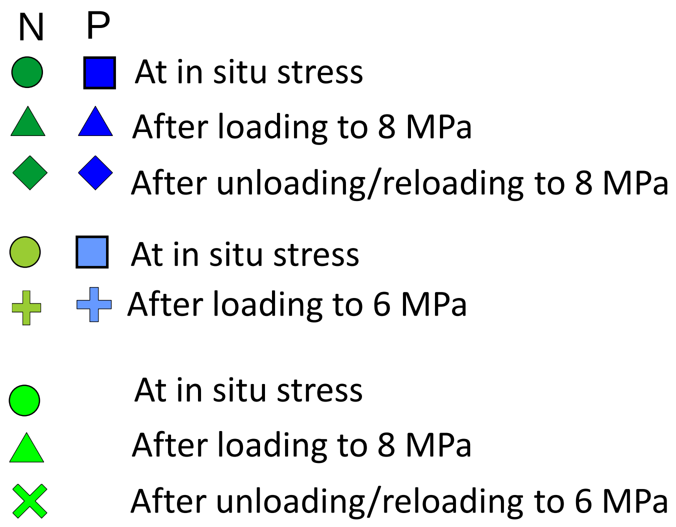

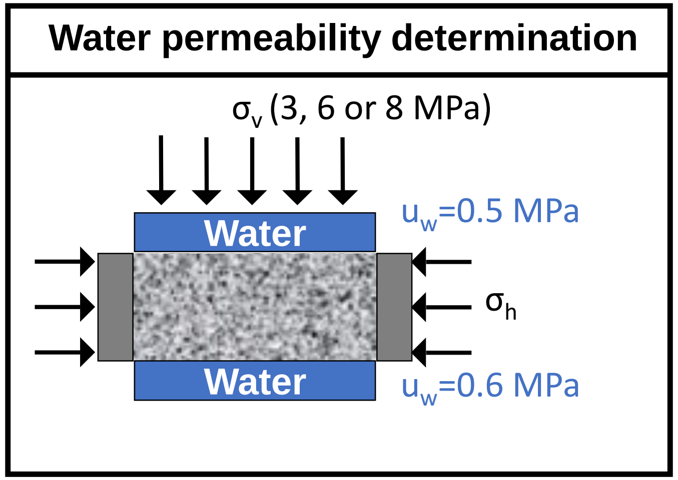

GAS INJECTION STAGES

A→B: Gas injection at constant volume rate
B: Shut-off of the injection system
B→C: Gas dissipation at constant gas injection volume

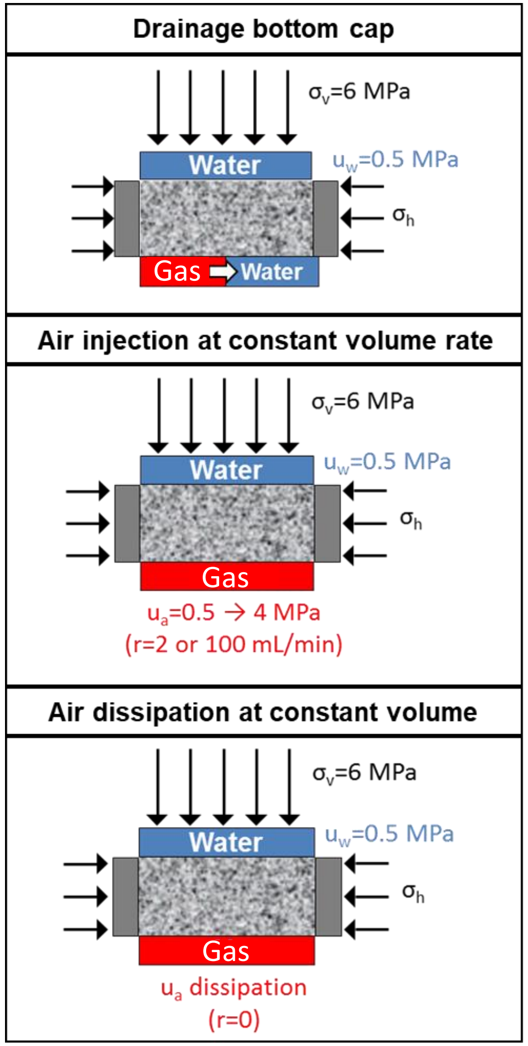

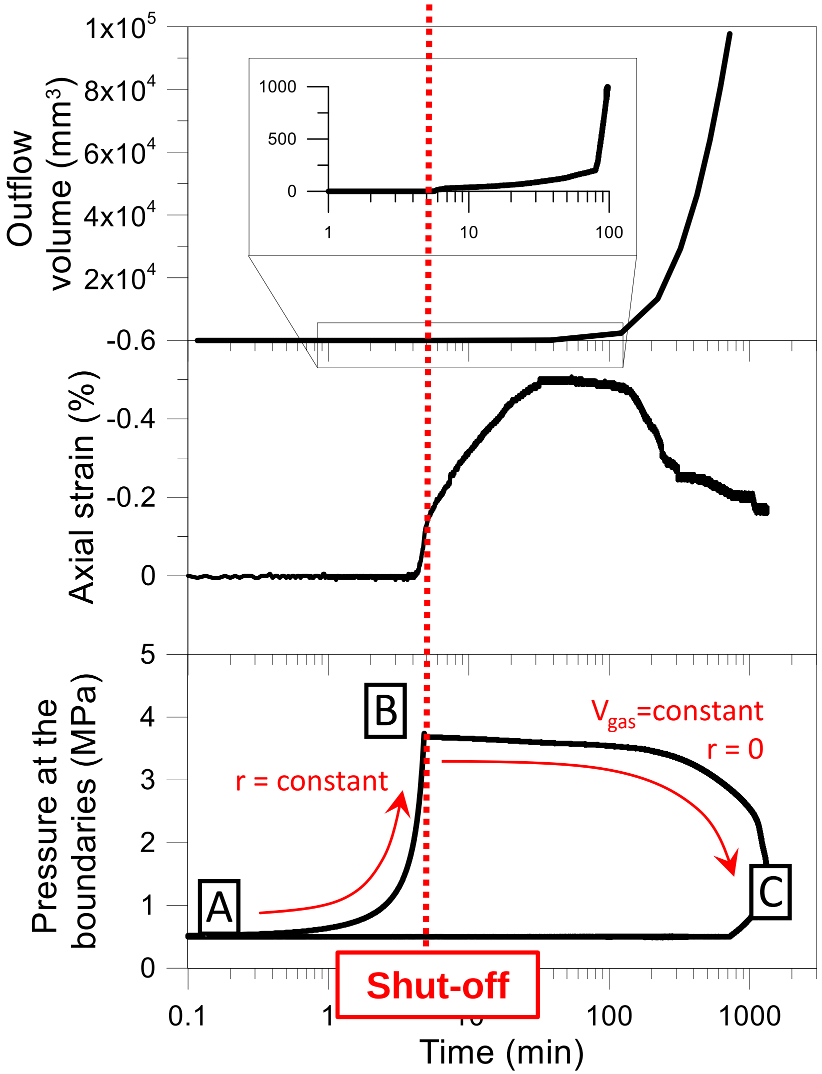

Tests performed:

Two orientations:

- flow normal to bedding planes
- flow parallel to bedding planes

Two volumetric rates:

- fast (r= 100 mL/min)
- slow (r= 2 mL/min)

Two gases:

- Air
- Helium

eurad

GAS INJECTION AND DISSIPATION
EFFECT OF BEDDING ORIENTATION AND INJECTION RATE

A→B: Fast air injection at constant volume rate 100 mL/min up to 4 MPa
- No important expansion detected
- No outflow detected

B→B': Shut-off and dissipation phase at constant injection volume
- Expansion while air pressure front propagates (constitutive stress decreases)

B'→C: Dissipation phase at constant injection volume
- When outflow volume rate increases, air pressure decreases and samples undergo compression (constitutive stress increases)

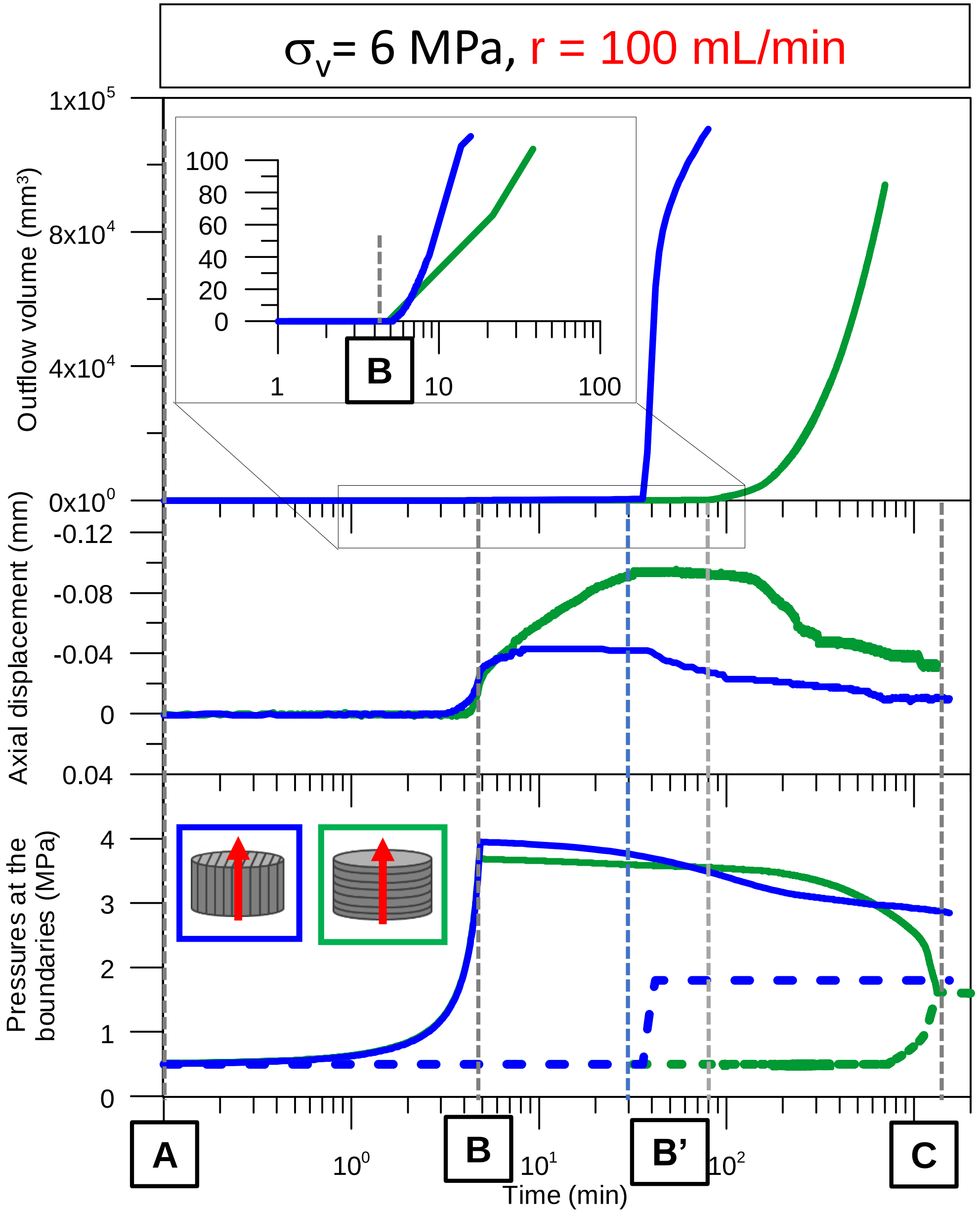

GAS INJECTION AND DISSIPATION
EFFECT OF BEDDING ORIENTATION AND INJECTION RATE

A→B: Slow air injection at constant volume rate 2 mL/min up to 4 MPa
- Expansion while air pressure front propagates (constitutive stress decreases)
- First outflow detected during the injection

B→C: Shut-off and dissipation phase at constant injection volume
- Immediately after shut-in, the outflow volume rate increases, the air pressure decreases and samples undergo compression (constitutive stress increases)

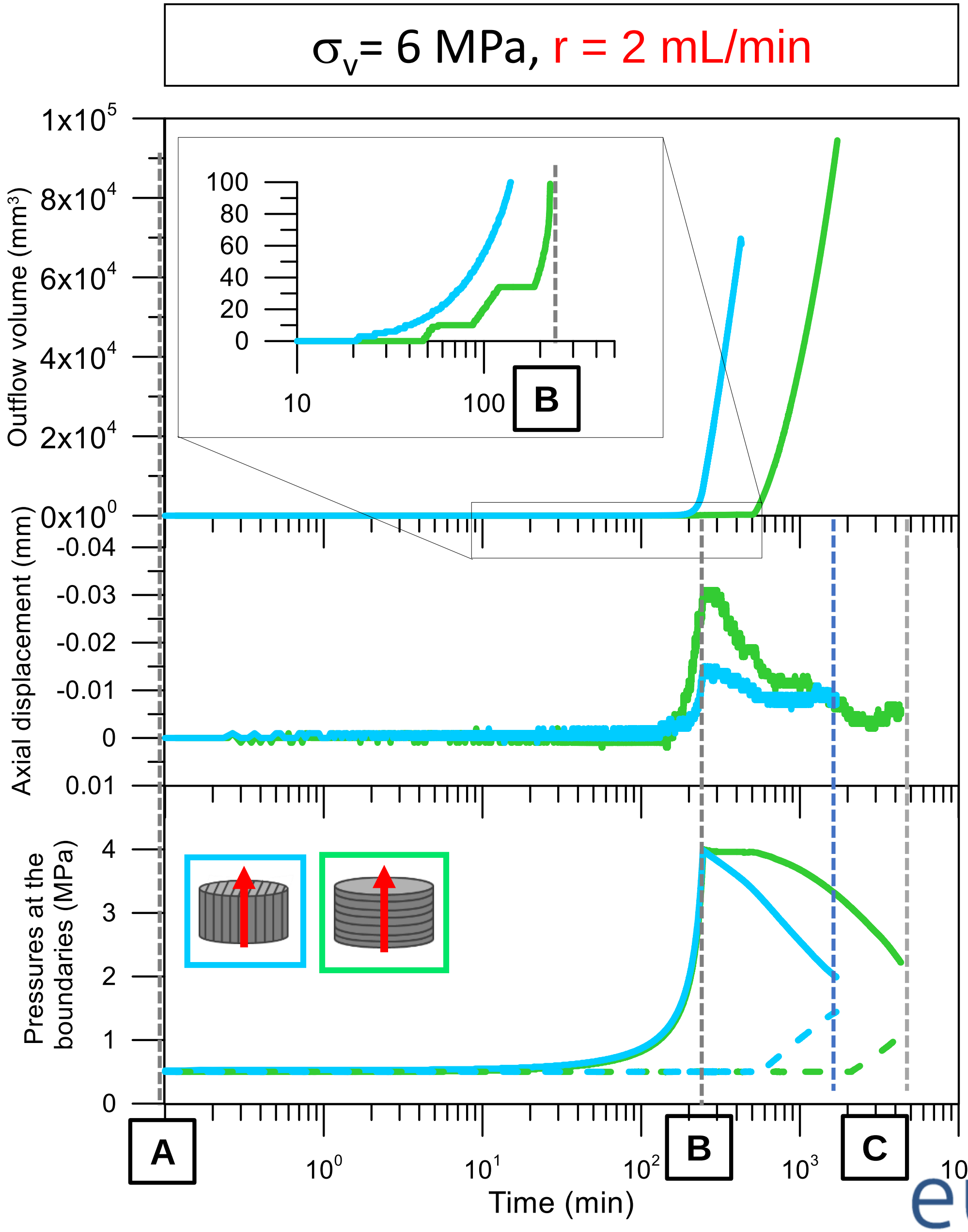

GAS INJECTION AND DISSIPATION
VOLUMETRIC BEHAVIOUR

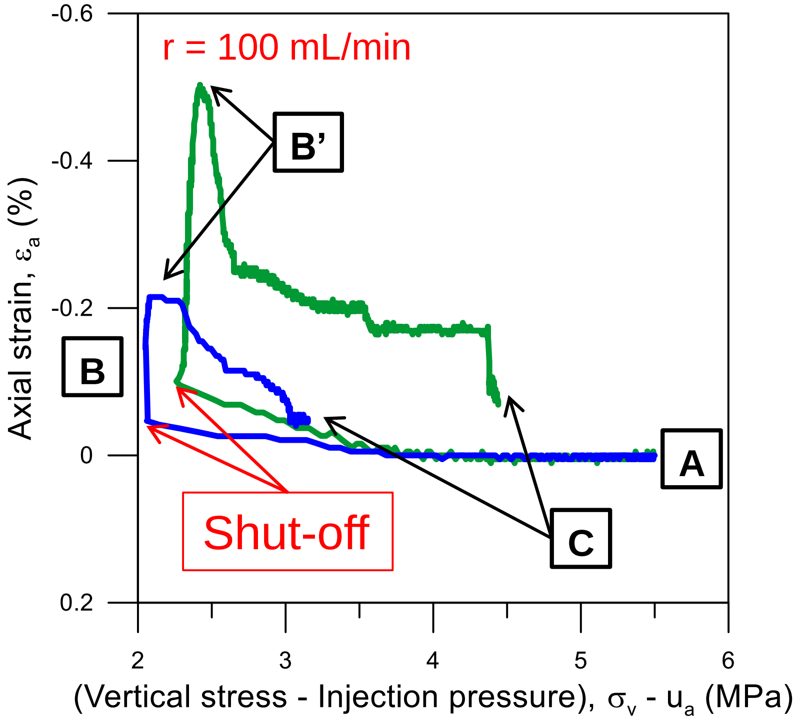

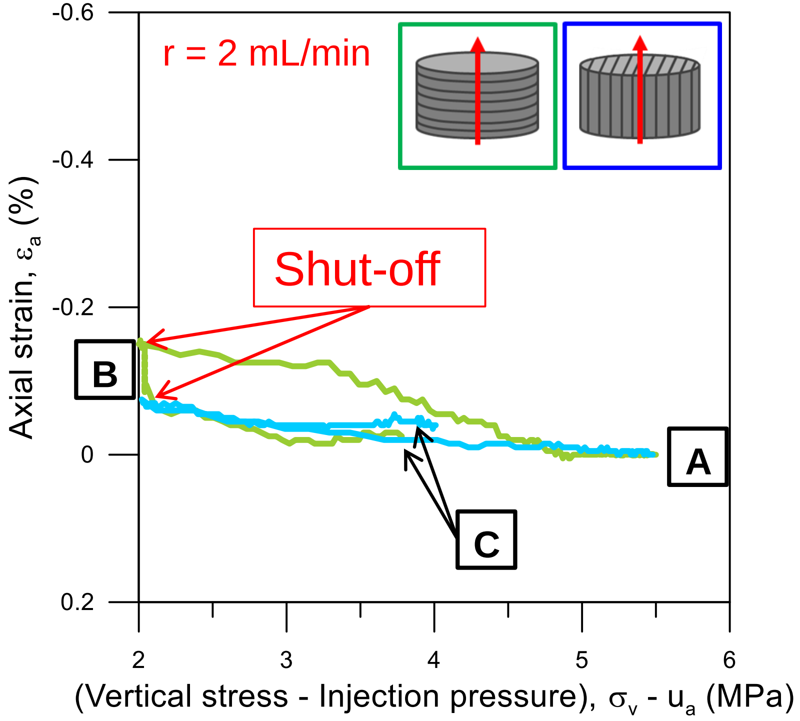

Significant effect of injection rate

Faster injections → higher expansions (samples expanded after shut-off during pressure front propagation)

Pore pressure nearly equilibrated during slower injections (no expansion after shut-off)

Important influence of bedding orientation under oedometer conditions

Samples with bedding planes normal to flow underwent higher expansions on air equalisation and larger compressions on the air dissipation stage (anisotropy)

GAS INJECTION AND DISSIPATION

AIR VS HELIUM

Similar behaviour found when Helium was used as injected gas in comparison with air:

- Slightly faster dissipation
- Slightly higher expansion

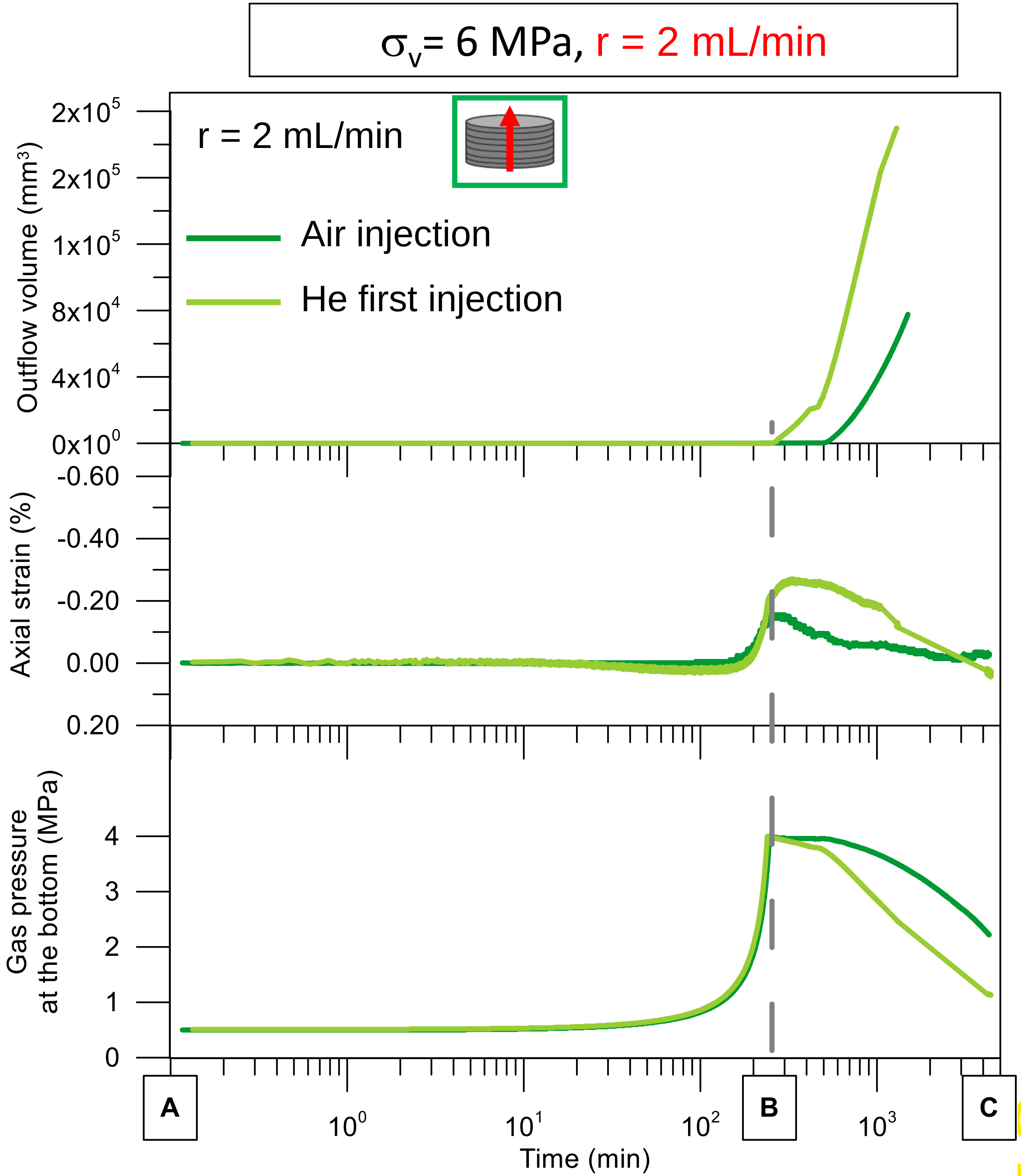

GAS INJECTION AND DISSIPATION
SUCCESSIVE INJECTION STAGES

The response during the second injection is rather similar to the first injection.

- Slightly higher expansion

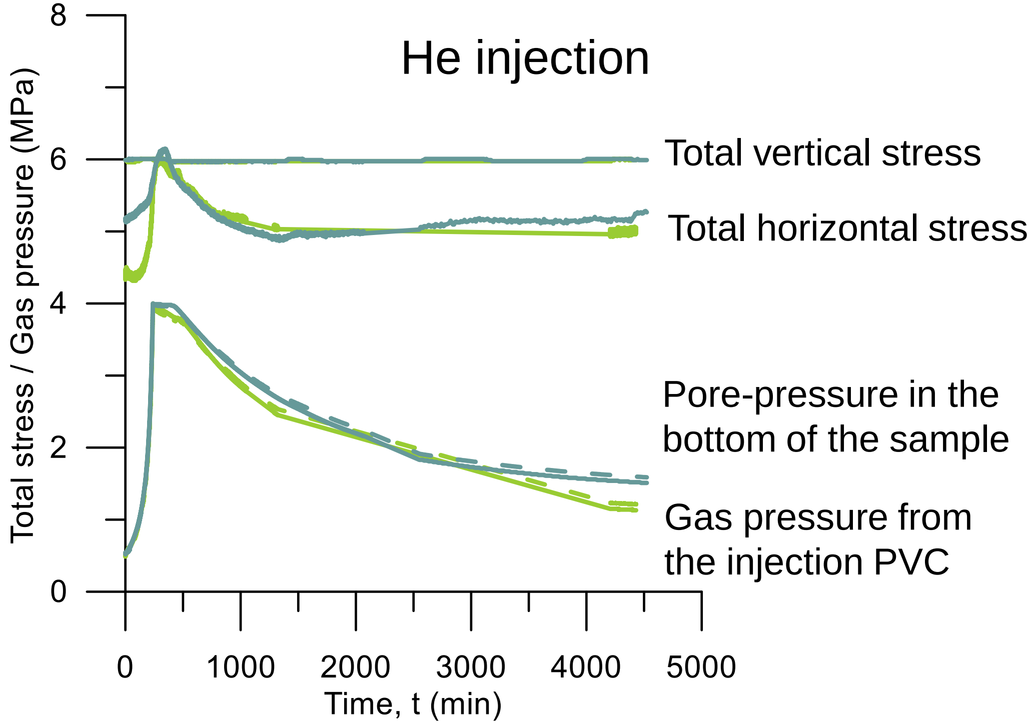

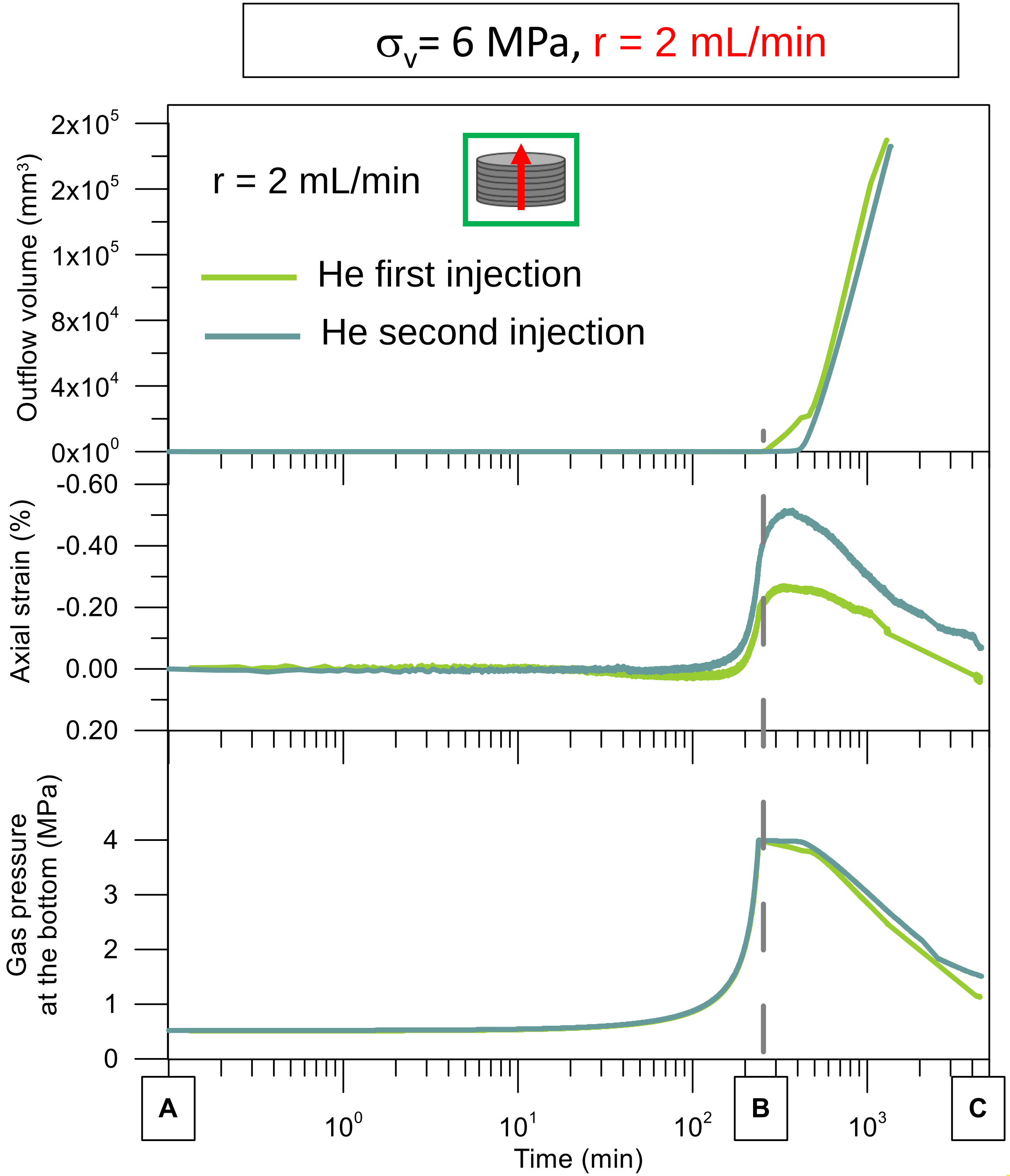

GAS INJECTION AND DISSIPATION
GAS PERMEABILITY FROM INJECTION PRESSURE DECAY DATA

$$K = -\frac{2LV_{in}\mu_g}{A((u_{in}(t))^2 - (u_{out}(t))^2)}\frac{du_{in}}{dt}$$

u_{in}: Injection pressure
u_{out}: pressure at recovery point
V_{in}: constant gas injection volume
L: height of sample
A: sample area
μ_g: gas viscosity

Assumptions:
- Steady-state conditions at high degrees of saturation (gas pathways desaturated)
- Flow cross-section equal to sample area
- Negligible gas diffusion though water

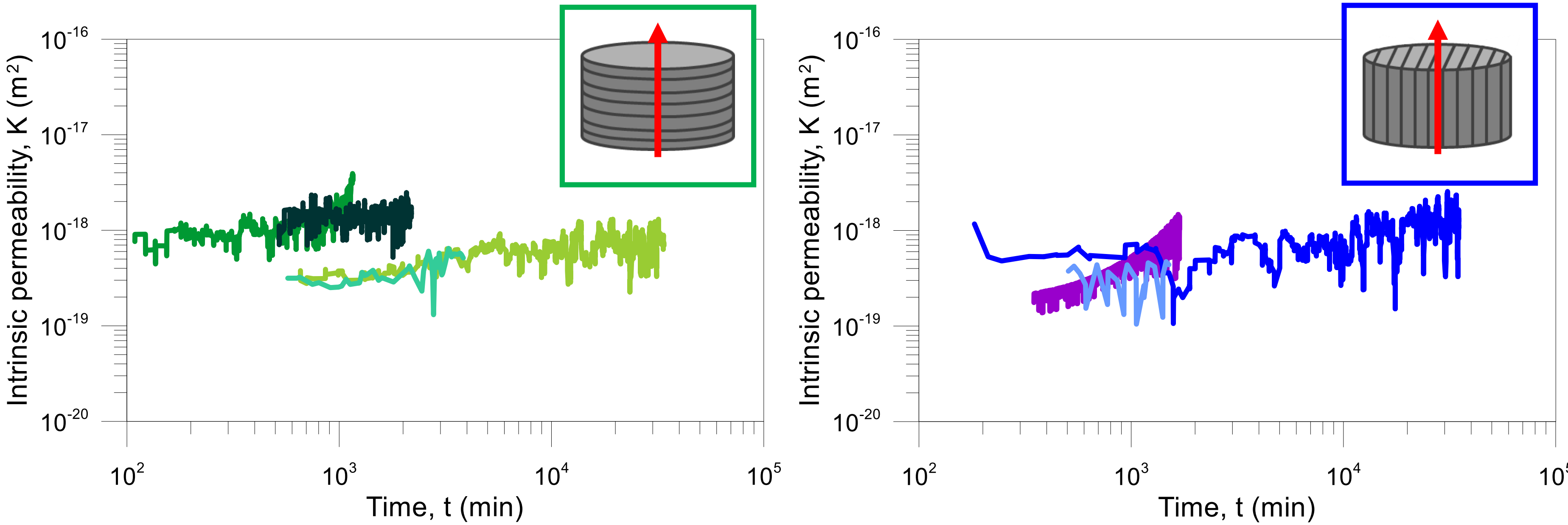

RE-SATURATION AFTER GAS INJECTION

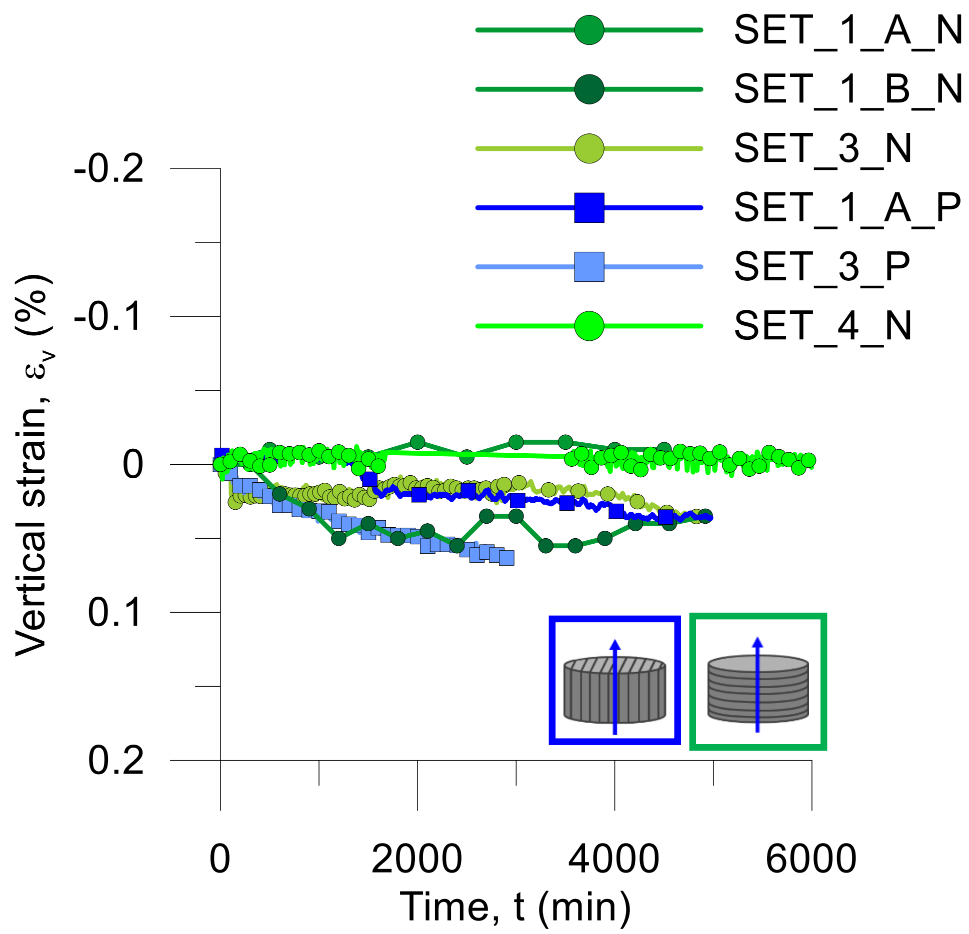

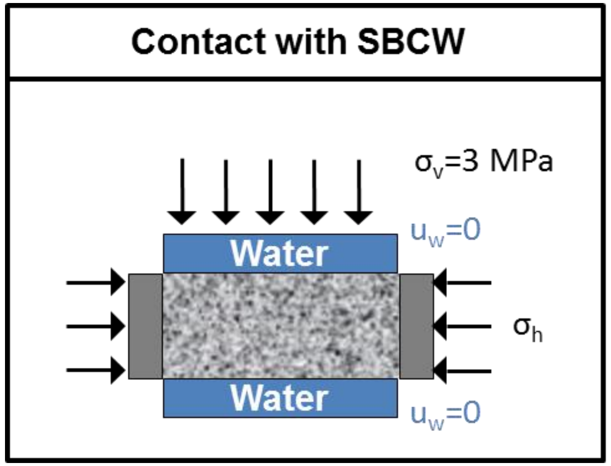

Very small deformations were recorded during the re-saturation stage, which indicated no important desaturation during gas migration

Bedding orientation	Injection stage	Volume of water expelled (mL)	Sr at the end of the injection
Bedding ⊥ flow	1st injection	2.22	0.87
	2nd injection	2.60	0.85
Bedding ⊥ flow	1st injection	2.82	0.83
	2nd injection	2.75	0.83

WATER PERMEABILITY AFTER GAS INJECTION

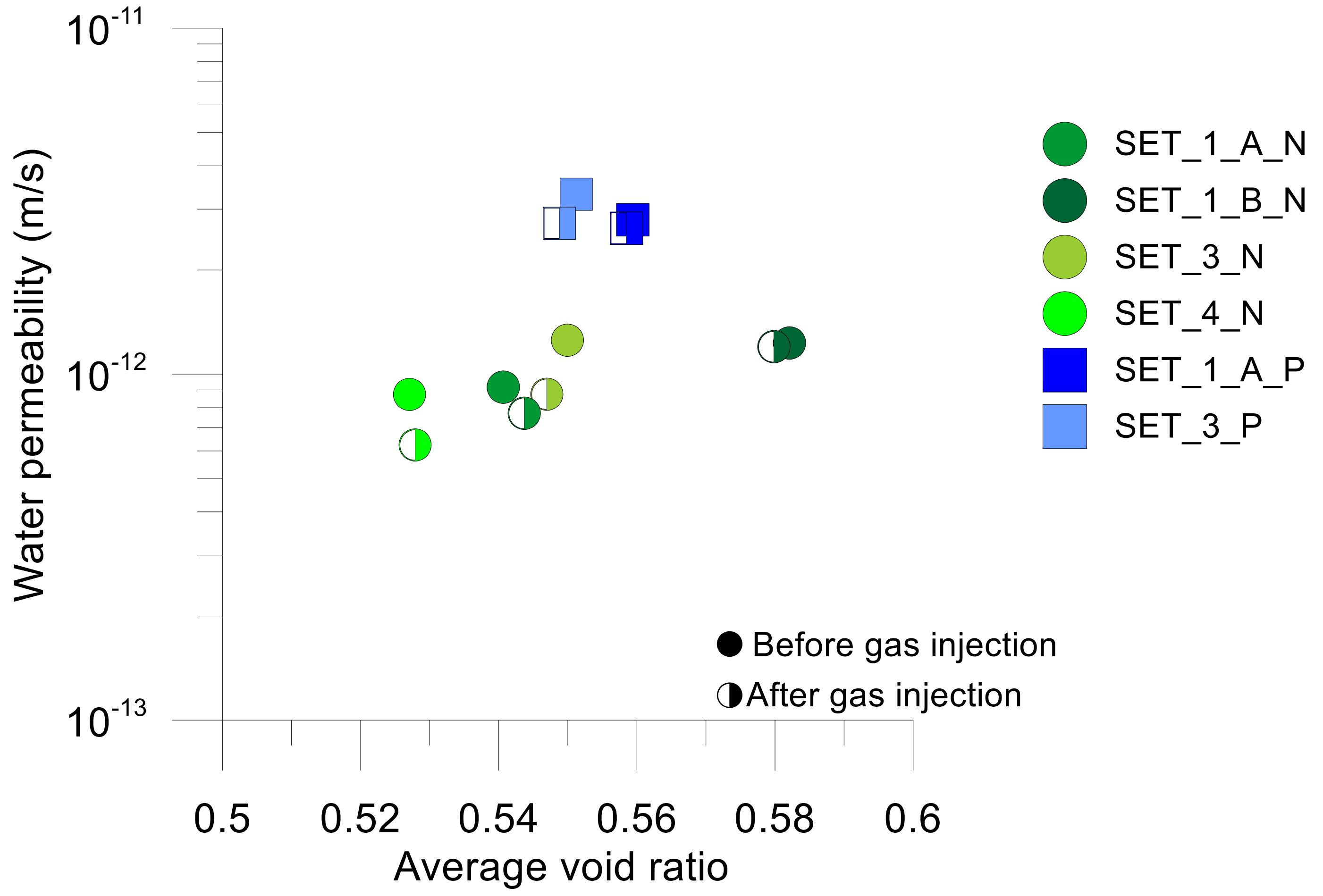

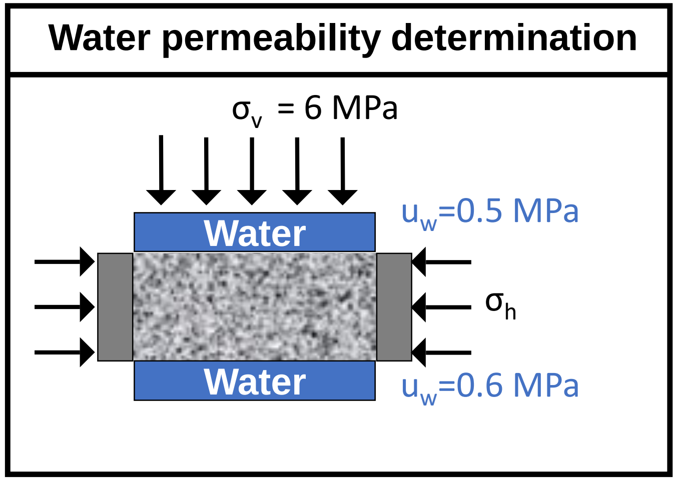

Water permeability before and after the gas injection does not present significant changes in either bedding orientations

Self-sealing of gas pathways due to the re-saturation process

eurad

WATER VS GAS PERMEABILITY

(Effective) permeability to gas determined during the dissipation stages was found to be higher than the (intrinsic) permeability to water.

No important anisotropic features were detected in the permeability to gas (it was not the case of the permeability to water with higher values with bedding planes parallel to flow).

(Effective) permeability to gas after re-saturation (2nd injection) is slightly higher than for the 1st injection. Although, after unloading/reloading this difference is insignificant.

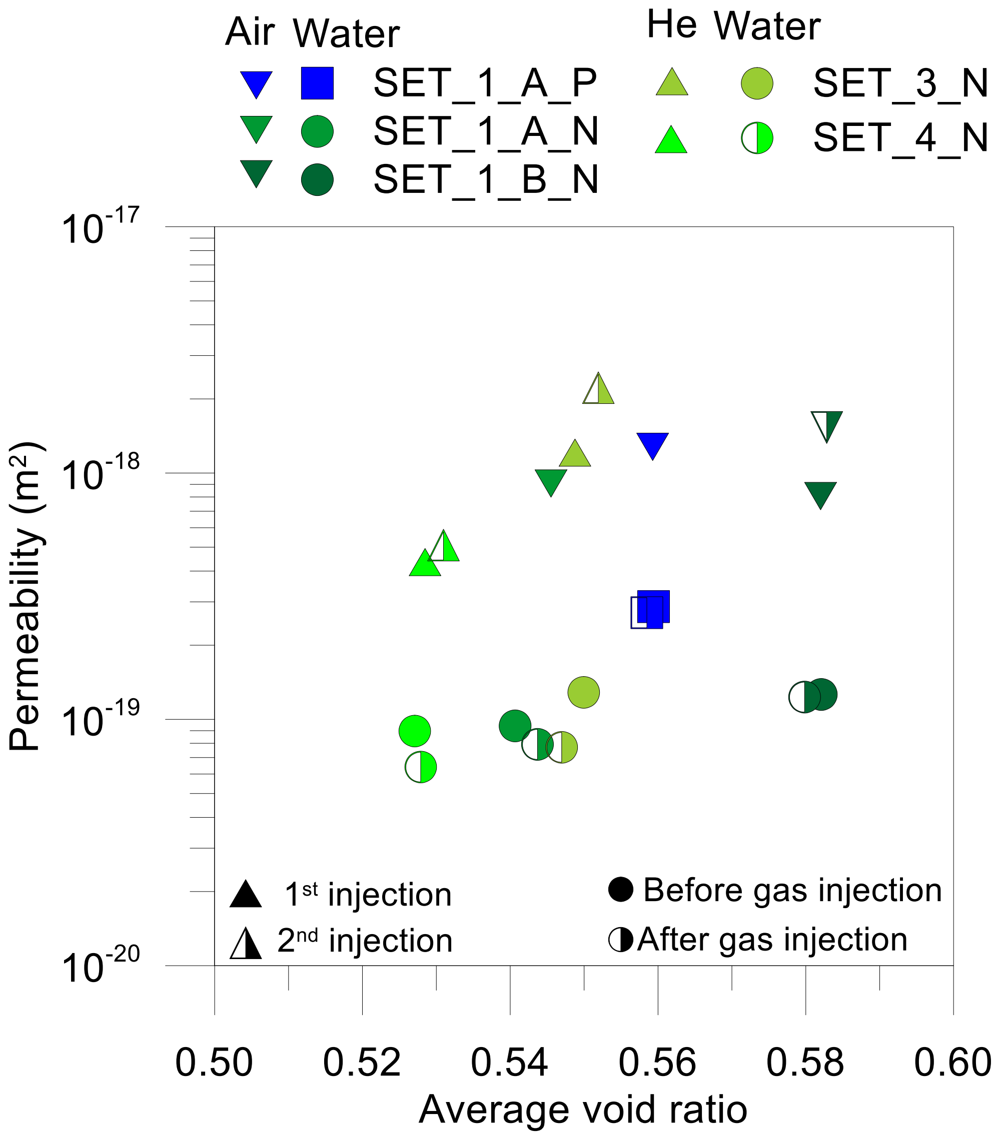

MICROSTRUCTURAL CHANGES INDUCED BY GAS MIGRATION: TECHNIQUES

- Quantitative technique
- Intruded (connected) porosity
- Discerning different scales
- Pore size detection: 7 nm - 100 µm
- Shape through fractal analysis

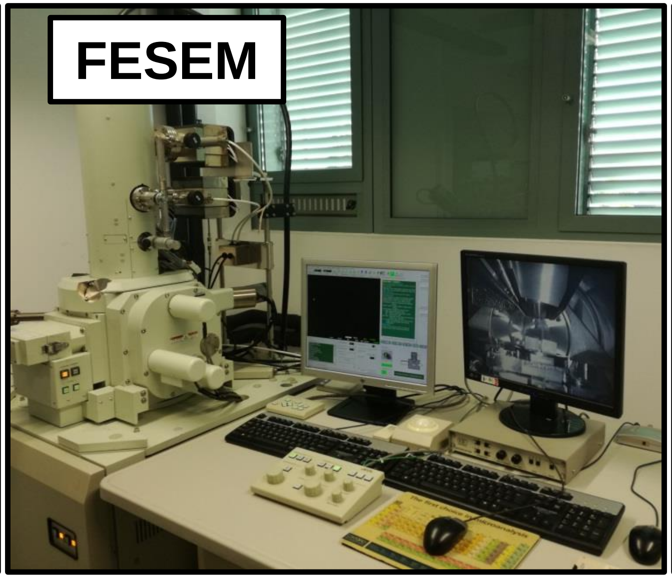

- Qualitative/quantitative technique
- Morphology of the surface
- Resolution depending on magnification (1 µm in this study)
- Image analysis (measuring distances, pores, aggregates, orientation etc.)

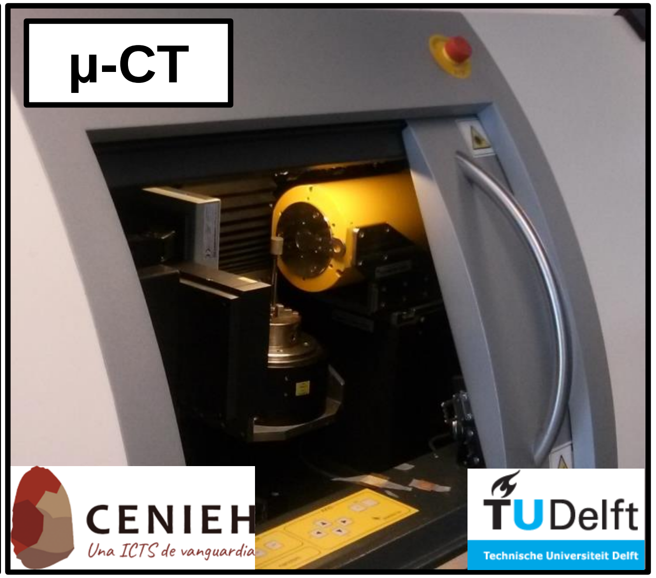

- Qualitative/quantitative technique
- 3D volume reconstruction
- Resolution depending on sample size (20 µm in this study)
- Image analysis (fissure volume through filtering process, connectivity, …)

Equivalent sizes and drying protocols (freeze-drying) to allow comparing techniques

eurad

MIP: PORE SIZE DISTRIBUTION AFTER GAS INJECTION

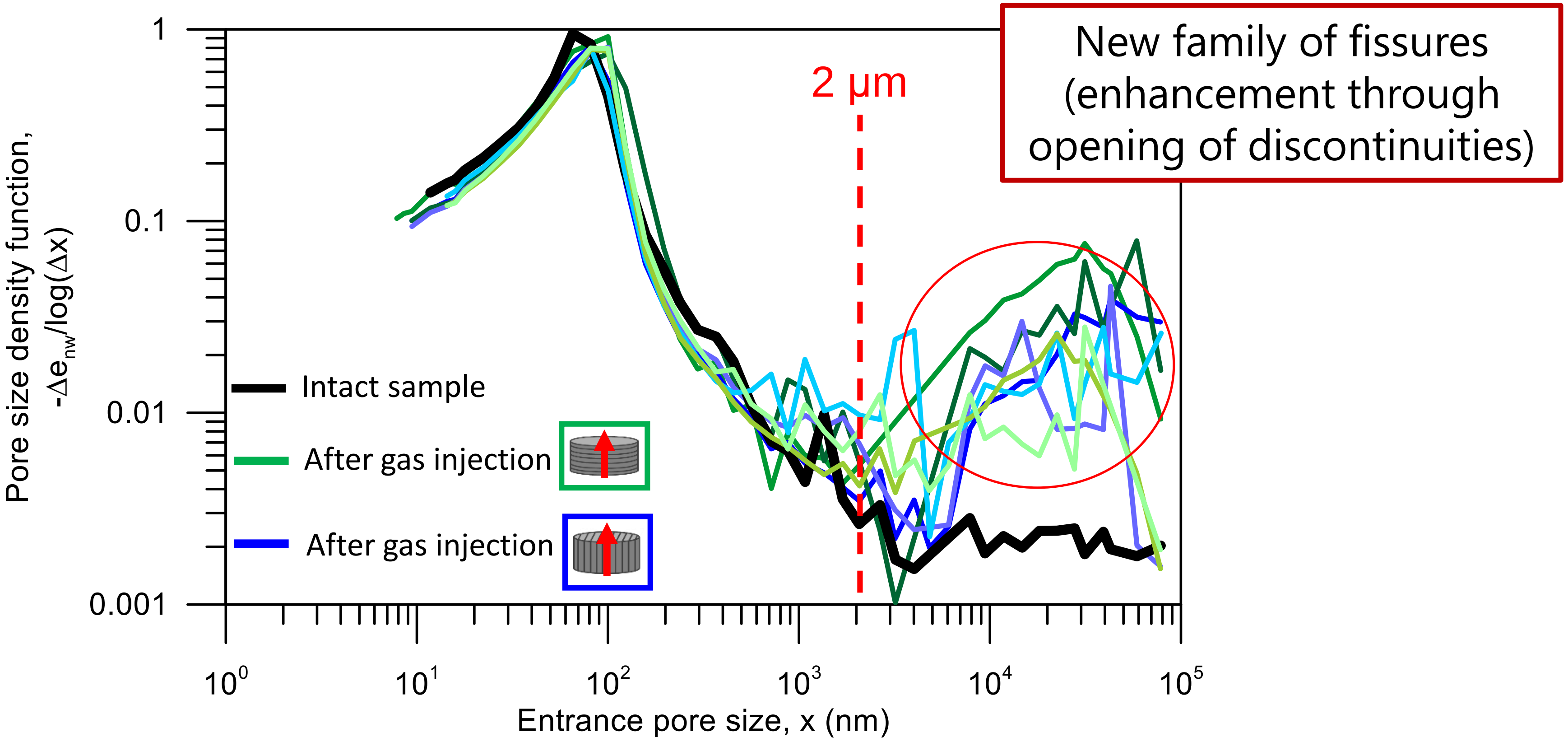

Bi-modal pore size distribution after air tests:
natural pores (matrix) and fissures (damage/degradation)

MIP: PORE SIZE DISTRIBUTION AFTER SELF-SEALING AND SECOND GAS INJECTION

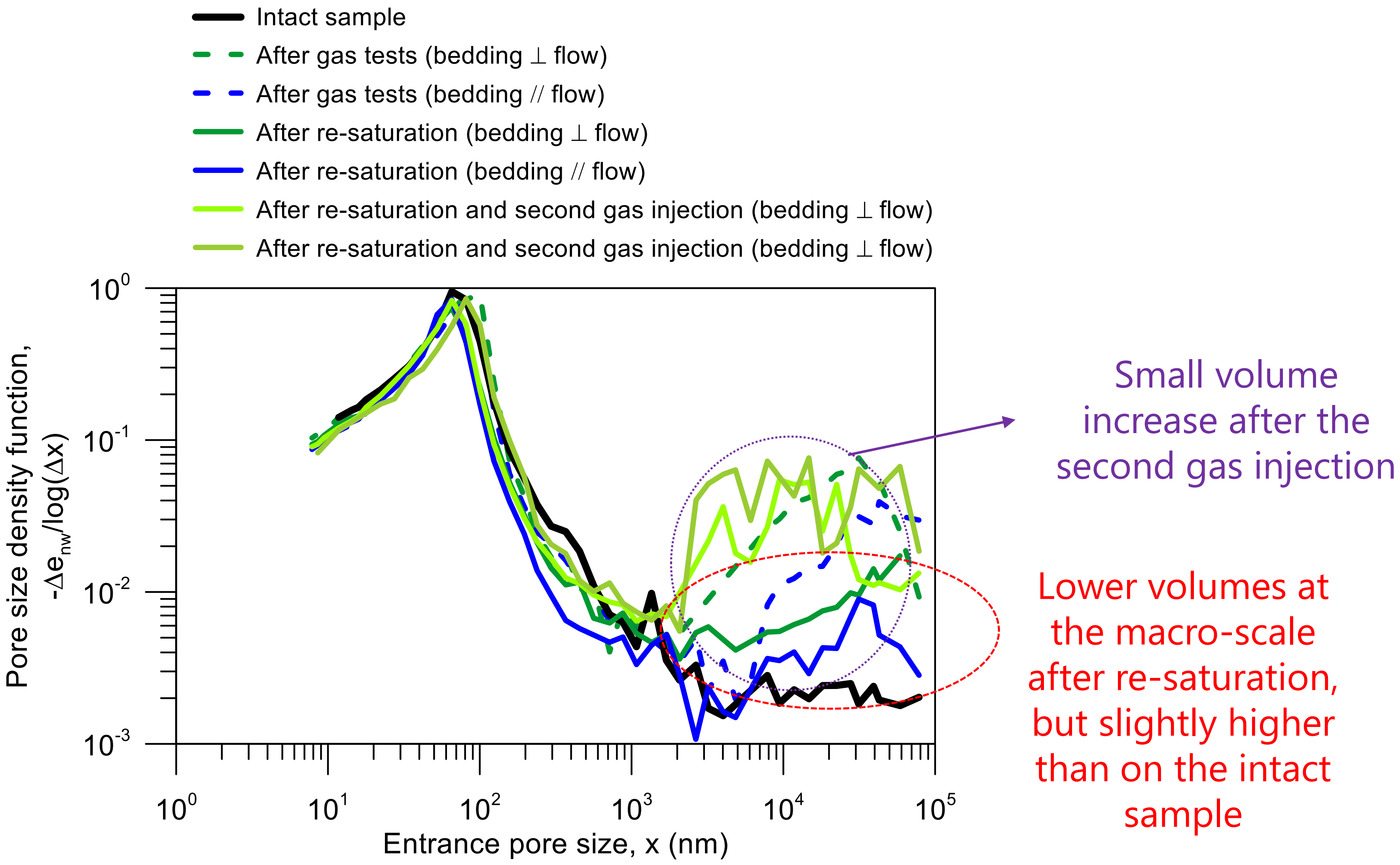

MIP: INFLUENCE OF THE UNLOADING PROCESS IN PORE SIZE DISTRIBUTION

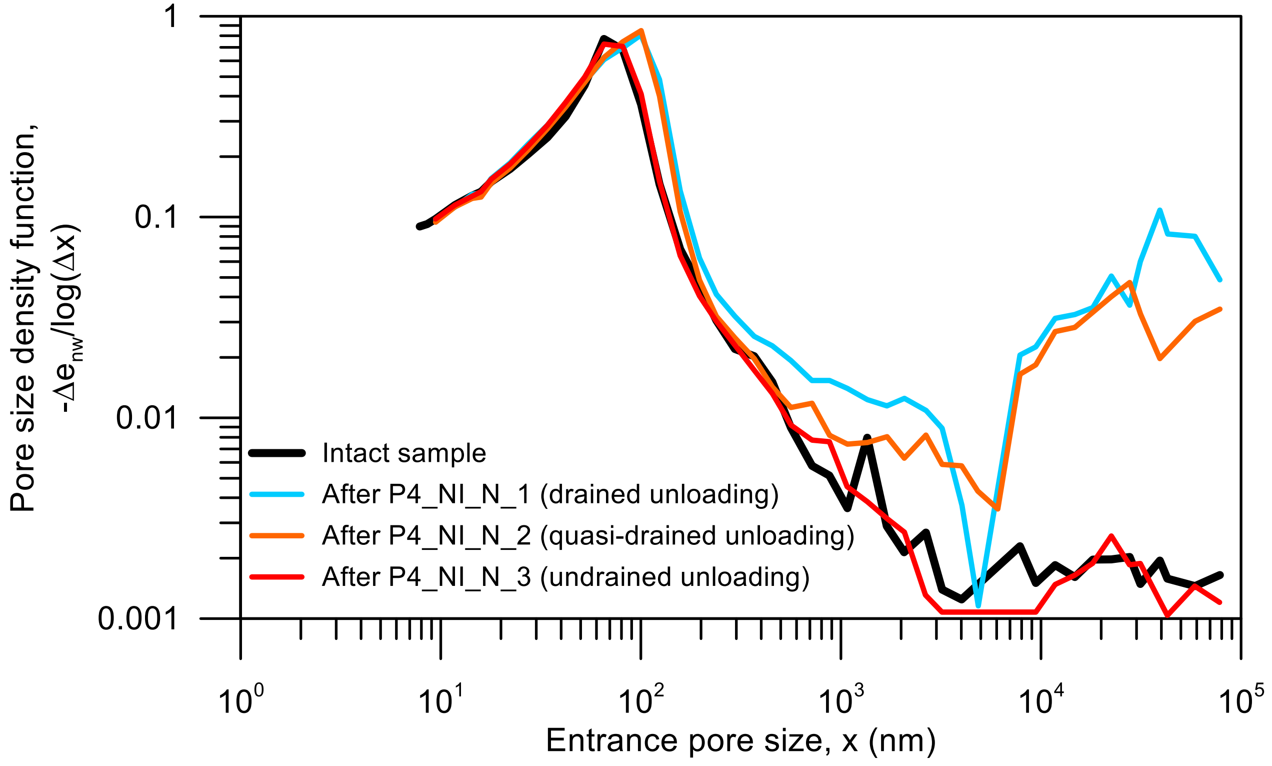

Influence of the unloading process on the final pore size distribution:

- Drained unloading process induces damage (opening of fissures) equivalent to air pressurization process
- Undrained unloading process does not modify the microstructure

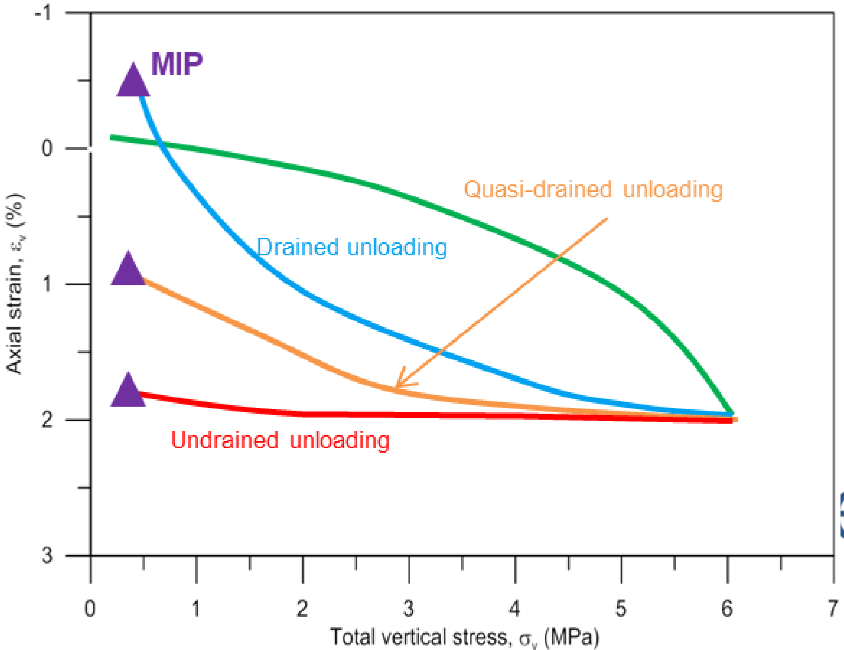

MICRO-CT: IMAGE TREATMENT

Procedure for μ-CT image analysis:

- Define Region of Interest (ROI)
- Identify features
- Volume reconstruction
- Filtering process (if required)
- Connectivity filter (if required)

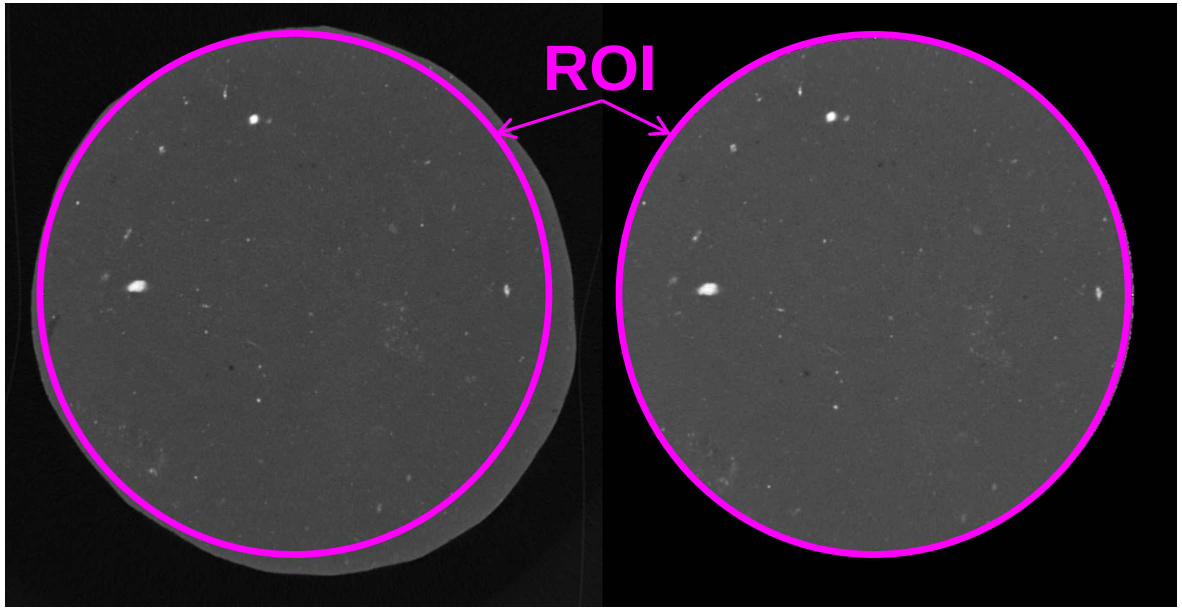

3D volume reconstruction (rendering) of intact sample

Bedding direction not visible

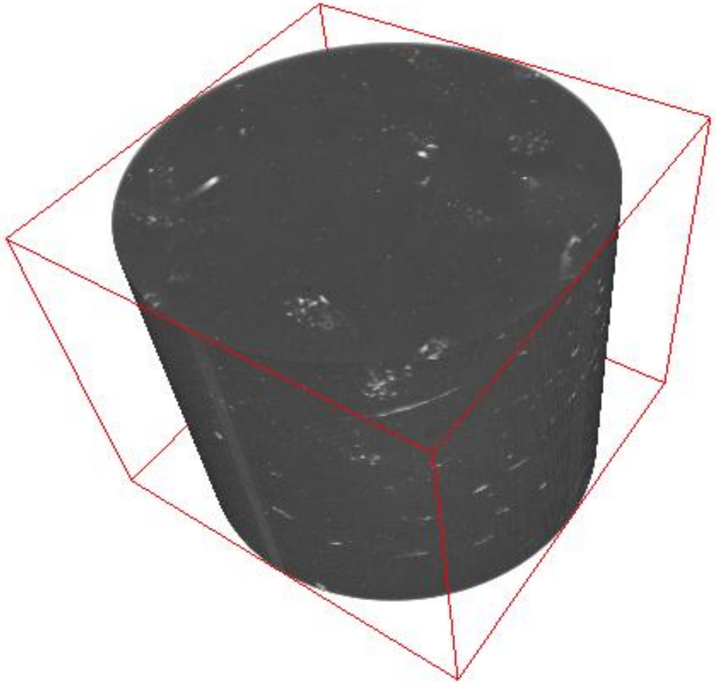

Software ImageJ

(Schneider et al, 2012)

MICRO-CT: FEATURES IDENTIFICATION

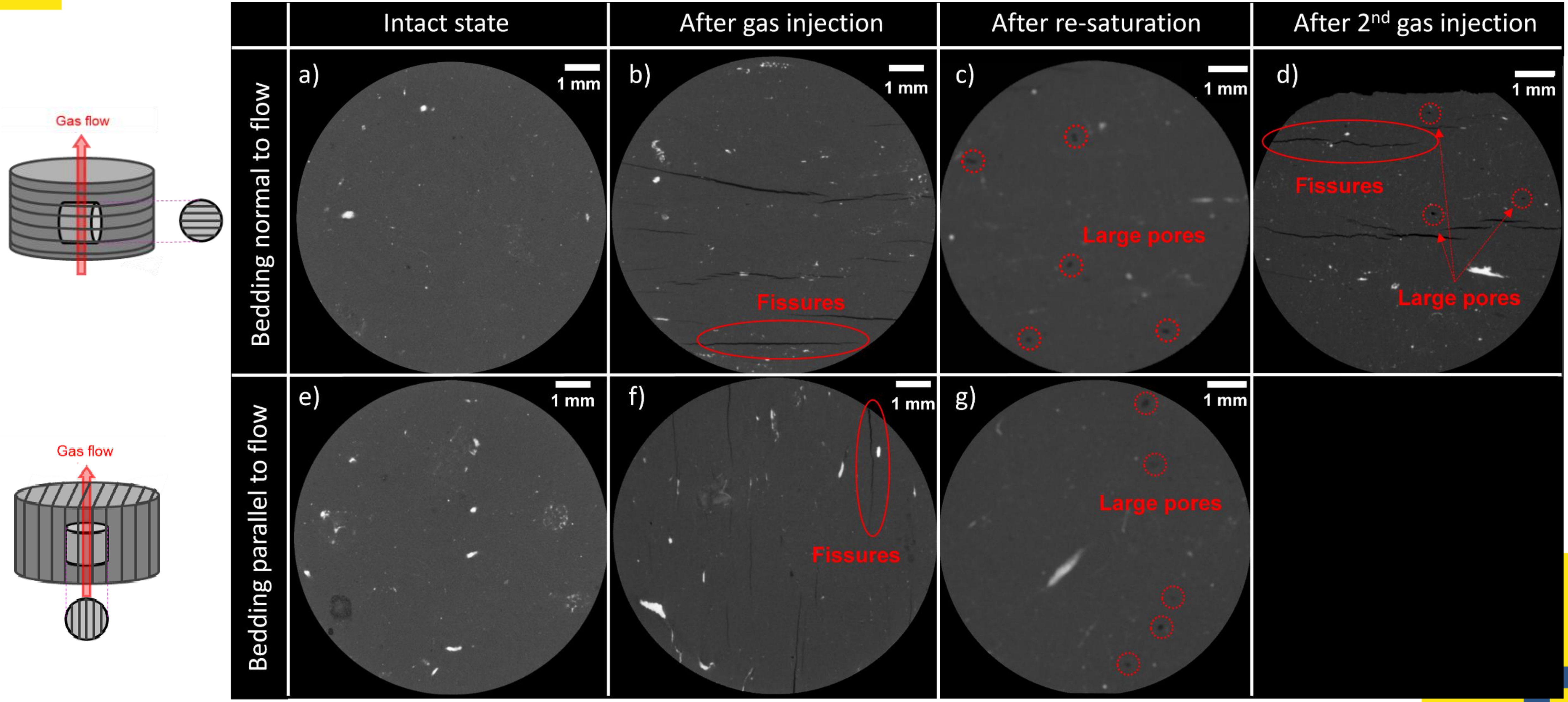

MICRO-CT: AFTER GAS INJECTION

Fissure filtering

Isolation of fissure pattern by using: Multiscale Hessian fracture filtering *(Voorn et al., 2013)*

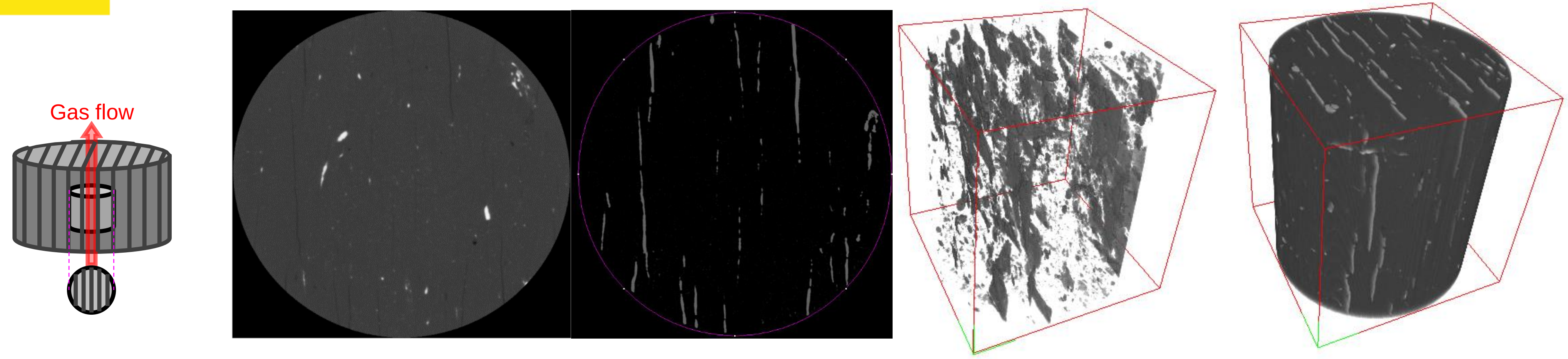

V_{sample} = 1900 mm^3
$V_{pores+fissures}$ = 712 mm^3
$V_{fissures}$ = 34.5 mm^3

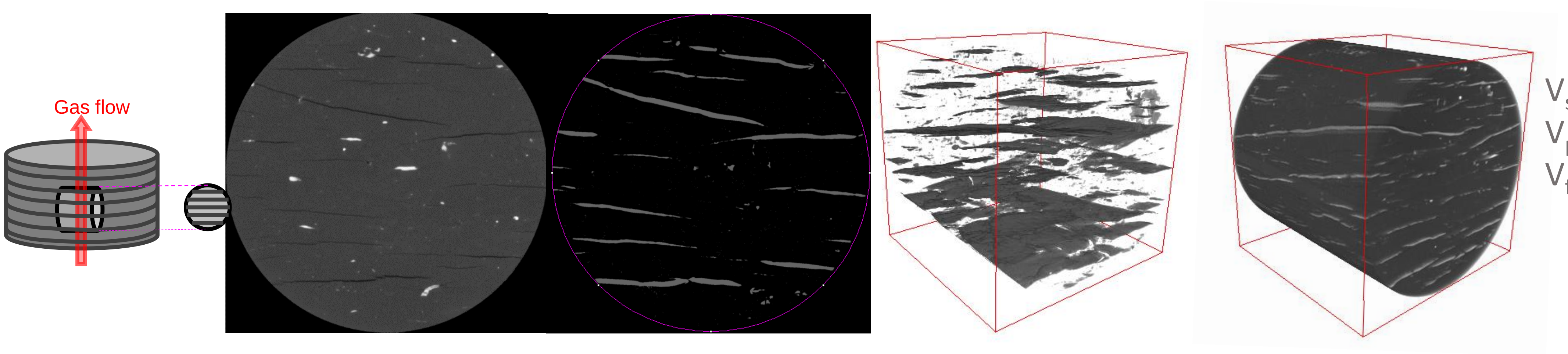

V_{sample} = 1600 mm^3
$V_{pores+fissures}$ = 960 mm^3
$V_{fissures}$ = 23.9 mm^3

MICRO-CT: FISSURE APERTURE

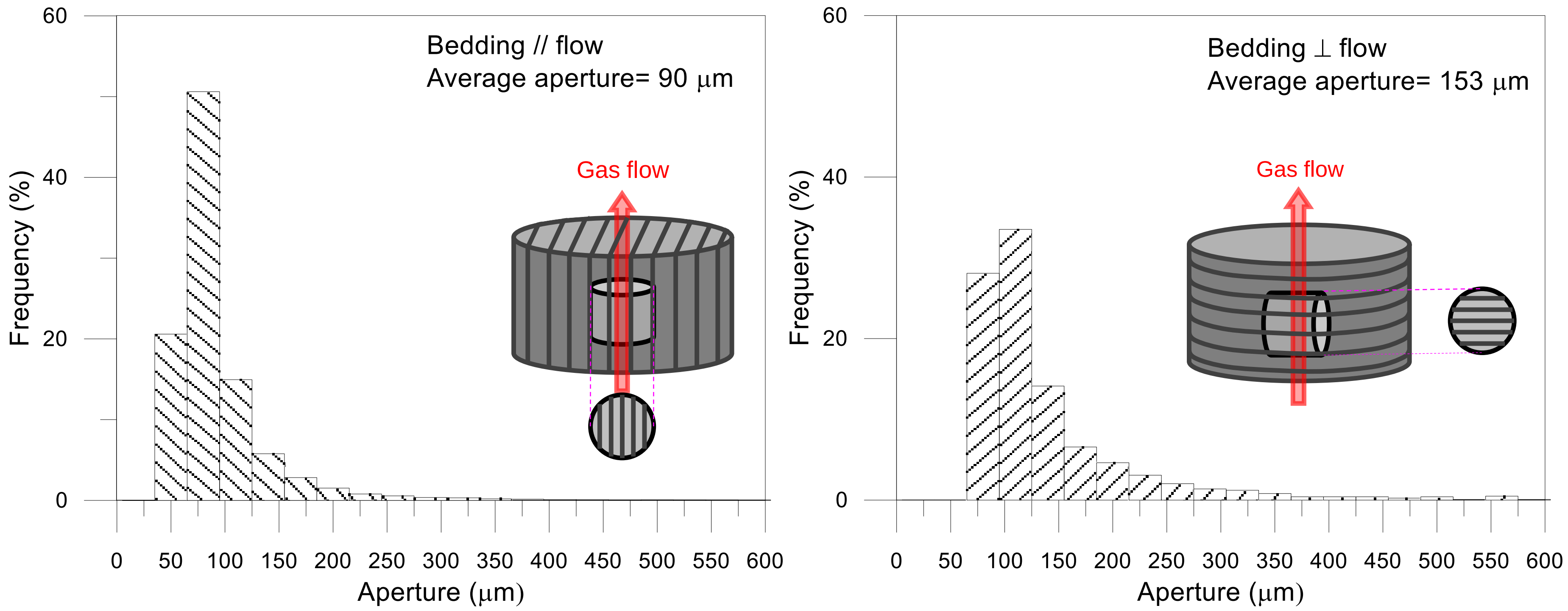

Fissures on the sample with bedding planes orientated parallel to gas flow were thinner than those with bedding planes oriented normal to flow

MICRO-CT: FISSURE SEPARATION

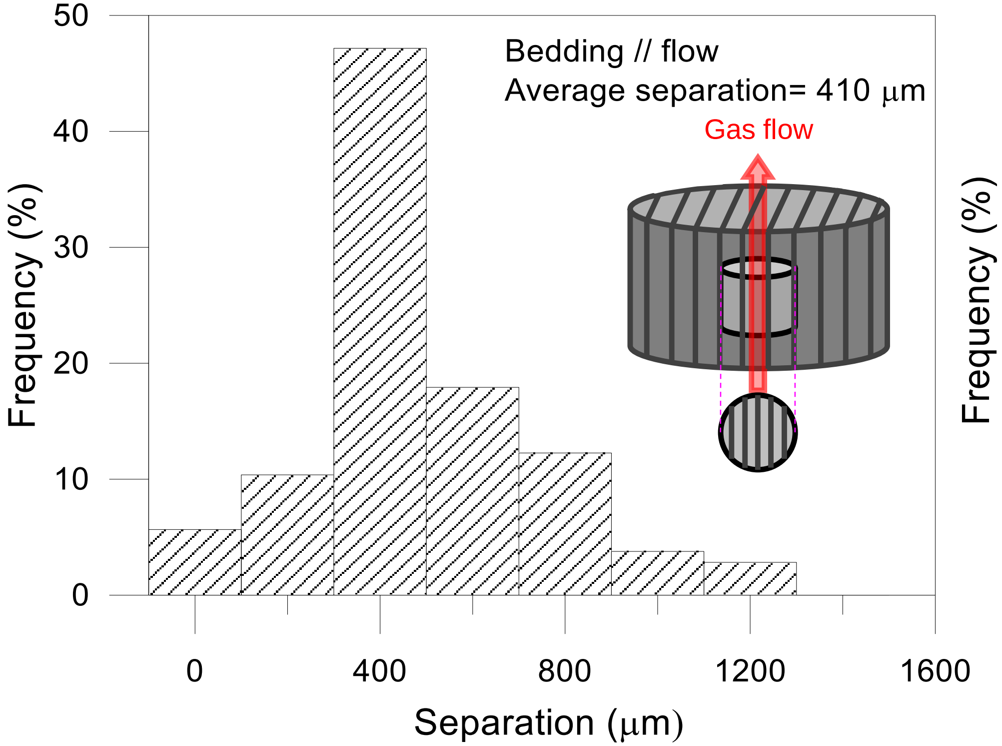

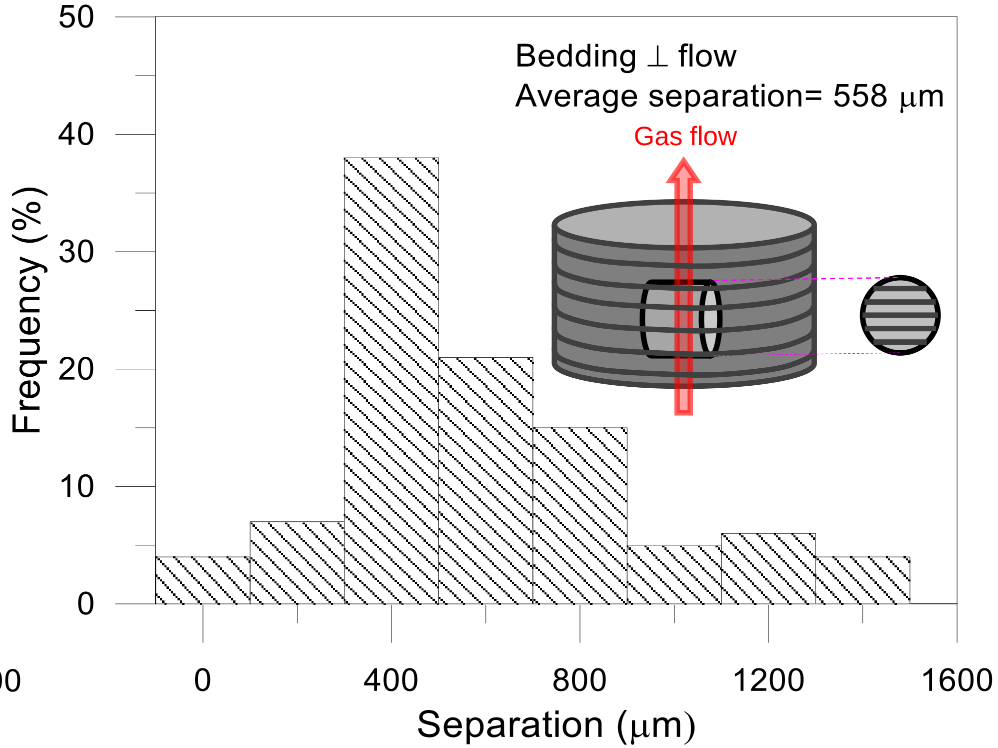

Fissures on the sample with bedding planes orientated parallel to gas flow were slightly closer than those with bedding planes oriented normal to flow

MICRO-CT: AFTER RE-SATURATION

After re-saturation

SET_1_A_P

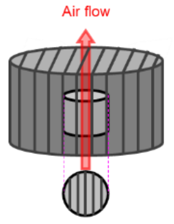

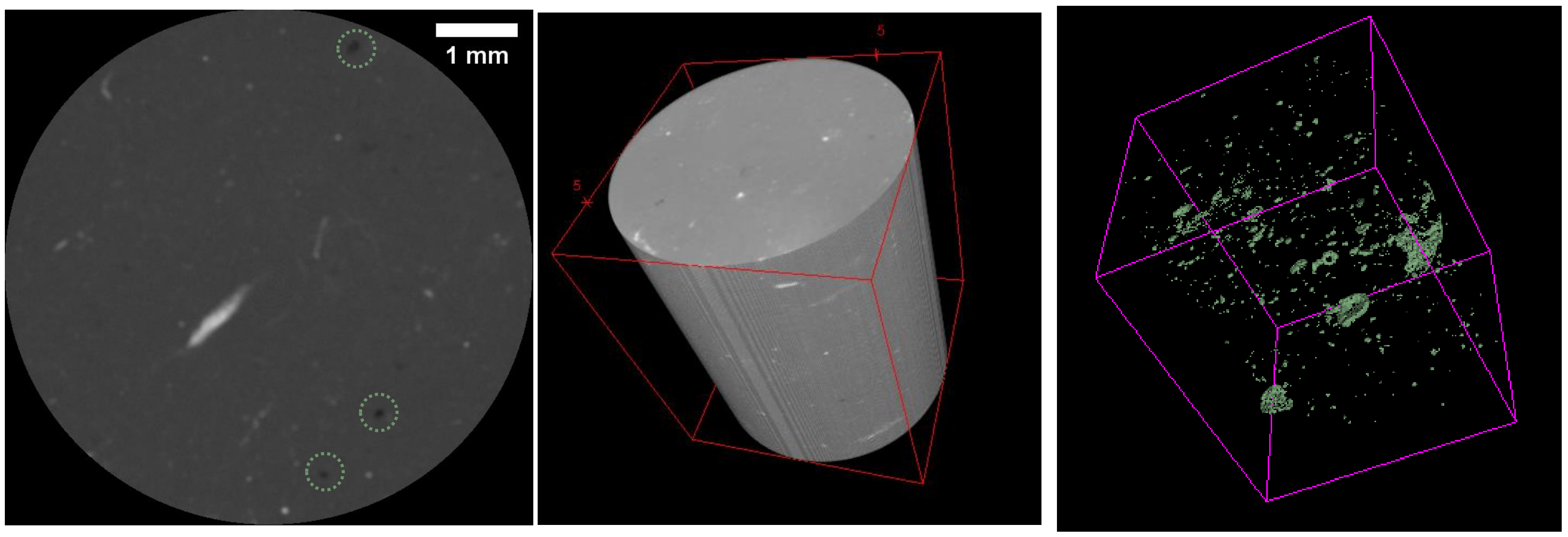

SET_1_A_N

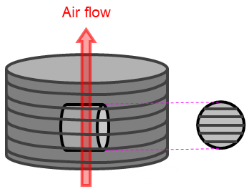

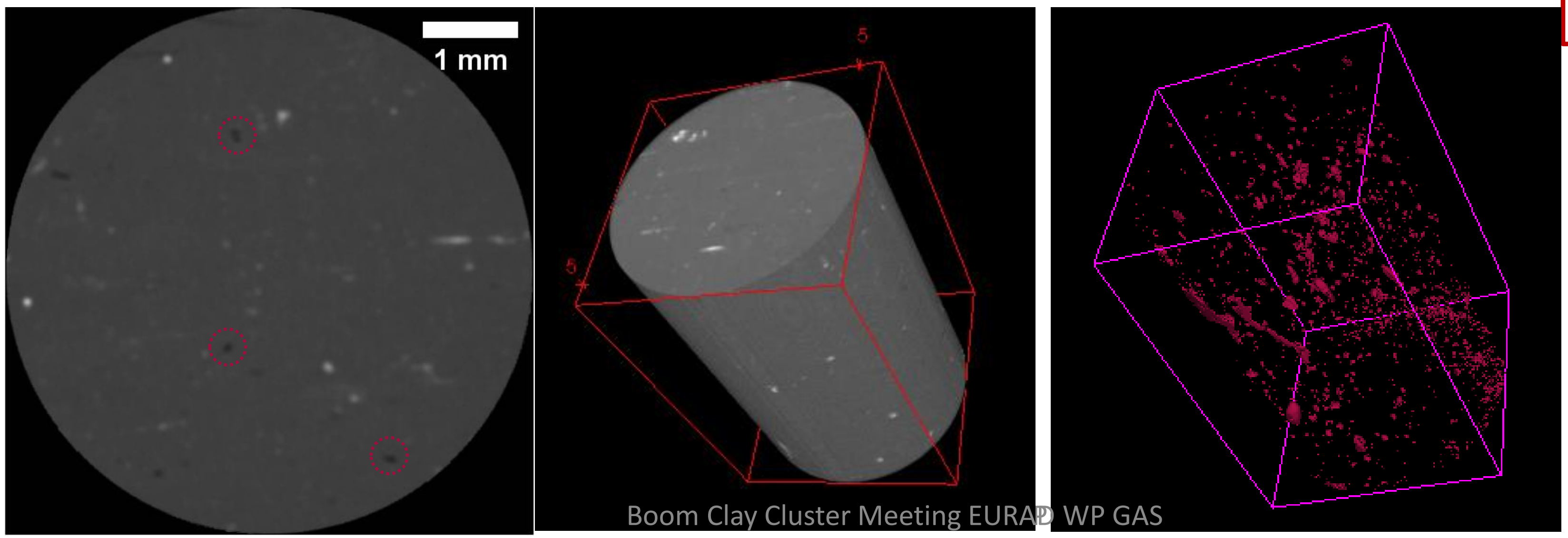

Pixel size 20 μm

Large pores not detected at the intact state, are identified at both orientations, possibly due to gas entrapment during re-saturation and gas exsolution / gas bubble coalescence during the undrained unloading

The connectivity between these large pores was not detected by μ-CT (< 40 μm)

MICRO-CT: AFTER SECOND GAS INJECTION

After second gas injection

SET_1_B_N

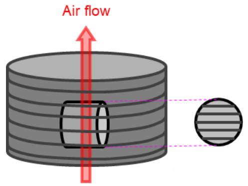

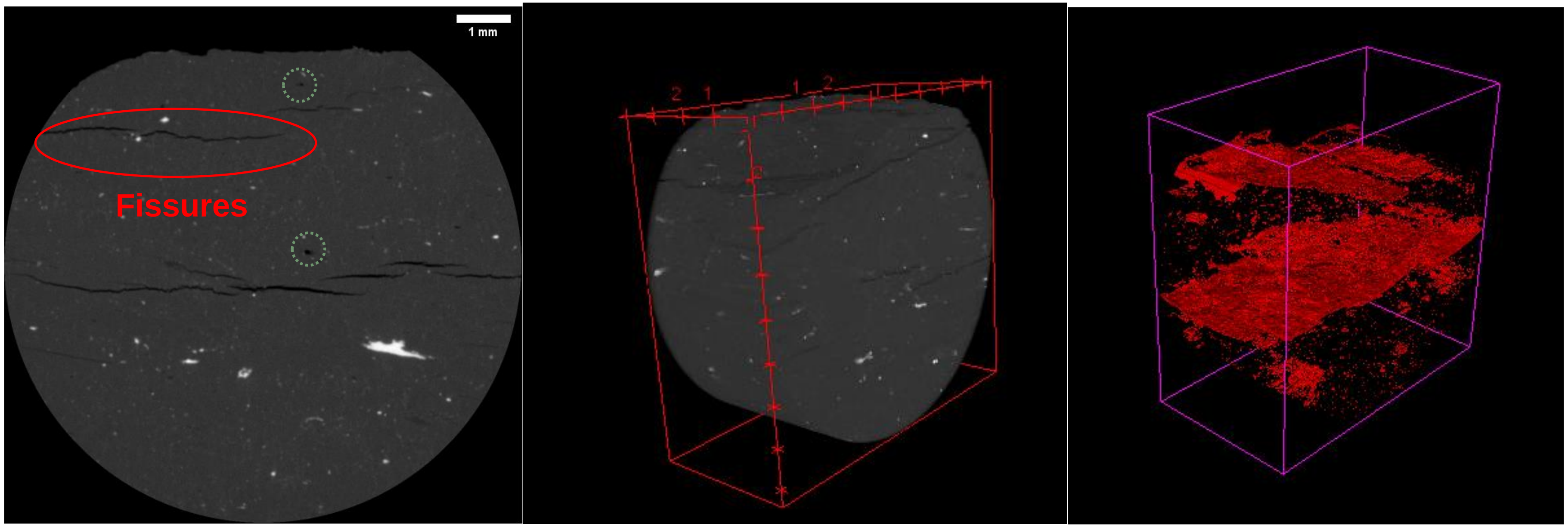

Large-aperture fissures and **large pores** are detected after the second gas injection. However, neither low-aperture fissures bridging bedding planes nor connection paths between large pores were detected (< 40 μm)

Pixel size 20 μm

MICRO-CT: AFTER SECOND GAS INJECTION

SET_3_N

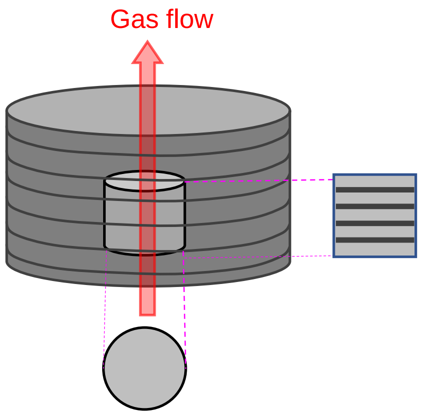

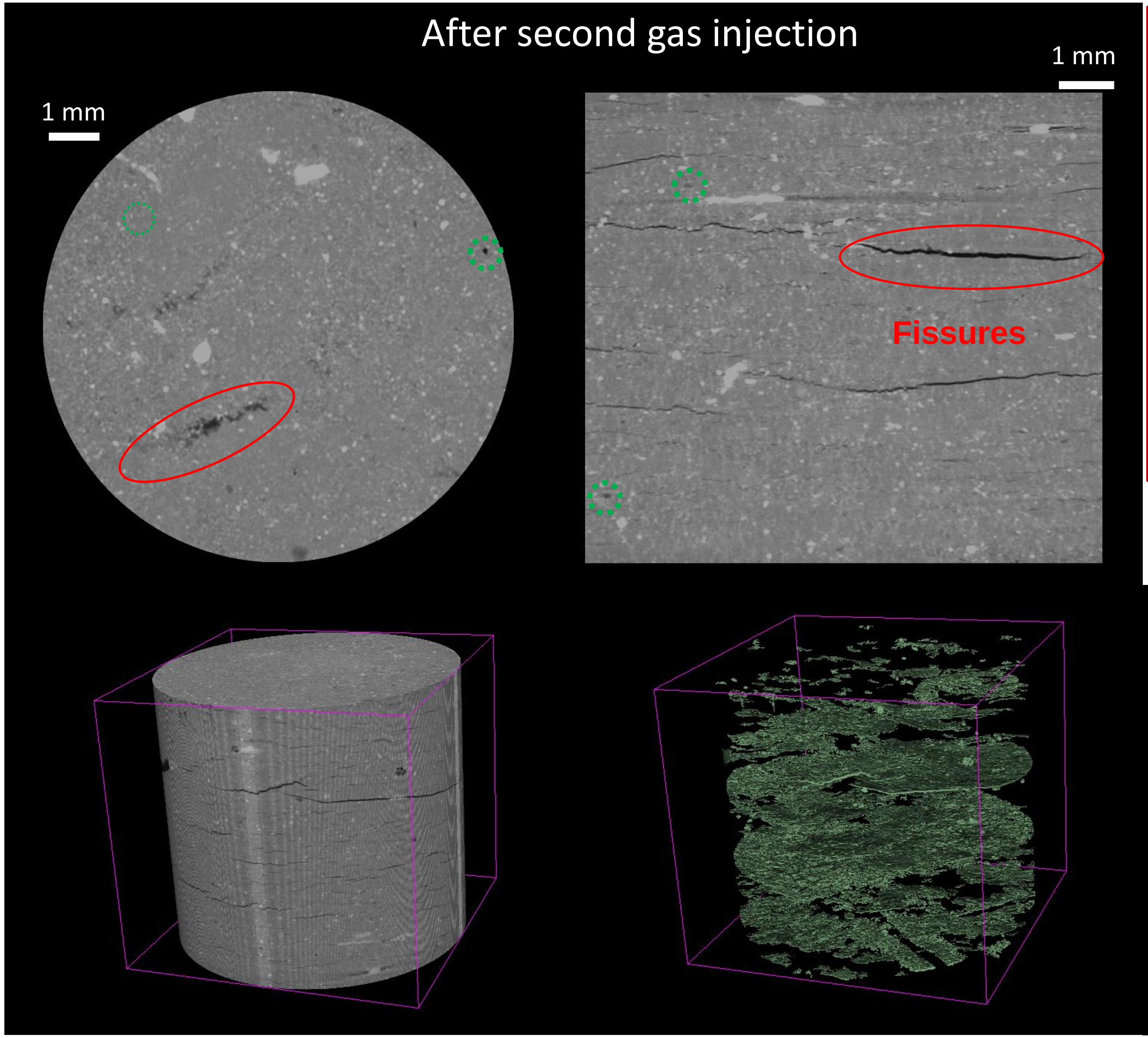

Large-aperture fissures and **large pores** are detected after the second gas injection. Low-aperture fissures bridging bedding planes can be discern, despite still unconnected (not continuous) (< 20 μm)

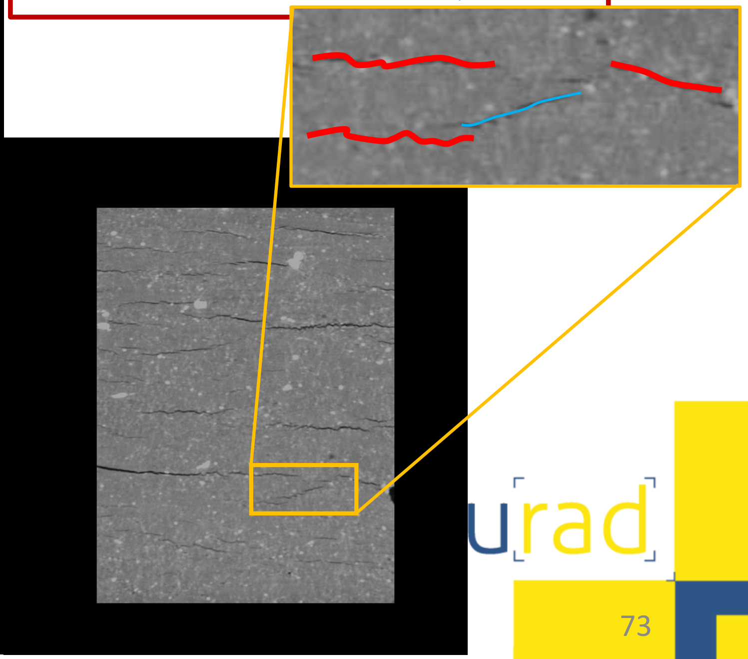

Pixel size 10 μm

FESEM: IMAGE BEFORE AND AFTER TESTS

Intact sample

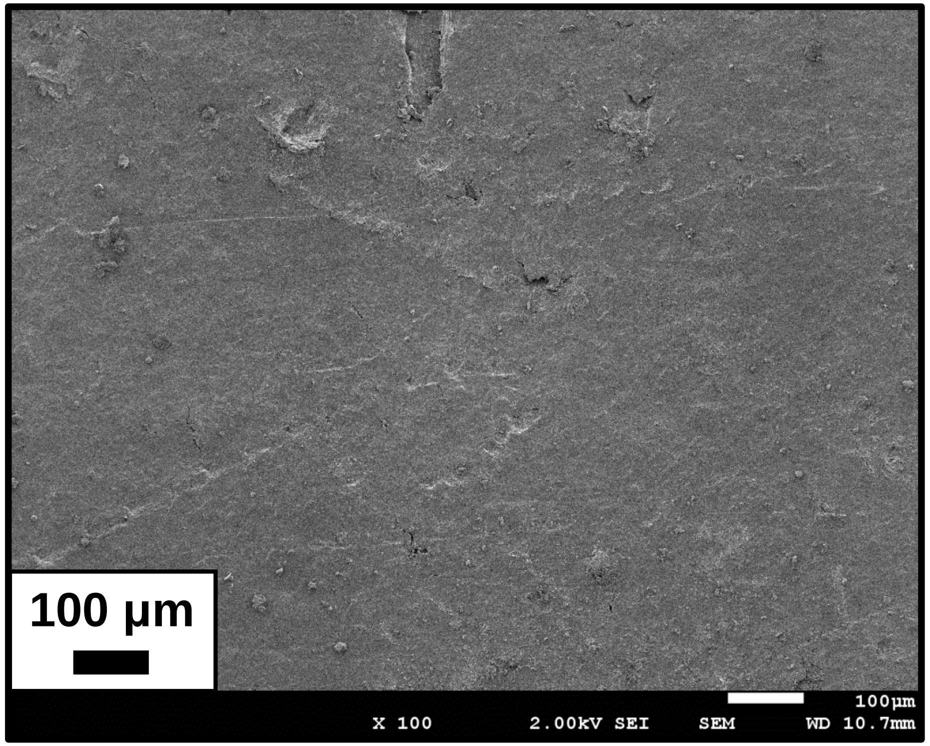

After air injection tests

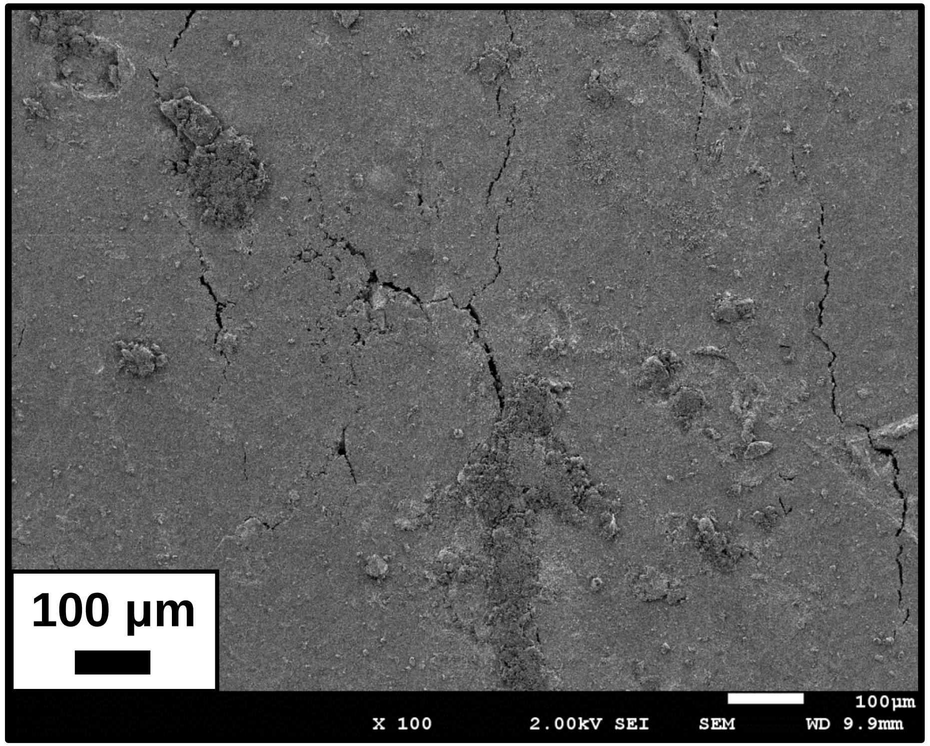

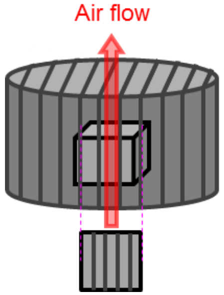

FESEM: IMAGE BEFORE AND AFTER TESTS

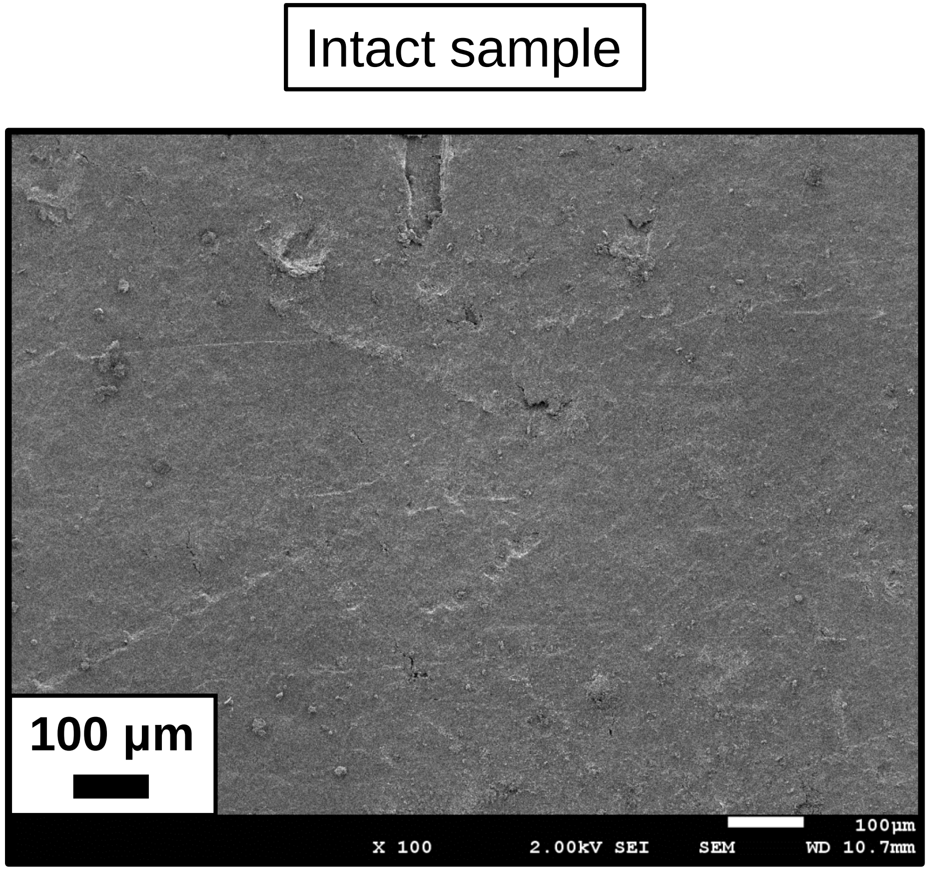

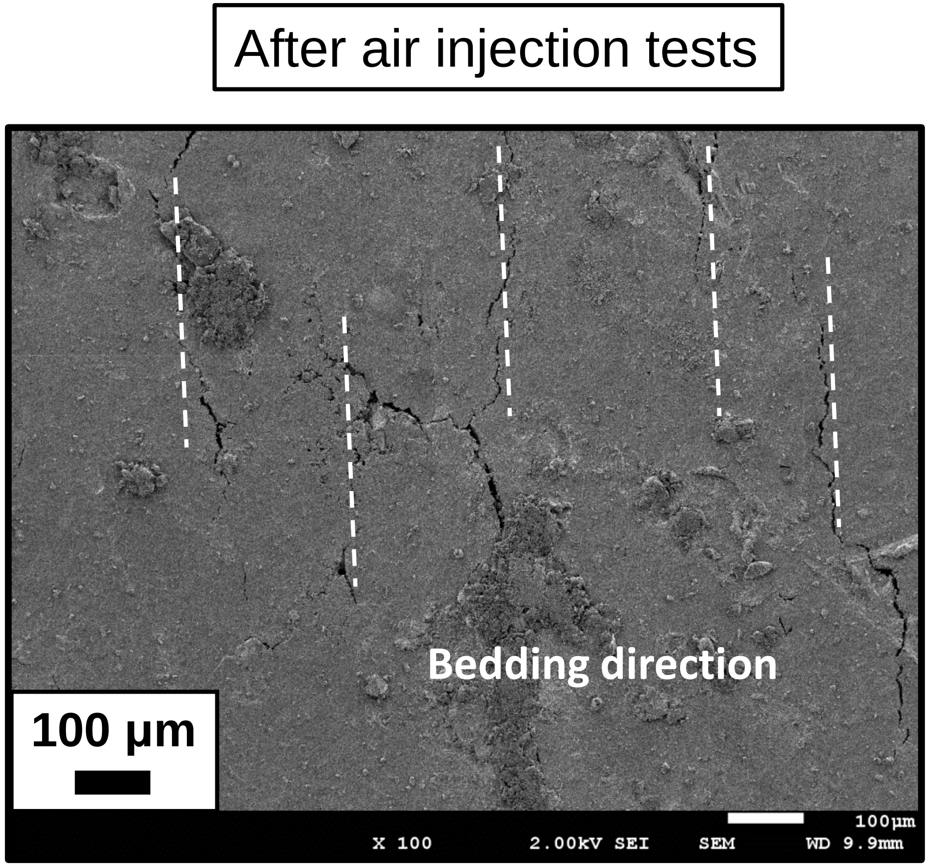

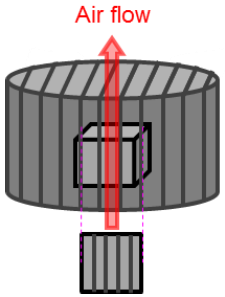

FESEM: IMAGE BEFORE AND AFTER TESTS

Intact sample

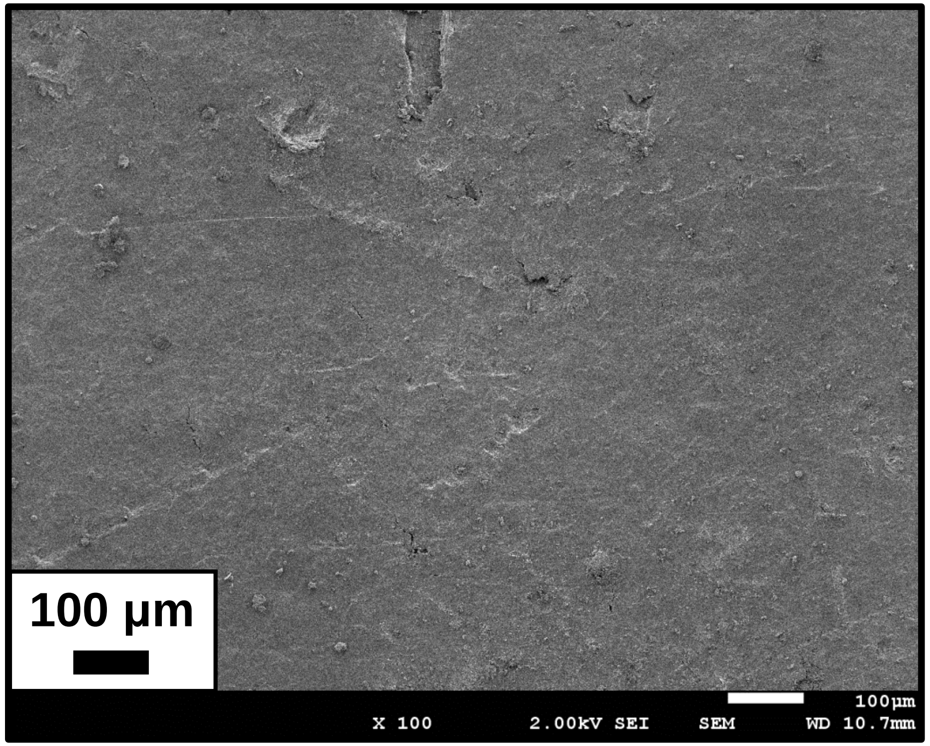

After air injection tests

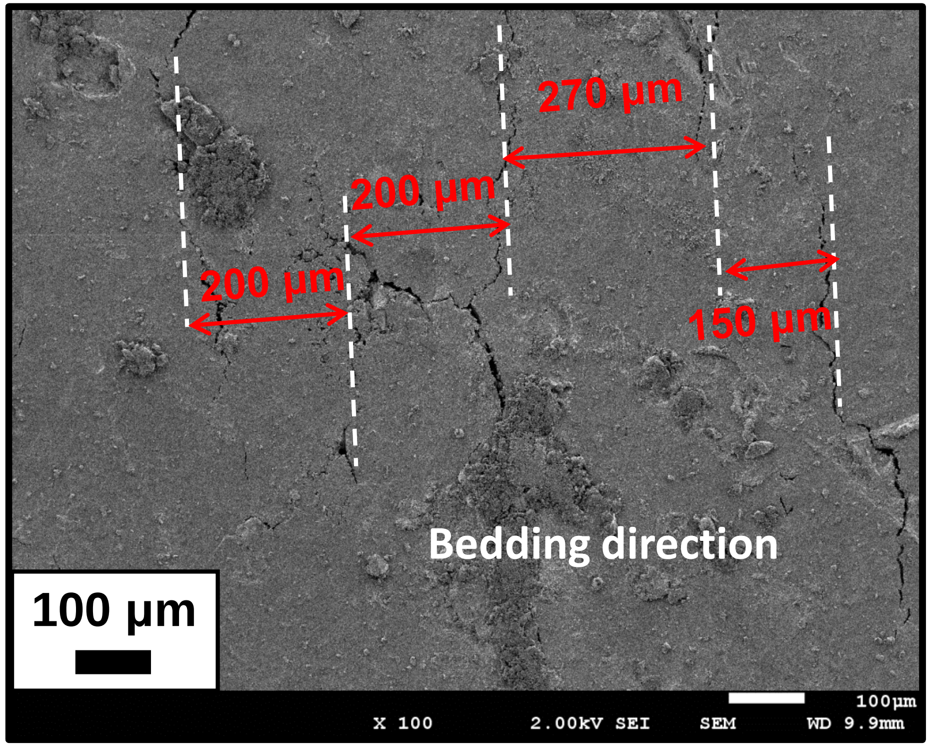

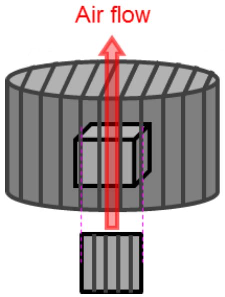

FESEM: IMAGE AFTER TESTS

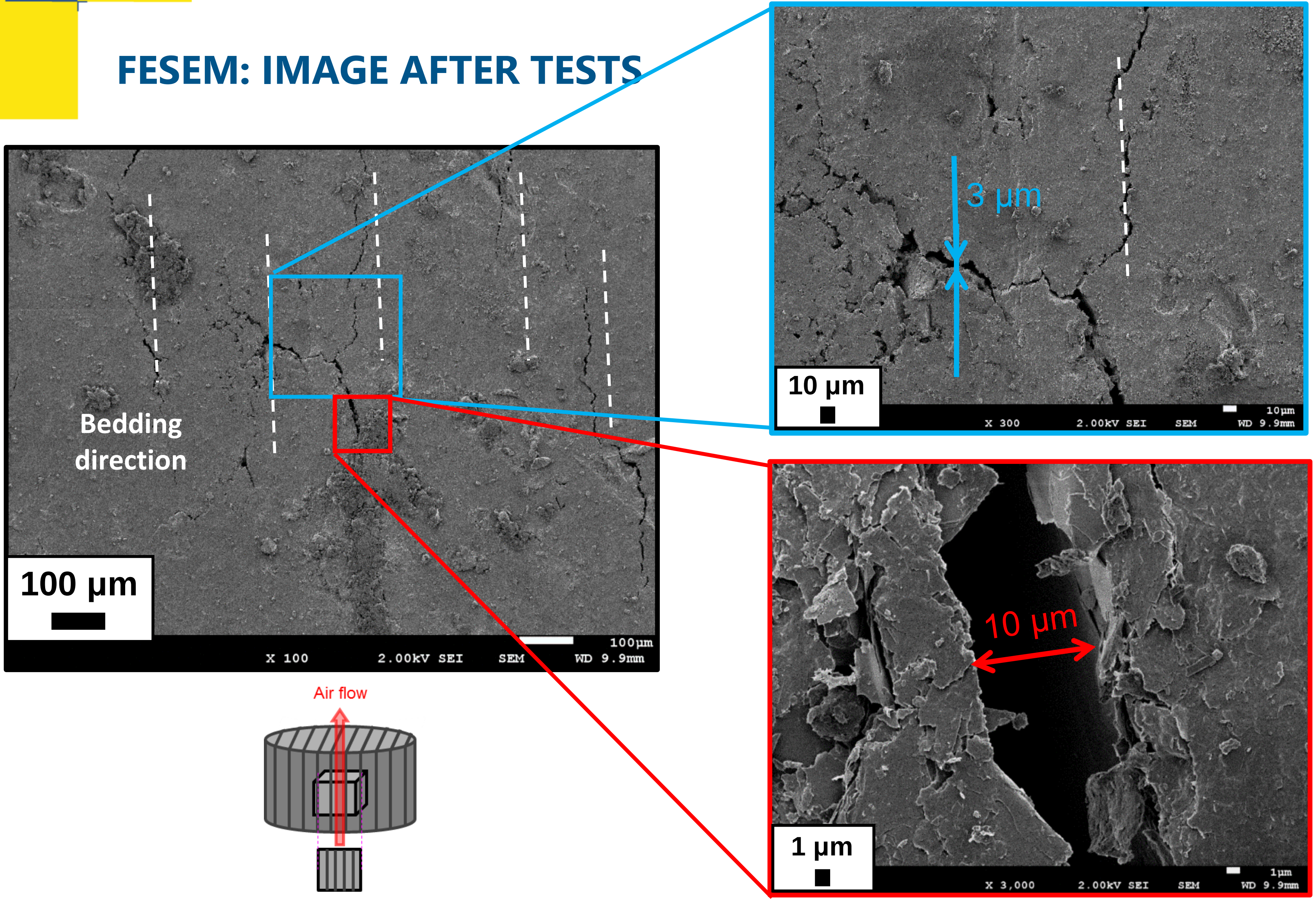

Low-aperture fissures bridging bedding planes

Large-aperture fissures following bedding direction

MICROSTRUCTURAL ANALYSIS: EVOLUTION OF PORE SIZE DISTRIBUTION

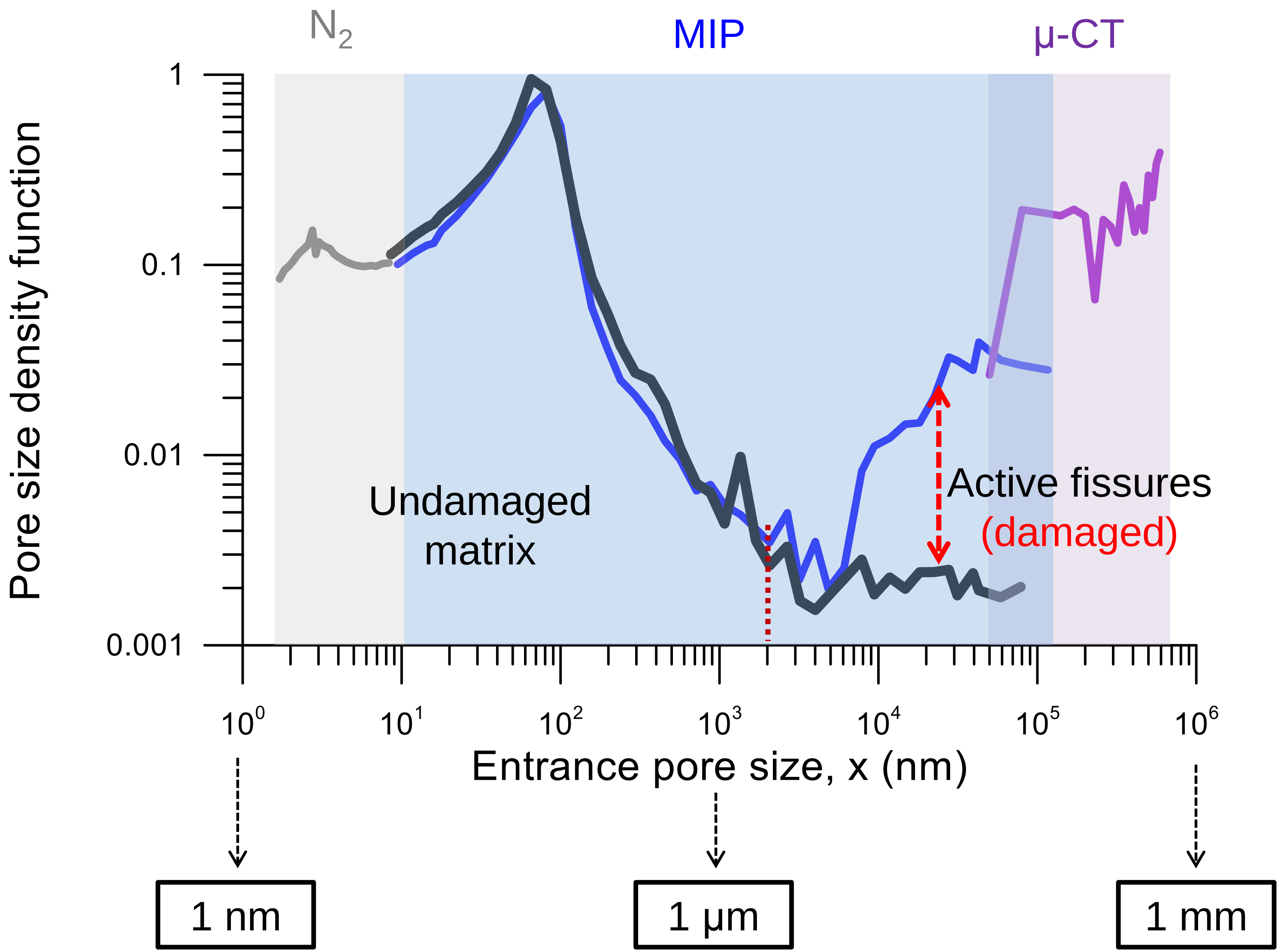

eurad

CONCEPTUAL MODEL

a) Water permeability: $k_{initial\ P} > \ k_{initial\ N}$

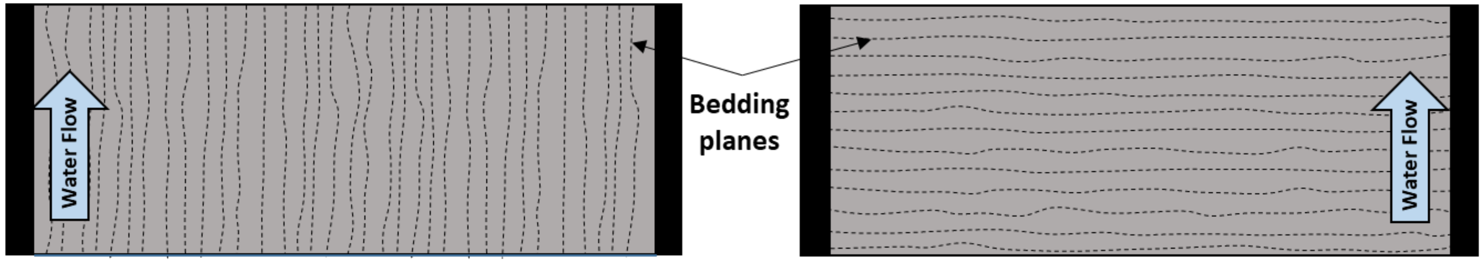

b) Gas injection: $k_P \approx k_N$ & $k_P/k_{initial\ P} < k_N/k_{initial\ N} \rightarrow \alpha_P < \alpha_N$

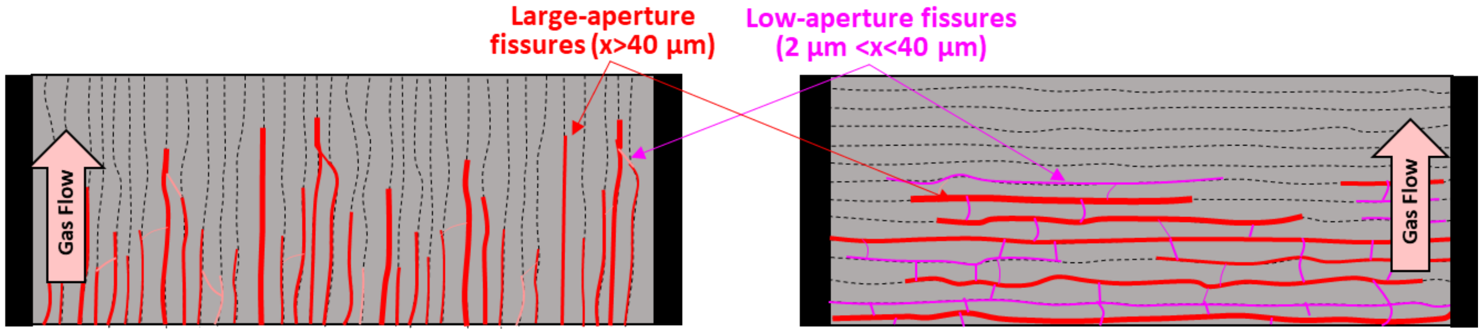

c) Re-saturation: $k_P \approx k_{initial\ P} > \ k_N \approx k_{initial\ N}$

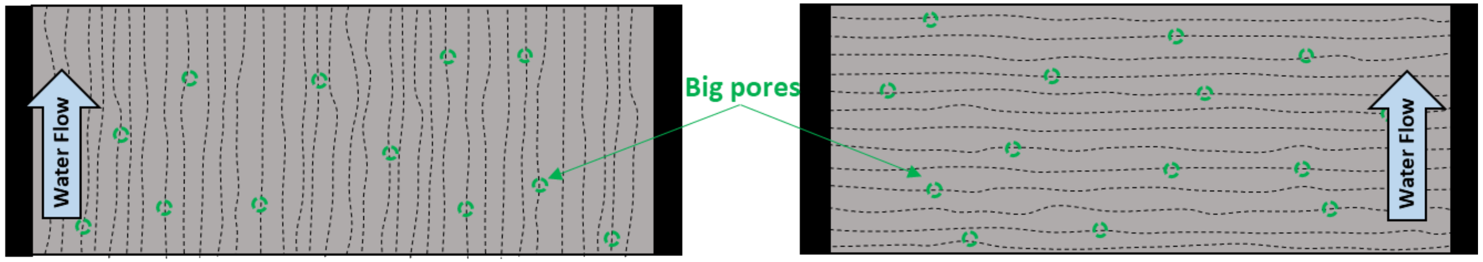

MACRO-FISSURED RATIO DETECTED AND FINAL DEGREE OF SATURATION

Void ratio: $e = \frac{V_m + V_M + V_f}{V_s}$

Macro void ratio:

$$e_M = \frac{V_M}{V_s}$$

e_M includes the 'connected' volume of large pores associated with (possible) gas entrapment / gas exsolution

Fissured void ratio:

$$e_f = \frac{V_{fissures}}{V_{solid}}$$

e_f includes the 'connected' volume of **large-aperture fissures** detected in the direction of the bedding planes with the μ-CT and low-aperture fissures bridging bedding planes which were not detected by μ-CT (< 40 μm)

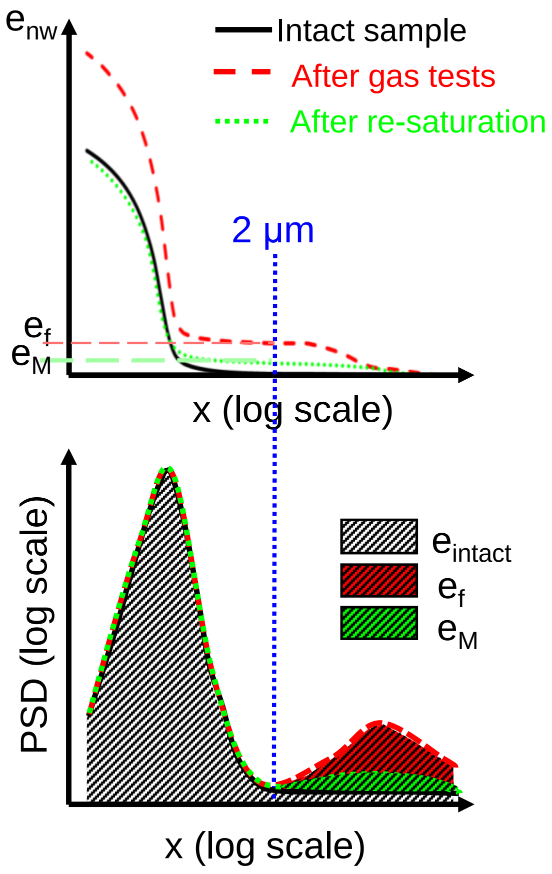

Macro-fissured ratio

$$f = \frac{e_f + e_M}{e}$$

Final degree of saturation*

$$S_r = 1 - f$$

*Assuming all the fissures are unsaturated

MICROSTRUCTURAL ANALYSIS: INTERPRETATION

Sample	Orientation	Technique	$e_f + e_M$	f	S_r
After gas injection (e=0.560)	Bedding // flow	MIP (b>2 µm)	0.039	0.069	0.931
		MIP (b>40 µm)	0.025	0.044	0.956
		µ-CT (b>40 µm)	0.028	0.050	0.950
After gas injection (e=0.563)	Bedding ⊥ flow	MIP (b>2 µm)	0.041	0.070	0.930
		MIP (b>40 µm)	0.020	0.034	0.966
		µ-CT (b>40 µm)	0.014	0.024	0.976
After re-saturation (e=0.559)	Bedding // flow	MIP (b>2 µm)	0.015	0.028	0.972
		MIP (b>40 µm)	0.011	0.019	0.981
		µ-CT (b>40 µm)	0.011	0.020	0.98
After re-saturation (e=0.540)	Bedding ⊥ flow	MIP (b>2 µm)	0.024	0.044	0.956
		MIP (b>40 µm)	0.017	0.031	0.969
		µ-CT (b>40 µm)	0.019	0.035	0.965
After second gas injection (e=0.582)	Bedding ⊥ flow	MIP (b>2 µm)	0.087	0.149	0.851
		MIP (b>40 µm)	0.032	0.056	0.944
		µ-CT (b>40 µm)	0.034	0.059	0.941
After second gas injection (e=0.565)	Bedding ⊥ flow	MIP (b>2 µm)	0.086	0.152	**0.848**
		MIP (b>20 µm)	0.043	0.076	0.924
		µ-CT (b>20 µm)	0.038	0.067	0.933

MULTI-SCALE ANALYSES

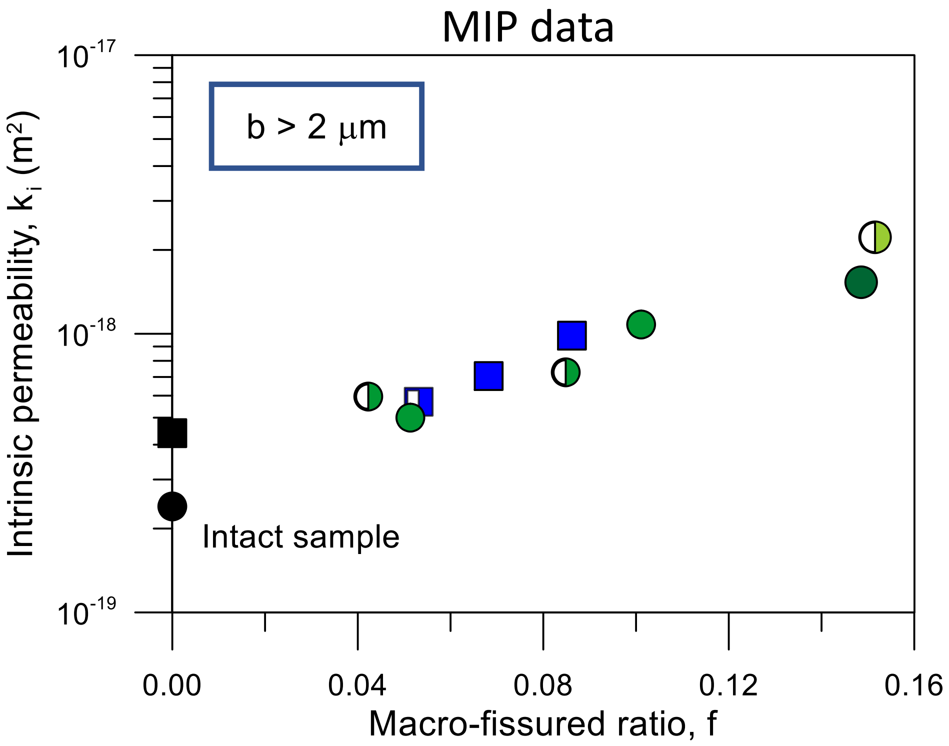

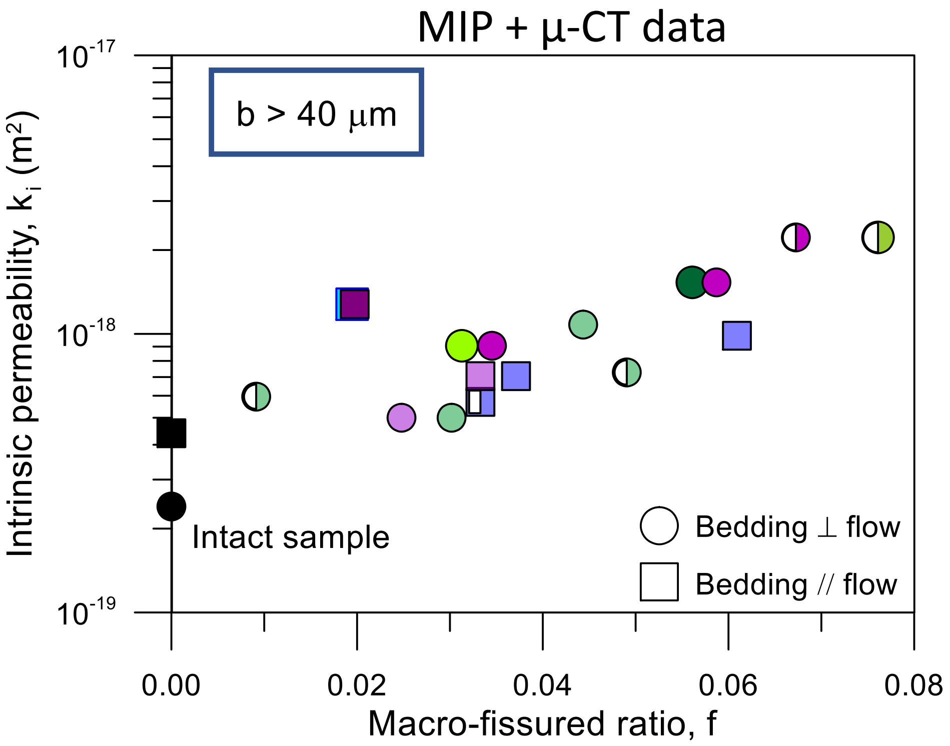

Intact sample

r=100 mL/min (MIP)

r=2 mL/min (MIP)

r=100 mL/min (μ-CT)

r=2 mL/min (μ-CT)

Macro-fissured ratio

$$f = \frac{e_f + e_M}{e}$$

eurad

MULTI-SCALE MODEL

Permeability determined in the last stage (water or gas) is normalised with respect to the initial permeability to water (before any injection) to obtain a permeability ratio.

$$\frac{k_i}{k_{ini}} = [\alpha(f - f_0) + 1]$$

Model parameters

$$f_0 = \frac{e_M}{e} = 0.02$$

→ Volume of macropores at the intact state (MIP data)
Independent of the bedding orientation

$$\alpha \begin{cases} \alpha_{\perp} = 84 \\ \alpha_{//} = 20 \end{cases}$$

→ Fitting parameter with experimental data
Dependent of bedding orientation

k_{ini} → Permeability to water before gas injection → **Anisotropy at the initial state is taken into account with k_{ini}**

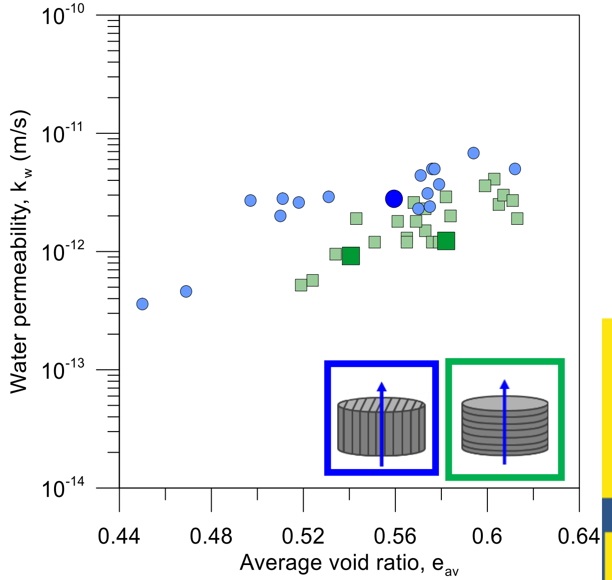

MULTI-SCALE MODEL

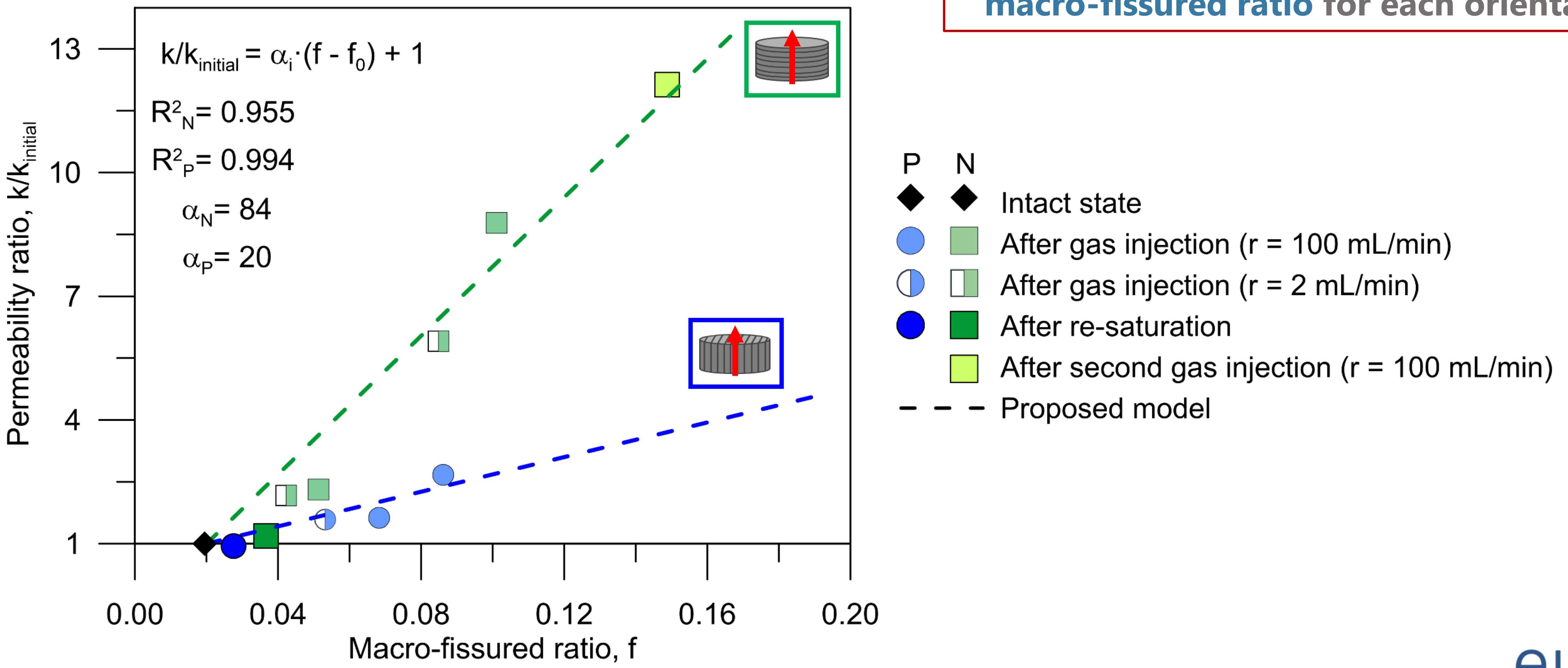

The permeability ratio relates linearly to the macro-fissured ratio for each orientation

eurad

REFERENCES OF THIS WORK

- Gonzalez-Blanco, L., Romero, E., Jommi, C., Li, X. & Sillen, X. (2016). Gas migration in a cenozoic clay: Experimental results and numerical modelling. *Geomechanics for Energy and the Environment*, 6, pp.81–100.
- Gonzalez-Blanco, L., Romero, E., Li, X., Sillen, X., Marschall, P. & Jommi, C. (2016) Air injection tests in two argillaceous rock formations: experimental results and modelling. *1st International Conference on Energy Geotechnics ICETG, Kiel, Germany, Wuttke, Bauer & Sánchez (Eds.).*
- Gonzalez-Blanco, L., Romero, E., Jommi, C. Li, X. & Sillen, X. (2017). Exploring fissure opening and its connectivity in a Cenozoic clay during gas injection. Chapter in Springer Series in Geomechanics and Geoengineering, January, 2017 In book: *Advances in Laboratory Testing and Modelling of Soils and Shales (ATMSS)*, 288-295.
- Gonzalez-Blanco, L., (2017). Gas migration in deep argillaceous formations: Boom Clay and indurated clays. *PhD Thesis, Universitat Politècnica de Catalunya, Barcelona, Spain.*
- Gonzalez-Blanco, L., Romero, E., Marschall, P & Levasseur, S. (2022) Hydro-mechanical response to gas transfer of deep argillaceous host rocks for radioactive waste disposal. *Rock Mechanics and Rock Engineering*, 55, 1159-1177.
- Gonzalez-Blanco, L. & Romero, E. (2022) A multi-scale insight into gas migration in a deep Cenozoic clay. *Géotechnique*. Ahead of print
- Gonzalez-Blanco, L., Romero, E. & Levasseur, S. (2023) Self-sealing of Boom Clay after gas transport. *Rock Mechanics and Rock Engineering* (accepted)

OUTLINE OF THE LECTURE

1. Motivation
2. Insight into gas transfer and self-sealing
3. Some observations regarding gas testing (experimental protocols)
4. A detailed research methodology on Boom Clay:
   - Material characterization
   - Stress paths followed
   - Gas test protocols
   - Test results at different scales (macroscopic results and microstructural features)
5. **Final comments. Future challenges**

eurad

FUTURE CHALLENGES

Multi-scale experimental research is needed to comprehend the gas transport and self-sealing phenomena in saturated argillaceous rocks.

Macroscopic behaviour:
- Effect of stress state
- Gas transport mechanisms
- Gas effective permeability
- Recovery of hydraulic function

Microscopic observation:
- Opening of gas pathways
- Role of bedding planes
- Quantification of microstructural changes
- Effectiveness of self-sealing

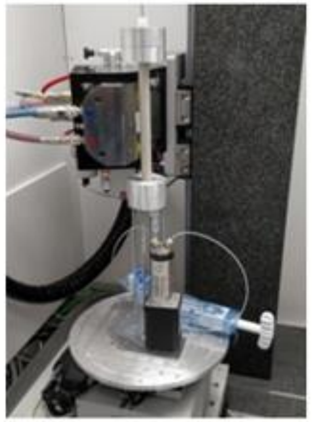

On-site tomography

- Real tracking of gas pathways during gas invasion
- No influence of unloading process or sample pre-treatment (freeze-drying)

eurad

eurad
European Joint Programme on Radioactive Waste Management

THANK YOU FOR YOUR ATTENTION!!

Financial support of ONDRAF/NIRAS (Belgium) and NAGRA (Switzerland) with CIMNE/UPC (Spain) through several research projects is greatly acknowledged

ONDRAF/NIRAS
Belgian Agency for Radioactive Waste and enriched Fissile materials

nagra.

REFERENCES

- Bernier, F, Li, X.L., Bastiaens, W., Ortiz, L., Van Geet, M., Wouters, L., Frieg, B., Blümling, P., Desrues, J., Viaggiani, G., Coll, C., Chanchole, S., De Greef, V., Hamza, R., Malinsky, L., Vervoort, A., Vanbrabant, Y., Debecker, B., Verstraelen, J., et al. (2007) Fractures and Self-healing within the Excavation Disturbed Zone in Clays (SELFFRAC). Final Report.
- Dao, L.Q. (2015) Etude du comportement anisotrope de l'argile de Boom. *PhD Thesis*, Université Paris-Est, France.
- Della Vecchia, G., Jommi, C., Lima, A., & Romero, E. (2011) Some remarks on the hydro-mechanical constitutive modelling of natural and compacted Boom clay. *International Conference of Unsaturated Soils*, Barcelona, Spain, Taylor & Francis Group, London.
- Di Donna, A., Charrier, P., Dijkstra, J., Andò, E. & Bésuelle, P. (2022) The contribution of swelling to self-sealing of claystone studied through x-ray tomography. *Physics and Chemistry of the Earth*, 127, 103191.
- Hemes, S., Desbois, G., Urai, J.L., Schröppel, B. & Schwarz, J.O. (2015) Multi-scale characterization of porosity in Boom Clay (HADES-level, Mol, Belgium) using a combination of X-ray μ-CT, 2D BIB-SEM and FIB-SEM tomography. *Microporous and Mesoporous Materials*, 208, 1–20.
- Marschall, P., Horseman, S., & Gimmi, T. (2005) Characterisation of Gas Transport Properties of the Opalinus Clay, a Potential Host Rock Formation for Radioactive Waste Disposal. *Oil & Gas Science and Technology*, 60(1), 121–139.
- ONDRAF/NIRAS (2016) Conceptualisations of gas related issues. *Workshop on gas related issues in clay based repository programmes.*
- Pineda, J., Alonso, E.E. & Romero, E. (2014) Environmental degradation of claystones. *Géotechnique*, 64(1), 64–82.

eurad

REFERENCES

- Pineda, J., Romero, E., Alonso, E. Pérez, T. (2014) A New High-Pressure Triaxial Apparatus for Inducing and Tracking Hydro-Mechanical Degradation of Clayey Rocks. *Geotechnical Testing Journal*, 37 (6), 1-15.
- Romero, E. & Gonzalez-Blanco, L. (2019) Hydro-mechanical processes associated with gas transport in MX-80 Bentonite in the context of Nagra's RD&D programme. Nagra Technical Report NAB 19-06.
- Romero, E., Arnedo, D., Alonso, E.E., & Marschall, P. (2010) Gas Injection Laboratory Experiments on Opalinus Clay. *In: Clays in Natural & Engineered Barriers for Radioactive Waste Confinement,* 4th International Meeting, March 2010, Nantes, France, pp. 113–114.
- Salehnia, F., Collin, F., Li, X., Dizier, A., Sillen, X. & Charlier, R. (2015) Coupled modeling of Excavation Damaged Zone in Boom clay: Strain localization in rock and distribution of contact pressure on the gallery's lining. *Computers and Geotechnics*, 69, 396-410.
- Sau, N. (2021) THM coupled behavior of a deep indurated argillaceous formation. *PhD Thesis*, Universitat Politècnica de Catalunya, Spain.
- Sau, N., Romero, R. & Van Baelen, H. (2020) Restoring initial conditions in a deep argillaceous formation with induced suction on retrieval. *E3S Web of Conferences* 195, 04012.
- Schneider, C.A., Rasband, W.S., & Eliceiri, K.W. (2012) NIH Image to ImageJ: 25 years of image analysis. *Nature Methods*, 9 (7), 671–675.

eurad

REFERENCES

- Sillen, X. & Marivoet, J. (2007) Thermal impact of a HLW repository in clay. *External Report SCK·CEN-ER-38*.
- Van Geet, M., Baestiaens, W. & Ortiz, L. (2008) Self-sealing capacity of argillaceous rocks: Review of laboratory results obtained from the SELFRAC project. *Physics and Chemistry of the Earth*, 33 (1), S396-S406.
- Voltolini, M. & Ajo-Franklin, J.B., 2020. The Sealing Mechanisms of a Fracture in Opalinus Clay as Revealed by in situ Synchrotron X-Ray Micro-Tomography. *Frontiers in Earth Science*, 8, 207.
- Voorn, M., Exner, U. & Rath, A. (2013) Multiscale Hessian fracture filtering for the enhancement and segmentation of narrow fractures in 3D image data. *Computers & Geosciences* 57, 44-53.
- Zhang, C.L. & Talandier, J. (2022) Self-sealing of fractures in indurated claystones measured by water and gas flow. *Journal of Rock Mechanics and Geotechnical Engineering*, 15(1), 227-238.
- Zhang, C.L. (2013) Sealing fractures in claystone. *Journal of Rock Mechanics and Geotechnical Engineering*, 5, 214-220.

eurad